

An ACI Technical Publication

SYMPOSIUM VOLUME



Cracking and Durability in Sustainable Concretes

SP-336

Editors:
Ralf Leistikow and Kimberly Waggle Kramer



American Concrete Institute
Always advancing

Cracking and Durability in Sustainable Concretes

Sponsored by
ACI Committees 130, Sustainability of Concrete
and 224, Cracking

The Concrete Convention and Exposition
October 15-19, 2017
Anaheim, California, USA

Editors:
Ralf Leistikow and
Kimberly Waggle Kramer



American Concrete Institute
Always advancing

SP-336

First printing, December 2019

Discussion is welcomed for all materials published in this issue and will appear ten months from this journal's date if the discussion is received within four months of the paper's print publication. Discussion of material received after specified dates will be considered individually for publication or private response. ACI Standards published in ACI Journals for public comment have discussion due dates printed with the Standard.

The Institute is not responsible for the statements or opinions expressed in its publications. Institute publications are not able to, nor intended to, supplant individual training, responsibility, or judgment of the user, or the supplier, of the information presented.

The papers in this volume have been reviewed under Institute publication procedures by individuals expert in the subject areas of the papers.

Copyright © 2019
AMERICAN CONCRETE INSTITUTE
38800 Country Club Dr.
Farmington Hills, Michigan 48331

All rights reserved, including rights of reproduction and use in any form or by any means, including the making of copies by any photo process, or by any electronic or mechanical device, printed or written or oral, or recording for sound or visual reproduction or for use in any knowledge or retrieval system or device, unless permission in writing is obtained from the copyright proprietors.

Printed in the United States of America

Editorial production: Susan K. Esper

ISBN-13: 978-1-64195-088-6

PREFACE

Cracking and Durability in Sustainable Concretes

ACI Committees 130 and 224 sponsored and moderated two sessions at The ACI Concrete Convention and Exposition – Fall 2017, held in Anaheim, California. The objective of the sessions was to review the use of innovative mixture designs which incorporated sustainable admixtures and supplemental cementitious materials, and the effect these sustainable technologies have on the cracking performance and durability of these concretes. In particular, cracking behavior in sustainable concretes or practices for mitigation of cracking in sustainable concretes was reviewed. This information was shared based on completed research and case studies of sustainable concrete mixture designs. The learning objectives of the two sessions follow:

- 1) Learn about innovative mixture designs that incorporate sustainable admixtures and supplemental cementitious materials;
- 2) Learn about the effect these sustainable technologies have on the cracking performance and durability of these concrete mixes;
- 3) Gain an understanding of the cracking behavior of sustainable concrete mixtures; and
- 4) Learn about practices used to mitigate cracking in sustainable concrete.

Twelve presentations were given, and the presenters came from all over the world. Following the sessions, some of the presenters authored papers that provided more extensive information about their research. This SP include copies of these seven research papers.

Editors

Mr Ralf Leistikow
Wiss Janney Elstner Associates, Inc.
Cary, NC, USA

Dr Kimberly Waggle Kramer
Kansas State University, Manhattan, KS, USA

TABLE OF CONTENTS

SP- 336-1:

Internal Curing and Supplementary Cementitious Materials in Bridge Decks1-20
Authors: James Lafikes, Rouzbeh Khajehdehi, Muzai Feng, Matthew O'Reilly, and David Darwin

SP- 336-2:

Zeolite Based Concrete- Durable Solution for Nation's Infrastructure21-40
Authors: Nidhi M. Modha and Pratanu Ghosh

SP- 336-3:

Freeze-Thaw and Salt Resistance of a Fly Ash Based Pervious Concrete 41-53
Authors: Gang Xu, Luis Gerardo Navarro, Kafung Wong, and Xianming Shi

SP- 336-4:

Multifunction Green Corrosion Inhibiting Admixtures for Mortar under Chloride Environment.....54-72
Authors: Yu Jiang, Gang Xu, Zhipeng Li, and Xianming Shi

SP- 336-5:

Understanding Shrinkage in Alternative Binder Systems..... 73-90
Authors: Craig McKee, Ralf Leistikow, Emily Lorenz, William P. Gaspar, and Tumer Akakin

SP- 336-6:

Durability of Recycled Aggregate Concrete 91-100
Authors: Nariman J. Khalil and Georges Aouad

SP- 336-7:

Low-Cracking High-Performance Concrete (LC-HPC) for Durable Bridge Decks 101-116
Authors: David Darwin, Rouzbeh Khajehdehi, Muzai Feng, James Lafikes, Eman Ibrahim, and Matthew O'Reilly

Internal Curing and Supplementary Cementitious Materials in Bridge Decks

James Lafikes, Rouzbeh Khajehdehi, Muzai Feng, Matthew O'Reilly, David Darwin

Synopsis: Supplementary cementitious materials (SCMs) in conjunction with pre-wetted fine lightweight aggregate to provide internal curing are being increasingly used to produce high-performance, low-shrinking concrete to mitigate bridge deck cracking, providing more sustainable projects with a longer service life. Additionally, the SCMs aid in concrete sustainability by reducing the amount of cement needed in these projects. This study examines the density of cracks in bridge decks in Indiana and Utah that incorporated internal curing with various combinations of portland cement and SCMs, specifically, slag cement, Class C and Class F fly ash, and silica fume, in concrete mixtures with water-cementitious material ratios ranging from 0.39 to 0.44. When compared with crack densities in low-cracking high-performance concrete (LC-HPC) and control bridge decks in Kansas, concrete mixtures with a paste content higher than 27% exhibited more cracking, regardless of the use of internal curing or SCMs. Bridge decks with paste contents below 26% that incorporate internal curing and SCMs exhibited low cracking at early ages, although additional surveys will be needed before conclusions on long-term behavior can be made.

Keywords: bridge decks, cracking, high-performance concrete, internal curing, sustainability

INTRODUCTION

Cracking in bridge decks is a serious concern because cracks provide corrosive agents a direct path to reinforcing steel and reduce the freeze-thaw resistance of the concrete, ultimately reducing the service life of the structure. Regardless of the type of concrete being used in bridge deck construction, sustainability is significantly improved through the reduction of cracking. One initiative in recent concrete construction includes the addition of shrinkage reducing technologies as a measure to reduce cracking. Concrete mixture proportioning and construction practices have also been examined as measures to result in longer-lasting bridge decks. Over the past two decades, the Kansas Department of Transportation (KDOT) has been working with the University of Kansas (KU) to minimize cracking in bridge decks. Through a pooled-fund study supported by KDOT, other state and federal transportation organizations, and concrete material suppliers and organizations, the University of Kansas has developed specifications for Low-Cracking High-Performance Concrete (LC-HPC) bridge decks.

These specifications address cement and water content, plastic concrete properties, construction methods, and curing requirements. The constituent that undergoes shrinkage in concrete is cement paste (cementitious materials plus water in a concrete mixture). As a measure to reduce shrinkage compared to conventional bridge deck concrete, LC-HPC specifications limit cement content and dictate a tight range of water-cementitious material (w/cm) ratios. Cement contents are limited to 500 to 540 lb/yd³ (296 to 320 kg/m³). Because of a lack of consensus on the effect of supplementary cementitious materials (SCMs) on drying shrinkage at the time LC-HPC specifications were first written, only portland cement is permitted in LC-HPC decks. A w/cm ratio (0.43 to 0.45) is specified to help limit strength because of the relationship between high strength and increased cracking due to reduced creep, which can result in increased cracking if drying shrinkage is restrained. For portland cement mixtures following LC-HPC specifications for w/cm ratio and cement content, the paste content is inherently limited to 24.6% by volume. The 28-day strength of concrete is limited to values between 3500 and 5500 psi (24.1 and 37.9 MPa), and the air content of fresh concrete must be $8.0 \pm 1.5\%$ to improve durability and reduce cracking. An optimized aggregate gradation is used in LC-HPC mixtures. This can be achieved with tools such as described by Shilstone (1990) or provided by the KU Mix Method (Lindquist et al. 2008, 2015). These criteria provide concrete with better workability at a lower slump. LC-HPC specifications limit slump between 1½ and 3 in. (40 and 75 mm) at the point of placement and 3½ in. (90 mm) at the truck because high slump increases settlement cracking above reinforcing bars. To limit thermal and plastic shrinkage cracking, the temperature of fresh concrete must be between 55 and 70 °F (13 and 21 °C). The temperature range may be extended to 50 to 75 °F with approval by the Engineer.

To reduce the amount of water lost during construction and to avoid plastic shrinkage limits, the evaporation rate during bridge deck placement is limited to 0.2 lb/ft²/hr (1.0 kg/m²/hr). If the evaporation rate exceeds this limit, special actions, such as cooling the concrete or installing wind breaks, are required. Procedures for ensuring proper consolidation of concrete (through the use of vertically mounted internal gang vibrators) are also specified along with strike-off and finishing. The surface must be finished using a burlap drag, a metal pan, or both, followed by bullfloating (only if needed). Finishing aids, including water, are prohibited. To minimize plastic shrinkage cracking caused by loss of surface water after placement, early initiation of curing is required using a layer of pre-saturated burlap placed on the deck within 10 minutes after final strikeoff. A second layer of burlap must be placed within the next 5 minutes. The burlap must be soaked for at least 12 hours prior to placement.

In Kansas, 16 bridge decks have been constructed following the LC-HPC specifications (Kansas Department of Transportation 2011, 2014a, 2014b), with 11 bridge decks constructed following normal KDOT specifications to provide a basis of comparison. To provide a consistent method to compare bridge decks, a specific crack survey procedure has been developed to minimize variations from year to year (Lindquist et al. 2008, Yuan et al. 2011, Pendergrass et al. 2014). Results from the pooled-fund study show that the LC-HPC bridge decks are performing better than the decks constructed in accordance with normal KDOT specifications across the state (Lindquist et al. 2008, McLeod et al. 2009, Darwin et al. 2010, 2012, Yuan et al. 2011, Pendergrass et al. 2014, Alhmoed et al. 2015, Darwin et al. 2016).

There are other approaches available in addition to LC-HPC to reduce cracking in bridge decks. These include the use of internal curing (IC) through a partial replacement of aggregate with pre-wetted fine lightweight aggregate (LWA). For concrete with water cementitious material (w/cm) ratios below about 0.42, the cement paste can experience self-desiccation during early hydration, resulting in autogenous shrinkage of the concrete. In cases where the concrete is restrained from shrinking, tensile stresses develop and crack the concrete. Proper distribution of IC water has been shown to improve performance of concrete due to the reduction of autogenous shrinkage by providing

additional water for hydration throughout the entire cement paste matrix (Bentz and Weiss 2011). IC water is also available to reduce drying shrinkage for concrete made with w/cm ratios both above and below 0.42. Applicability of this technology for bridge deck cracking and durability is discussed in this report.

The initial survey results of six bridge decks in Indiana are the primary focus of this report. The first deck (IN-IC) was placed with IC concrete that contained 100% portland cement with IC, obtained by replacing a portion of aggregate with pre-wetted fine LWA. The control deck for IN-IC, designated IN-Control, incorporated mixture proportions similar to the IN-IC deck but with no IC water provided (no LWA replacement). The other four bridges were constructed with internally cured high-performance concrete (IN-IC-HPC) containing SCMs, either Class C fly ash or slag cement along with silica fume. The IN-IC-HPC decks contained higher quantities of IC water than IN-IC.

In addition to the six bridges in Indiana, the results of crack surveys conducted by Brigham Young University (BYU) on two internally cured decks in Utah (UT-IC-1 and UT-IC-2) are also included in this paper for comparison. UT-IC-1 and UT-IC-2 were constructed in spring 2012 and are similar in structure type (including precast panels to support an internally cured deck topping) and mixture proportions. The concrete used in both UT-IC decks incorporated a partial replacement of cement with Class F fly ash. The age of both Utah bridges was 24 months at the time of most recent surveys and followed a procedure similar to that used by KU for visually inspecting bridge decks for cracks. This report analyzes the cracking performance of the eight bridge decks and compares them with that of the LC-HPC and conventional KDOT bridge decks being analyzed in the pooled-fund study.

RESEARCH SIGNIFICANCE

Cracking of concrete bridge decks can lead to rapid deterioration and shortened service life. It follows that the sustainability of concrete bridge decks is significantly increased with improved cracking performance. Based on research findings at the University of Kansas (KU), specifications for Low-Cracking High-Performance Concrete (LC-HPC) bridge deck construction were developed and include requirements for cementitious material and cement paste contents, curing, maximum concrete compressive strength, slump, and finishing operations. LC-HPC specifications do not currently specify the use of SCMs or IC. The bridge decks included in this paper serve as a basis for evaluating cracking and durability performance of concrete with IC or SCMs and IC at early ages.

CRACK SURVEY PROCEDURE

Crack surveys for both LC-HPC and control bridge decks are performed on an annual basis during late spring, summer, and early fall. The survey procedures are summarized next.

Procedure

To provide accurate and comparable results, a standard procedure is followed for crack surveys as outlined by Lindquist et al. 2005. Crack surveys should be performed only on a day that is at least mostly sunny with an air temperature not less than 60°F (16°C) at the time of surveying. Moreover, the bridge deck should be completely dry. The crack survey is invalid if it rains during the time of the survey or if the sky becomes overcast.

A scaled plan (map) for the bridge deck is developed and printed before the survey and serves as the template to indicate the location and length of the cracks on the actual bridge deck. A grid on a separate sheet of paper is included underneath the deck plan. The grid helps the surveyor keep track of crack location and length. Some variations are expected when drawing the cracks.

Traffic control is provided to ensure the safety of the surveyors during the bridge survey. After closing at least one lane of the bridge to traffic, two surveyors draw a 5 ft × 5 ft (1.52 m × 1.52 m) grid on the bridge deck using sidewalk chalk or lumber crayons. This is called the bridge grid and should match the grid prepared for use with the plans. Surveyors mark cracks on the deck they can see while bending at waist height (cracks that cannot be seen from waist height should not be marked). At least two surveyors should inspect each section of the bridge. This method results in consistent crack survey results between surveys (Lindquist et al. 2005, 2008). After cracks are marked on the bridge, another surveyor draws the marked cracks on the scaled bridge plan.

To determine crack density, the bridge plans with the marked cracks are scanned into a computer and converted to digital drawing files. Any lines on the bridge plan not representing cracks (such as bridge abutments or barriers) are erased in post-processing. The total length of the cracks can then be measured using drawing software. Crack density is calculated by dividing the total length of the cracks by the area of the bridge deck. Crack densities

are reported in m/m^2 for the whole bridge, each placement, and each span ($1 m/m^2 = 0.305 ft/ft^2$). For most bridge decks, the majority of cracks present are transverse, although longitudinal cracks form, especially adjacent to abutments (Schmitt and Darwin 1995; Krauss and Rogalla 1996). As will be shown later in this paper, the cracks in the Indiana decks tended to be longitudinal. For the two Utah decks discussed in this paper, crack surveys were conducted by BYU researchers using a similar procedure for identifying, measuring, and recording crack lengths and widths (Guthrie et al. 2014).

BRIDGES

The Indiana bridges are located in two Indiana Department of Transportation (INDOT) districts, Seymour and Vincennes. The four IN-IC-HPC decks are supported by steel girders and have steel stay-in-place forms; the other two are supported by prestressed box beams. Two Utah IC deck toppings, surveyed by Brigham Young University researchers (included as an additional reference for comparison) are supported by precast half-deck concrete panels supported by precast prestressed concrete girders. Information on the decks is summarized in Table 1. In this report, the IC and control decks in Indiana are designated IN-IC and IN-Control, respectively, and the internally cured high-performance concrete decks are designated IN-IC-HPC-1 through IN-IC-HPC-4. The internally cured Utah deck toppings are designated UT-IC-1 and UT-IC-2.

Table 1—Bridge properties

Bridge ID	District	Type of Support	Spans	Skew (deg.)	Length		Width	
					(ft)	(m)	(ft)	(m)
IN-IC	Seymour	Prestressed box beam	1	10.6	40.3	12.3	29	8.8
IN-Control	Seymour	Prestressed box beam	1	0	50	15.2	29	8.8
IN-IC-HPC-1	Vincennes	Steel beam	3	0	224	68.3	34.5	10.5
IN-IC-HPC-2	Seymour	Steel beam	1	0	55	16.8	43.5	13.3
IN-IC-HPC-3	Seymour	Steel beam	4	34.8	256	78.0	33	10.1
IN-IC-HPC-4	Vincennes	Steel beam	2	6.7	230	70.1	43.8	13.4
UT-IC-1	-	Prestressed girder	1	34	127.5	38.9	50.8	15.5
UT-IC-2	-	Prestressed girder	1	4	119.8	36.5	50.8	15.5

IN-IC

IN-IC is a single-span bridge located in the INDOT Seymour district near the city of Bloomington and spans over Stephens Creek on North Gettys Creek Rd. The deck was placed in September 2010 in a single placement. It is supported by prestressed concrete box beams. IN-IC is 29 ft (8.4 m) wide, and the deck varies in depth from 4½ in. (114 mm) at edge gutters to 8 in. (205 mm) at the roadway centerline. A single layer of reinforcing steel was placed at the mid-depth of the decks. The IN-IC bridge deck spans approximately 40.3 ft (12.3 m). The concrete contained 657 lb/yd³ (390 kg/m³) of Type I/II portland cement, compared to a maximum of 540 lb/yd³ (320 kg/m³) used for LC-HPC bridge decks. IN-IC contained pre-wetted fine LWA for providing IC water. The w/cm ratio was 0.39, well below the range of 0.43 to 0.45 used for LC-HPC bridge decks. The paste content was 27.6%, by volume, which is higher than the 22.8 to 24.6% used in LC-HPC bridge decks and threshold of 27% based on the work by Schmitt and Darwin (1995, 1999). Without internal curing, these parameters typically lead to concrete with high crack densities. The lightweight aggregate used in this bridge provided an average IC water content of 7.2% by weight of cement. The average 28-day strength of the lab-cured cylinders was 4900 psi (33.8 MPa), which is within the suggested range of 3500 to 5500 psi (24.1-37.9 MPa) for LC-HPC. The strength, however, was low considering the w/cm ratio of 0.39.

Fresh concrete properties including slump, temperature, and air content are not available for this deck.

IN-Control

IN-Control is a single-span bridge located in close proximity to IN-IC and also spans over Stephens Creek on North Gettys Creek Rd. It serves as the control deck for IN-IC and did not utilize internal curing. Like IN-IC, IN-Control is supported by prestressed concrete box girders. The deck was, like IN-IC, constructed in September 2010 in a single placement. Deck geometry and reinforcement layout are similar to IN-IC. IN-Control spans approximately 50 ft (15.2 m). This bridge deck used the same type and amount of cement and w/cm ratio as the IN-IC deck. The average 28-day strength of the cylinders was 4380 psi (30.2 MPa), which is again low, considering the low w/cm ratio. Fresh concrete properties including slump, temperature, and air content are not available for this deck.

IN-IC-HPC-1

IN-IC-HPC-1 is located north of West Baden Springs on US 150 crossing the Lost River. It is a three-span bridge with a length and width of 224 ft (68.3 m) and 34.5 ft (10.5 m), respectively. The deck is supported by steel girders and was constructed in two placements, in July and October 2013. The deck has a depth of 8 in. (205 mm), with 2.5 in. (64 mm) of top cover over reinforcing bars. The concrete contained 568 and 567 lb/yd³ (324 kg/m³) of cementitious material for placements 1 and 2, respectively, 18% of which was slag cement and 4% of which was silica fume (by weight). For IC, the concrete also contained pre-wetted fine LWA, accounting for approximately 15% of total aggregate volume. The actual absorption of the LWA, determined prior to casting, was 18.7% for both placements (versus 14.9% used in design). This resulted in average IC water contents of 9.1 and 8.5% by weight of binder for placements 1 and 2, respectively. The w/cm ratios for placements 1 and 2 were 0.401 and 0.426, respectively, which are below the range for LC-HPC decks. The paste contents for placements 1 and 2 were 24.6 and 25.2% of total volume, respectively. The paste content for placement 2 was slightly outside of the range used in LC-HPC decks (22.8-24.6%). The average slumps for placements 1 and 2 were 4¾ in. (120 mm) and 5¾ in. (145 mm) as measured at the point of placement, respectively, which exceed the maximum slump of 3½ in. (90 mm) for LC-HPC decks. The average air contents for placements 1 and 2 were 5.1 and 5.5%, respectively, which are below the range (8.0 ± 1.5%) in the LC-HPC specifications. The average 28-day strengths for placements 1 and 2 were 7680 and 6640 psi (53.0 and 45.8 MPa), respectively, which exceed the upper limit for compressive strength under LC-HPC specifications.

IN-IC-HPC-2

IN-IC-HPC-2 is located in the town of Austin on US 31 over Hutto Creek. It is a single-span bridge with a length and width of 55 ft (16.8 m) and 43.5 ft (13.3 m), respectively, and is supported by steel girders. The deck was placed in October 2013. The deck is 8 in. (205 mm) thick. The concrete contained 575 lb/yd³ (340 kg/m³) of cementitious material, 25% of which was Class C fly ash, and 4% of which was silica fume. For internal curing, the concrete also contained pre-wetted fine LWA, accounting for 15% of total aggregate volume. The actual absorption of LWA determined prior to casting for this deck was 20% (versus a design absorption of 13.75%). This resulted in an average IC water content of 9.2% by weight of binder. The w/cm ratio for this deck was 0.418, which is lower than the 0.43 to 0.45 range used in LC-HPC specifications. The paste content was 25.3% which is slightly outside of the range used in LC-HPC decks (22.8-24.6%). The average slump was 5 in. (125 mm), and the average air content was 6.4%. The average 28-day strength was 6720 psi (46.3 MPa). The concrete slump, air content, and compressive strength were outside of the ranges specified by LC-HPC specifications.

IN-IC-HPC-3

IN-IC-HPC-3 is located on SR 46 over interstate highway I-74 in the town of West Harrison. This four-span bridge has a length and width of 256 ft (78 m) and 33 ft (10.1 m), respectively, and is supported by steel girders. The deck was constructed in a single placement in November 2014. The concrete contained 600 lb/yd³ (355 kg/m³) of cementitious material, 24% of which was Class C fly ash and 4% of which was silica fume. The concrete also contained 21% pre-wetted fine LWA of total aggregate volume to provide an IC water content of 11.6% by weight of binder. The average w/cm ratio was 0.417 for this deck, outside the range suggested in the LC-HPC specifications (0.43 to 0.45). The paste content was 25.9%, which is outside of the range used in LC-HPC decks (22.8 to 24.6%). The average slump was 5½ in. (140 mm), and the average air content was 7.0%. The average 28-day strength was 5500 psi (37.9 MPa). Air content and strength met the LC-HPC requirements, but slump was higher than the limit specified within LC-HPC specifications.

IN-IC-HPC-4

IN-IC-HPC-4 is located on SR 61 crossing over I-64. The two-span bridge has a length and width of 230 ft

(70.1 m) and 43.8 ft (13.4 m), respectively and is supported by steel girders. The deck was constructed in two placements, in July and October of 2015. The concrete contained 582 and 585 lb/yd³ (345 and 347 kg/m³) of cementitious material for placements 1 and 2, respectively, 20% of which was slag and 4% of which was silica fume (by weight). The concrete also contained 21% pre-wetted fine LWA of total aggregate by volume for internal curing. The actual absorption of the LWA determined prior to casting was 20.1% (versus a design absorption of 13%). This resulted in average IC water contents of 12.0 and 11.2% by weight of binder for placements 1 and 2, respectively. The average *w/cm* ratios for placements 1 and 2 were 0.414 and 0.420, respectively, lower than those used in the LC-HPC decks. The actual paste contents for placements 1 and 2 were 25.7% and 26%, respectively, slightly outside of the range used in LC-HPC decks (22.8-24.6%). The average slumps for placements 1 and 2 were 4¾ in. (120 mm) and 5¼ in. (130 mm), respectively. The average air content was 6.2% for the first placement and 5.5% for the second placement. Strength data were not provided for separate placements. The average 28-day compressive strength was given as 6120 psi (42.2 MPa). Slump, air content, and strength are outside the ranges given in the LC-HPC specifications.

UT-IC-1 and UT-IC-2

UT-IC-1 and 2 are located in the city of West Jordan. UT-IC-1 is along Dannon Way Road, and UT-IC-2 is on 8200 South Road. Both are single span bridges supported by prestressed concrete girders and were placed in the spring of 2012. The length and width of UT-IC-1 are 127.5 ft (38.9 m) and 50.8 ft (15.5 m), respectively. The length and width of UT-IC-2 are 119.8 ft (36.5 m) and 50.8 ft (15.5 m), respectively. Precast half-deck concrete panels support the IC deck topping for both bridges. The deck topping was specified to have 2½ in. (75 mm) of cover over top reinforcing bars and varies in thickness. The IC deck toppings had identical mix designs and contained 605 lb/yd³ (347 kg/m³) of cementitious material, 21% of which was Class F fly ash. The concrete also contained 16% pre-wetted fine LWA of total aggregate volume to provide an IC water content of 7% by weight of binder. The *w/cm* ratio was 0.44, which is within the range suggested in LC-HPC specifications. The paste content was 28%, above of the range used in LC-HPC decks (22.8-24.6%).

The average slumps for UT-IC-1 and UT-IC-2 were 3½ in. (90 mm) and 3¼ in. (85 mm), respectively. The average air contents for UT-IC-1 and UT-IC-2 were 6.4% and 6%, respectively. The average 28-day strengths of the concrete for UT-IC-1 and UT-IC-2 were 5710 psi (39.4 MPa) and 5370 psi (37.0 MPa), respectively. Air content for both decks and strength for UT-IC-1 did not meet LC-HPC specifications.

Concrete Properties and Construction Procedures

The mixture proportions used for the bridge decks are shown in Table 2. Plastic concrete properties along with 28-day compressive strengths are listed in Table 3. Two concrete mix designs were used for internally cured bridge decks in Indiana, IN-IC and IN-IC-HPC. The IN-IC concrete contained 657 lb/yd³ (390 kg/m³) of portland cement, the only binder, and a *w/cm* ratio of 0.39, which resulted in a paste volume of 27.6%, exceeding the paste content range in Kansas LC-HPC specifications. For IC concrete mixtures, current literature typically reports the amount of IC water in lb per 100 lb (kg per 100 kg) of cementitious material. For this paper, the amount of IC water is reported as a percentage by weight of cementitious material. IC water for the IN-IC deck was provided through replacement of 24% of total aggregate (by volume) with pre-wetted fine LWA that provided 7.2% of IC water by weight of cement in the mixture (Di Bella et al. 2012). Determination of absorption in laboratory was based on soaking the material for 24 hours before placing it in a pre-wetted surface dry (PSD) condition. For fine LWA, absorption tends to increase with longer soak times, so properties are described in terms of the PSD condition rather than the SSD condition since the material is not fully saturated. A commercially available fine LWA with a 24-hour absorption of 10.4% and a PSD specific gravity of 1.56 was used. All LWA referenced in this paper is expanded shale. The mixture proportions conformed to INDOT specifications and determination of LWA properties followed procedures outlined by the New York State DOT (NYSDOT) for construction of a series of internally cured bridge decks (Wolfe 2012). A modified paper towel test method (NY 703-19E Test Method) that includes instructions for determining LWA properties in the field as well as in the lab was used in lieu of ASTM C128.

IN-IC-HPC mixtures that were used for construction of the remaining four internally cured bridge decks in Indiana were designed to improve cracking and ionic transport properties of concrete (Barrett et al. 2015). First, to reduce ion transport and have a denser microstructure, a ternary binder system with cement, silica fume (3 to 7% by mass), and slag cement (15 to 20% by mass) or Class C fly ash (20 to 25% by mass), was used to produce a refined pore system and greater calcium hydroxide consumption. For all the IN-IC-HPC bridges in this study, absorption of the pre-wetted LWA obtained before batching exceeded the values determined in laboratory testing. IN-IC-HPC

mixtures, as batched, had between 8.8 and 12% of IC water by weight of binder. The fine LWA used for the IN-IC-HPC decks had a 24-hour absorption capacity (based on dry weight) and PSD specific gravity of approximately 13% and 1.70, respectively. Second, the IN-IC-HPC specifications placed a 25% ($\pm 1.0\%$) limit on the paste content of the mixtures to improve the shrinkage and cracking performance of the concrete. The actual paste contents of the four IN-IC-HPC decks ranged from 24.6% to 26.0% by volume. As explained by Barret et al. (2015), this limitation was applied based on the recommendations by Schmitt and Darwin (1995) as a result of their study of 33 bridge deck placements in Kansas that showed a clear relationship between paste content and bridge deck cracking. Schmitt and Darwin (1995) concluded that when volume of the paste exceeded 27%, cracking significantly increases. A 7-day wet burlap curing regime was used for all Indiana bridges. INDOT removed the requirement for bridge decks to be covered by a commercial sealant for the internally cured decks.

Table 2—Mixture proportions (SSD/PSD basis)

Bridge ID	Date Placed	Cementitious Material Percentages ^b	Coarse Aggregate	Fine Aggregate	Fine LWA (PSD)
			lb/yd ³ (kg/m ³)	lb/yd ³ (kg/m ³)	lb/yd ³ (kg/m ³)
IN-IC	9/24/2010	100% C	1764 (1046)	528 (313)	455 (270)
IN-Control	9/23/2010	100% C	1764 (1046)	1224 (726)	-
IN-IC-HPC-1 ^a	7/19/2013	78% C, 18% S, 4% SF	1805 (1071)	795 (472)	375 (222)
	10/18/2013		1800 (1068)	801 (475)	348 (206)
IN-IC-HPC-2	10/1/2013	71% C, 25% C-FA, 4% SF	1726 (1024)	819 (486)	334 (198)
IN-IC-HPC-3	11/1/2014	72% C, 24% C-FA, 4% SF	1758 (1043)	644 (382)	446 (265)
IN-IC-HPC-4 ^a	7/14/2015	76% C, 20% S, 4% SF	1763 (1046)	665 (395)	447 (265)
	10/3/2015		1768 (1049)	663 (393)	448 (266)
UT-IC-1	Spring 2012	79% C, 21% F-FA	1721 (1021)	706 (419)	324 (192)
UT-IC-2	Spring 2012	79% C, 21% F-FA	1721 (1021)	706 (419)	324 (192)

^a – First row is for placement 1 and the second row is for placement 2.

^b – C = portland cement; S = slag cement; SF = silica fume; C-FA = Class C fly ash; F-FA = Class F fly ash

Table 2—Mixture proportions (continued)

Bridge ID	Cementitious Material Content	Water Content	Design IC Water	Actual IC Water	<i>w/cm</i> Ratio	Paste Content
	lb/yd ³ (kg/m ³)	lb/yd ³ (kg/m ³)	Percent of Binder by Weight	Percent of Binder by Weight		Percent
IN-IC	657 (390)	256 (152)	7	7.2	0.39	27.6
IN-Control	657 (390)	256 (152)	-	-	0.39	27.6
IN-IC-HPC-1*	568 (337)	228 (135)	8	9.1	0.401	24.6
	567 (336)	238 (141)	8	8.5	0.426	25.2
IN-IC-HPC-2	567 (336)	237 (141)	8	9.2	0.418	25.3
IN-IC-HPC-3	600 (356)	250 (148)	8	11.6	0.417	25.9
IN-IC-HPC-4*	582 (345)	241 (143)	8	12	0.414	25.7
	585 (348)	246 (146)	8	11.2	0.42	26
UT-IC-1	605 (359)	266 (158)	7	7	0.44	28
UT-IC-2	605 (359)	266 (158)	7	7	0.44	28

* = First row is for placement 1 and the second row is for placement 2.

Table 3—Average plastic properties and compressive strengths

Bridge ID	Slump	Air Content	28-day Strength
	in. (mm)	(%)	psi (MPa)
IN-IC	-	-	4900 (33.8)
IN-Control	-	-	4380 (30.2)
IN- IC-HPC-1*	4¾ (120)	5.1	7680 (53.0)
	5¾ (145)	5.5	6640 (45.8)
IN-IC-HPC-2	5 (125)	6.4	6720 (46.3)
IN-IC-HPC-3	5½ (140)	7.0	5500 (37.9)
IN-IC-HPC-4*	4¾ (120)	6.2	6120 (42.2) ^a
	5¾ (135)	5.5	
UT-IC-1	3½ (90)	6.4	5710 (39.4)
UT-IC-2	3¼ (85)	6.0	5370 (37.0)

* = First row is for placement 1 and the second row is for placement 2

^a = Data on separate placements not available

For the IC bridge decks in Indiana, the *w/cm* ratio was permitted to be between 0.39 and 0.42 to achieve high compressive strength and maintain durability, notably lower than the *w/cm* ratios used in the LC-HPC bridge decks in Kansas (0.44 to 0.45). IC water for these bridges was used to eliminate chemical shrinkage, defined as the change in volume due to the chemical reaction between cement and water (Barret et al. 2015), and autogenous shrinkage, defined as the change in volume due to self-desiccation, particularly in mixtures with low *w/cm* ratios (Di Bella et al. 2012, Barret et al. 2015). For mixtures without SCMs, the amount of IC water was specified to be 7% of the cement weight, based on work by Bentz and Weiss (2011), which indicated that chemical and autogenous shrinkage of portland cement can be mitigated by providing 7% internal curing water by weight of cement. For the IN-IC-HPC mixtures, which had a ternary binder system, the amount of IC water was specified to be 8% of the binder weight. The shrinkage behavior and rate of hydration for SCMs requires a higher amount of internal curing water to counteract the effects of

chemical and autogenous shrinkage (Bentz and Weiss 2011). For the Indiana bridges, the 24-hour absorption (based on dry weight) and the PSD specific gravity of pre-wetted fine LWA, determined before construction, were used to design and batch the internally cured concrete mixtures. At the batching plant, the LWA stockpile was sprinkled for at least 48 hours and drained for 12 hours prior to batching. Prior to batching, the absorption, surface moisture, and specific gravity of the LWA were determined using the centrifuge method developed by Miller et al. (2014). Surface moisture and specific gravity values obtained before batching were used to adjust the mixture proportions to achieve a proper yield and w/cm ratio. The amount of fine LWA and subsequent amount of IC water in the mixtures, however, were adjusted only if the absorption was lower than that of the 24-hour absorption obtained in laboratory testing (Barrett et al. 2015). The four IN-IC-HPC decks had a total of six placements. The placements were 10.5 to 37.2 months old when the first crack surveys were performed. The IN-IC deck concrete was placed using buckets, but the IN-Control concrete was pumped. Concrete in the four IN-IC-HPC decks was also pumped. All Indiana decks were tined shortly after concrete placement.

The internally cured deck toppings in Utah were placed on precast half-deck concrete panels supported by five precast prestressed single span concrete girders. The topping concrete had a w/cm of 0.44 and a paste content of 28% by volume. This paste content exceeds Kansas LC-HPC concrete. The deck topping concrete incorporated Class F fly ash (21% by mass) as a partial replacement for portland cement; 16.7% of the total aggregate (by volume) was replaced with pre-wetted fine LWA with an absorption capacity of 15% and PSD specific gravity of 1.56 to provide IC water equal to 7% of the weight of binder (Guthrie et al. 2014). The 24-hour absorption of the pre-wetted fine LWA was used to proportion the aggregates. The LWA stockpile was sprinkled for a minimum of two days prior to mixing. The absorption was measured periodically, and when an absorption of 15% was achieved, the stockpile was drained. A curing compound was sprayed on the deck after finishing, followed by a 14-day period of curing under plastic. The two Utah IC deck toppings were constructed by the same contractor and utilized conventional wooden formwork. The deck surfaces were tined shortly after placement.

RESULTS

The crack surveys for the Indiana decks were completed between August 8 and 11, 2016. Placement ages range between 10.5 and 71.6 months. Additional surveys are planned for summer 2018. The two-year survey results presented for the Utah decks were completed in by 2012 Brigham Young University researchers (Guthrie et al. 2014). Crack densities for the Indiana and Utah decks ranged from 0 to 0.784 m/m^2 and are listed in Table 4. Based on previous work at KU, surveys should be conducted one and three years after placement and the survey at three years has proven to be a good predictor of long-term performance (Shrestha et al. 2013 and Pendergrass and Darwin 2014). Thus, ideally, the surveys conducted on the IC-HPC and Utah decks should be repeated but do serve as a baseline for future surveys and lend to the conclusions presented in this report.

Table 4—Summary of LWA information and crack densities

Bridge ID	LWA Used	IC Water (percent of binder)	Age at Survey (months)	Crack Density (m/m^2)
IN-IC	Expanded Shale	7.2	71.6	0.347
IN-Control	-	-	71.6	0.507
IN-IC-HPC-1*	Expanded Shale	9.1	34.7	0
		8.5	37.2	0.020
IN-IC-HPC-2	Expanded Shale	9.2	34.8	0.003
IN-IC-HPC-3	Expanded Shale	11.6	21.6	0.016
IN-IC-HPC-4*	Expanded Shale	12	10.5	0.021
		11.2	15.6	0.005
UT-IC-1	Expanded Shale	7	24	0.784
UT-IC-2	Expanded Shale	7	24	0.427

* = First row is for placement 1 and the second row is for placement 2.

IN-IC and Control

IN-IC was surveyed at an age of 71.6 months with a resultant crack density of 0.347 m^2 . Figure 1(a) shows the crack survey results for IN-IC. The majority of the cracks in this deck are oriented in the longitudinal direction, with the longest cracks appearing to occur at the prestressed box girder boundaries. The average crack width for this bridge was 0.006 in. (0.15 mm).

IN-Control was surveyed at an age of 71.6 months. The crack survey results are shown in Fig. 1(b). The crack density was 0.507 m^2 . Like IN-IC, most of the cracks are oriented in the longitudinal direction, with the longest cracks occurring at or near the prestressed box girder boundaries. There are more transverse cracks in IN-Control than IN-IC. The average crack width in this bridge was 0.010 in. (0.25 mm). In some cases, the box girders experienced differential settlement with respect to each other of as much as $3/8$ in. (10 mm). This uneven settlement of adjacent girders may have contributed to the high number of longitudinal cracks on the deck.

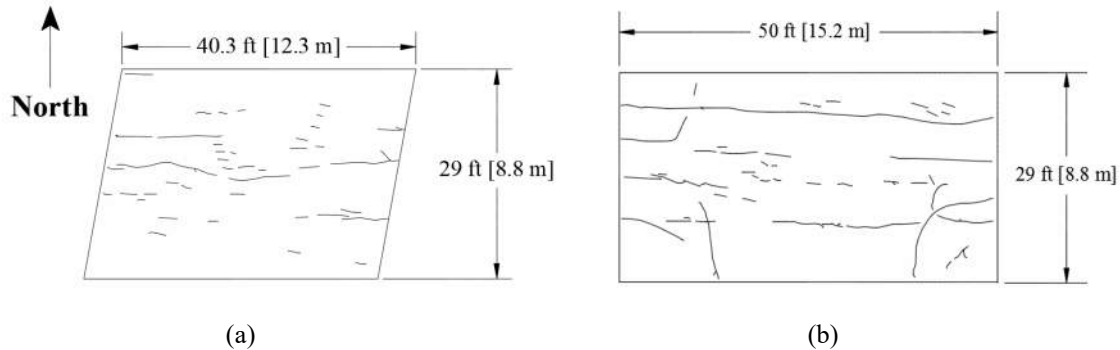


Fig. 1—Crack survey results for: (a) IN-IC and (b) IN-Control

IN-IC-HPC

The two placements of IN-IC-HPC-1 were surveyed at ages of 34.7 and 37.2 months and have crack densities of 0 and 0.02 m^2 , respectively. Both placements showed noticeable coarse aggregate pop-outs throughout the deck, more so on placement 2 than placement 1. Placement 2 showed a few short longitudinal cracks on an end span, close to the abutment, and a few longer transverse cracks over the pier between the other two spans. The average crack width was 0.006 in. (0.15 mm). The deck surface showed moderate scaling damage near the north end. Minor freeze-thaw damage was observed on both placements. Figure 2, although showing IN-IC-HPC-2, is representative of this damage.

IN-IC-HPC-2 was surveyed at an age of 34.8 months. The crack density was 0.003 m^2 . There was only one short longitudinal crack on the deck, with a width of 0.006 in. (0.15 mm). As shown in Fig. 2, there were some coarse aggregate pop-outs and deterioration on the walls of tined surface grooves that may have been caused by a combination of freeze-thaw damage and poor tining.



Fig. 2—Freeze-thaw damage and aggregate pop-outs on IN-IC-HPC-2

IN-IC-HPC-3 was surveyed at 21.6 months. The overall crack density was found to be 0.016 m/m^2 . The highest concentration of cracking on this deck was observed on one of the end spans. Most of the cracks were short, longitudinal, and narrow, located at the two abutments. The average crack width of all cracks recorded was 0.006 in. (0.15 mm). There were no transverse cracks, even over the piers. The surface of the deck did not show any indication of freeze-thaw damage or aggregate pop-outs. With the deck being relatively young, little cracking was expected.

The two placements of IN-IC-HPC-4 were surveyed at ages of 10.5 and 15.6 months, respectively, and have the lowest ages of the decks in this study. The crack densities for placements 1 and 2 were 0.021 and 0.005 m/m^2 , respectively, as shown in Fig. 3. Span 1 of placement 1 had some plastic shrinkage cracking close to the abutment and there were some short longitudinal cracks on span 2 for both placements; the cracks in placement 2 were closer to the abutment. No transverse cracks were observed, even over the piers. The average crack width was 0.006 in. (0.15 mm) for this bridge. The cracks located in span 1 were significantly wider (average width of 0.014 in. [0.36 mm]) than those located in span 2 (average width of 0.004 in. [0.10 mm]). Similar to the defects shown in Fig. 2, freeze-thaw damage and poor surface finishing (poor tining/grooving) were observed on the surface of the deck; more so on placement 1 than placement 2. No aggregate pop-outs were observed.

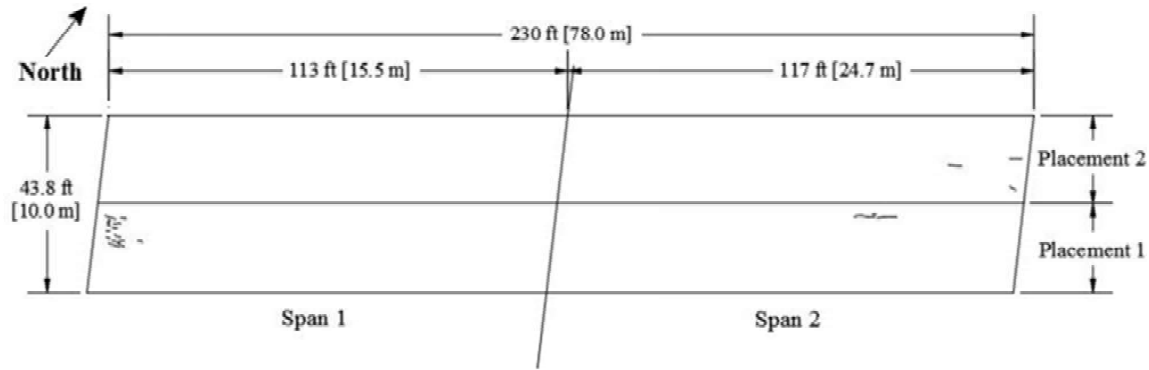


Fig. 3—IN-IC-HPC-4 crack survey result

UT-IC

UT-IC-1 and UT-IC-2 were surveyed by a Brigham Young University research team at the ages of 2, 5, 8, 12, and 24 months (Guthrie et al. 2014). According to the most recent surveys, the crack densities for UT-IC-1 and UT-IC-2 were found to be 0.784 and 0.427 m/m^2 , respectively at 24 months. For UT-IC-1, longitudinal, transverse, and map cracks were spread along the driving lanes of the deck with less cracking observed along the shoulders. Short longitudinal cracks formed adjacent to the left abutment across the entire width of the deck. For UT-IC-2, most of the cracks were transverse, with longitudinal cracks adjacent to the abutments. UT-IC-2 had less map cracking compared to UT-IC-1. The majority of transverse and longitudinal cracks were at the pre-cast half deck panel joints in both decks. For both decks, the crack width ranged from 0.008 to 0.050 in. (0.20 to 1.27 mm); the majority of cracks had widths ranging from 0.01 to 0.02 in. (0.25 to 0.51 mm).

Internal Curing with Pre-Wetted Fine LWA

To study the effectiveness of internal curing in reducing cracking in bridge decks, the crack densities of the five Indiana IC bridge decks and two Utah IC deck toppings are compared with Kansas control and LC-HPC decks and the control deck in Indiana. Information on the seven IC decks is summarized in Table 4. Data is plotted for individual placements when more than one placement was used, which is the case for IN-IC-HPC-1 and IN-IC-HPC-4. As shown in Fig. 4, the IN-IC-HPC decks exhibited significantly less cracking than the IN-IC and UT-IC deck toppings. Because these bridges have different ages, different mixture types, varying amounts of IC water, and different superstructure (steel girders, prestressed box beams, and prestressed girders) and deck (monolithic or topping over precast panels) types, it is difficult to make a fair comparison and explain why there are differences, significant in some cases, in crack densities between these decks. However, it appears that having a low paste content is a dominant factor in reducing the occurrence of cracking. The reduction in shrinkage when using SCMs combined with internal curing has been shown previously (De la Varga et al. 2012, Pendergrass and Darwin 2014). A greater amount of IC water and inclusion of a ternary binder system in IN-IC-HPC decks may have also contributed to low crack densities, but these decks were all placed at close to or less than three years at the time of the most recent survey. Although the UT-IC deck toppings are fundamentally different in terms of structure type from the Indiana decks, previous work at KU that included deck toppings with an SCM and low paste content (below 25%) placed on top of precast deck panels exhibited low crack densities (at or below 0.10 m/m^2) through more than 40 months after construction (Shrestha et al. 2013). Additional surveys at later dates are needed to monitor cracking and durability issues and establish a better estimate of long-term behavior.

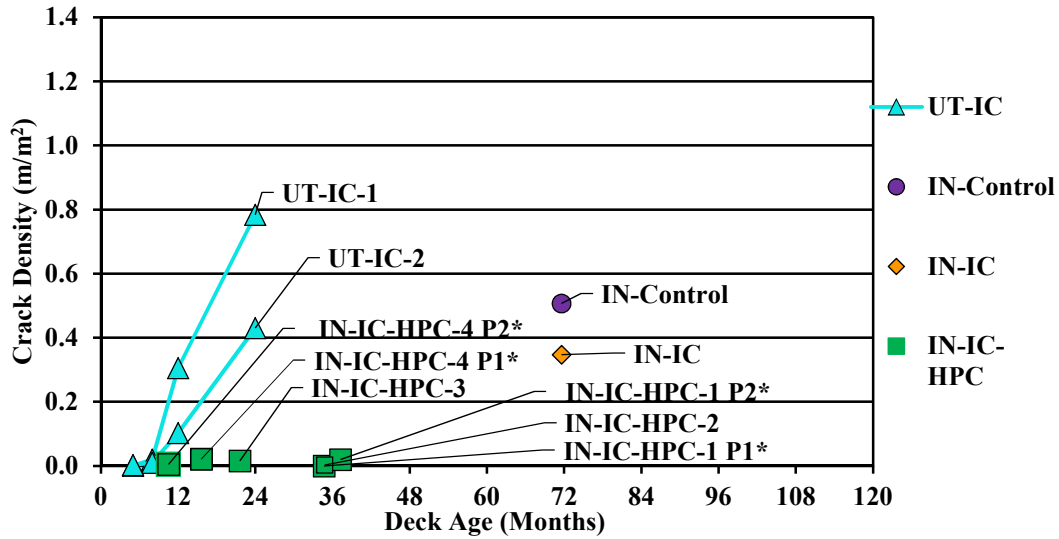


Fig. 4— Crack densities of Indiana and Utah IC bridge decks and Indiana control deck vs. deck age. *P1 and P2 denotes the first and second placement of the bridge, respectively.

Figure 5 compares the crack densities of the IC decks in Indiana and IC deck toppings in Utah with the crack densities of the control decks in Kansas (denoted as KS-Control) as a function of age. As shown in Fig. 5, the six IN-IC-HPC placements (IN-IC-HPC-1 through IN-IC-HPC-4) exhibited lower crack densities than Kansas control decks at similar ages. The IN-IC deck, performing better than the IN-Control deck at the same age, falls within the spread of Kansas control deck data. The internally cured Utah deck toppings (UT-IC-1 and UT-IC-2), despite their relatively young ages, exhibited the highest cracking density among all IC decks in this study. The crack density of UT-IC-1 was higher at 24 months than all but one of the Kansas control decks. The crack density for UT-IC-2 is also greater than most Kansas control decks surveyed at a similar age.

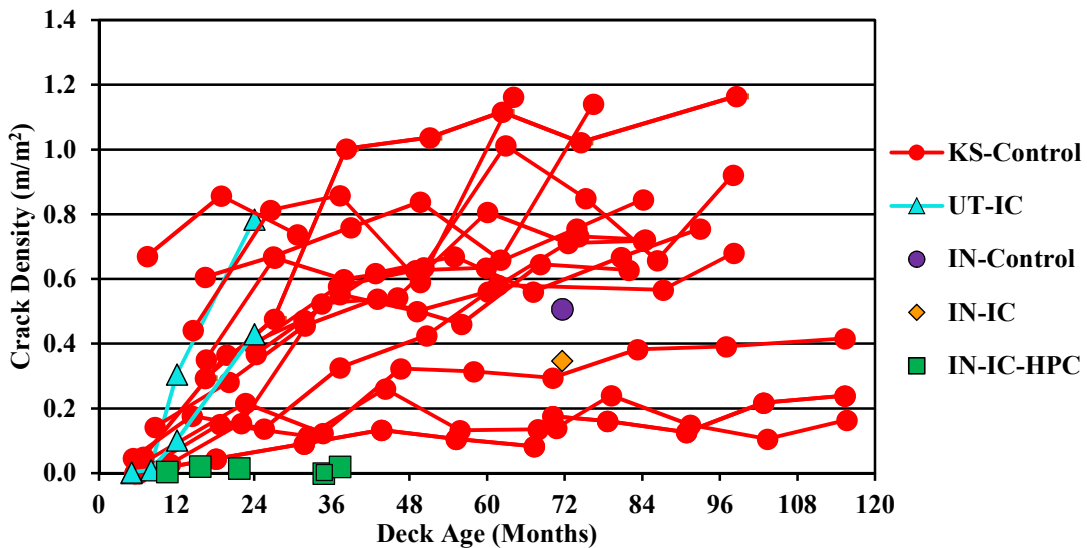


Fig. 5—Crack densities of Kansas control decks and IC decks vs. deck age

Figure 6 compares the crack densities as a function of age for the IC decks in Indiana and IC deck toppings in Utah against LC-HPC decks in Kansas. As shown in the figure, the IN-IC-HPC decks had lower crack densities than most of the LC-HPC decks at similar ages. IN-IC and IN-Control exhibited greater crack densities than most LC-HPC decks; at 24 months, the Utah IC deck toppings had higher crack densities than all LC-HPC decks at similar ages. It appears that internal curing and SCMs contributed greatly to reducing the cracking of IN-IC-HPC bridges.

Internal curing and SCMs or internal curing alone, however, provided no advantage for the Utah IC deck toppings (UT-IC-1 and UT-IC-2) or the Indiana IC deck (IN-IC), which had paste contents above 27% by volume and, thus, greater than both the IN-IC-HPC and LC-HPC decks.

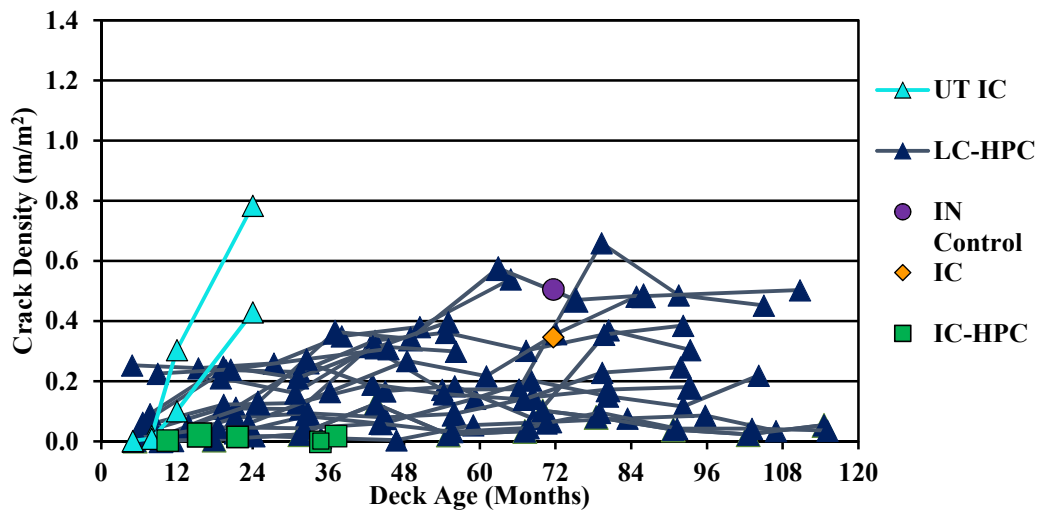


Fig. 6—Crack densities of LC-HPC decks and IC decks vs. deck age

Figure 7 shows the crack density on bridge decks in this study as a function of paste content. Aggregate has a high stiffness, making it dimensionally stable, regardless of moisture loss. Paste in the constituent of concrete that undergoes shrinkage. Studies conducted by University of Kansas dating back to over twenty years ago (Schmitt and Darwin 1995; Miller and Darwin 2000; Lindquist et al. 2008) have shown that increased paste content, independent of other factors, leads to increased cracking in bridge decks. Paste contents less than 27% by volume consistently result in reduced cracking. Figure 7 clearly supports this finding. The Utah deck toppings, with paste contents of 28%, and the IN-Control and IN-IC decks, with paste contents of 27.6%, exhibited significantly greater cracking than the IN-IC-HPC decks, with paste contents lower than 26%. Both Utah deck toppings and the IN-Control and IN-IC decks also had higher crack densities than almost all Kansas LC-HPC decks, and most Kansas control decks at similar survey ages. The internally cured Utah deck toppings had the highest cracking densities in spite of having the required amount of IC water and being supported by prestressed concrete girders, which are also believed to be more helpful in improving cracking performance of the deck than steel girders (*Durability* 1970). These findings demonstrate that a high paste volume can significantly increase bridge deck cracking, even when a crack reduction technology is used.

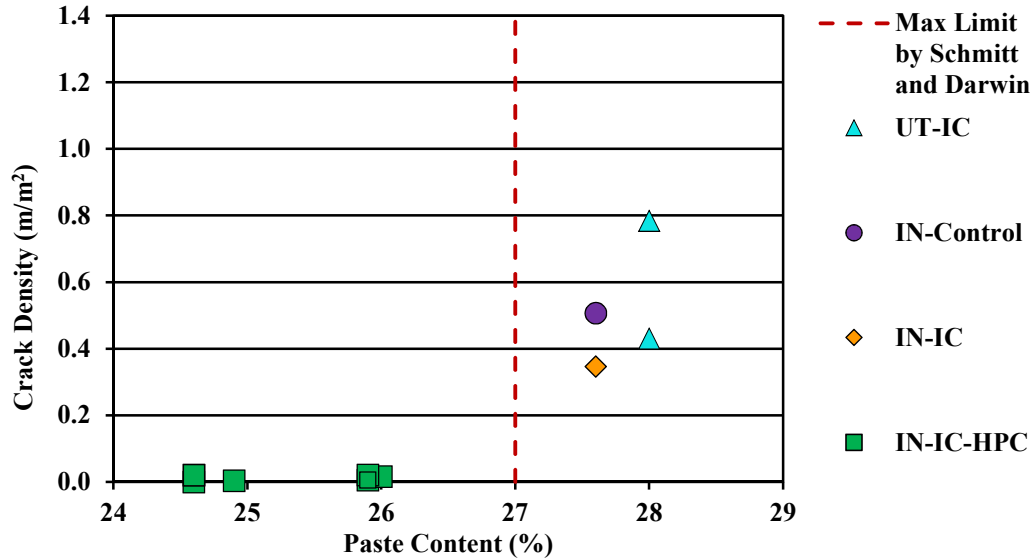


Fig. 7—Crack densities of Indiana and Utah IC bridge decks and Indiana control deck vs. paste content

Figure 8 shows the crack density of bridge decks in this study as a function of 28-day compressive strength. Schmitt and Darwin (1995), Miller and Darwin (2008), and Lindquist et al. (2008), in addition to showing the benefits of decreased paste content, also showed the benefits of having decks constructed with lower-strength concrete. As concrete compressive strength increases, creep decreases. Creep reduces stresses caused by restrained shrinkage and, thus, reduces the potential for cracking. As shown in Fig. 8, the IN-IC and IN-Control decks have 28-day compressive strengths of 4900 and 4380 psi (33.8 and 30.2 MPa), respectively, which are within the recommended range in the LC-HPC specifications, exhibited crack density values of 0.347 and 0.507 m/m², respectively – greater than all IN-IC-HPC decks and also greater than most of LC-HPC decks at a similar age. It appears that the higher paste contents of IN-IC, IN-Control and UT-IC deck toppings were more influential in increasing cracking than their lower compressive strengths in reducing cracking. However, it must be mentioned that two oldest IN-IC-HPC decks (37.2 month old IN-IC-HPC-1 and 34.8 month old IN-IC-HPC-2) exhibited the lowest crack densities among all IC decks and better than almost all LC-HPC decks despite having the highest 28-day compressive strength (6640 and 6720 psi [45.8 and 46.3 MPa], respectively) among the decks investigated in this study. Recent studies have suggested that the use of internal curing and one SCM, fly ash, reduce the modulus of elasticity and increase creep (De la Varga et al. 2012). Menkulasi et al. (2010) showed that IC mixtures exhibited lower shrinkage and higher creep coefficients than mixtures that did not contain any lightweight aggregate.

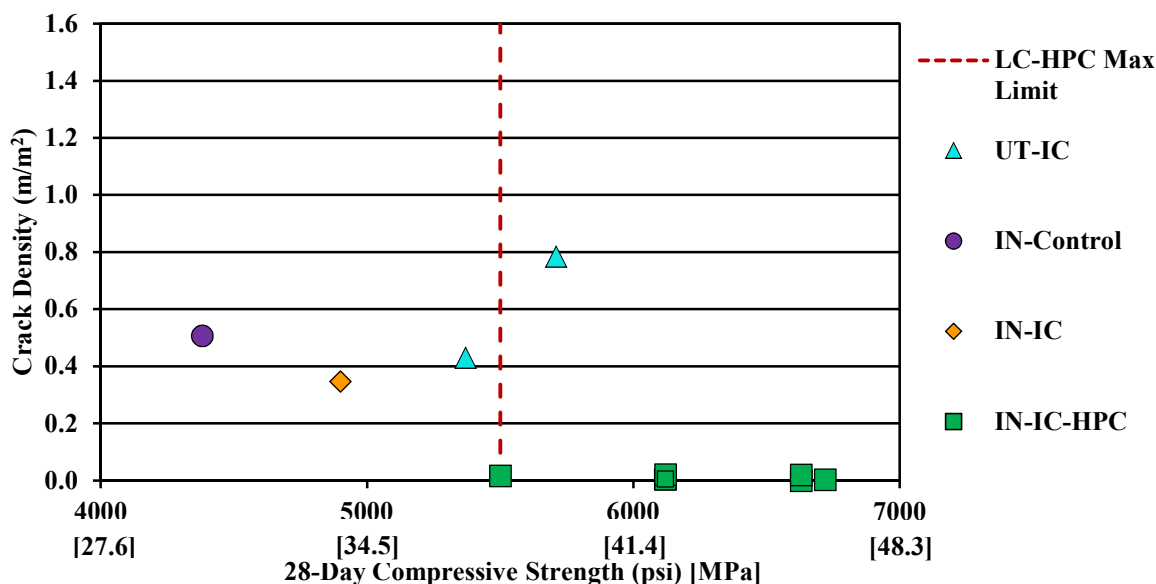


Fig. 8—Crack density vs. 28-day compressive strength of concrete for Indiana and Utah IC and Indiana control bridge decks

Figure 9 compares the crack density for Utah and Indiana IC bridge decks with the actual amount of IC water. The amount of IC water is also listed in Tables 2 and 4. The results indicate that decks that had more than 8% IC water by weight of binder exhibited lower cracking. Pendergrass and Darwin (2014) showed that mixtures containing pre-wetted LWA, slag, and silica fume exhibit a reduction in both early-age (0 to 90 days) and long-term (90 to 360 days) drying shrinkage. They concluded that drying shrinkage was reduced as slag was added in conjunction with lightweight aggregate. An additional reduction in shrinkage was observed as silica fume was added in conjunction with the lightweight aggregate and slag. A possible explanation for the lower crack densities in the IN-IC-HPC decks is that in addition to including SCMs, providing more IC water than required for eliminating chemical and autogenous shrinkage can also help reduce drying shrinkage.

The effectiveness of internal curing in reducing drying and autogenous shrinkage of concrete has been shown by many researchers (for example Henkensiefken et al. 2009; Browning et al. 2011). When used in bridge decks, pre-wetted LWA can potentially reduce cracking caused by restrained shrinkage. One area of concern for internally cured bridge decks is with freeze-thaw durability. For concrete with excess IC water, trapped water can remain in the pores of the LWA (Jones et al. 2014). Depending on the degree of saturation, on freezing, this water can cause local failures, such as scaling damage and pop-outs, or general freeze-thaw damage (Powers 1975). For concrete placed later in the construction season and prone to freezing prior to the system drying out, excess IC water would tend to compromise durability. The freeze-thaw performance of IC concrete has also been shown to depend on the type and proportions of the fine LWA used (Jones et al. 2014). Scaling resistance of concrete, including internally cured mixtures, depends heavily on finishing procedures. For the noted freeze-thaw and scaling damage on the affected IN-IC-HPC decks, it is possible that specifying a longer curing time would have helped mitigate these issues. Providing additional curing time for concrete mixtures with SCMs has also been shown to be beneficial in increasing strength and reducing shrinkage (Tazawa et al. 1989). Based on results described by Jones et al. (2014), scaling resistance does not appear to be negatively affected by providing internal curing to concrete mixtures. Future surveys of the IN-IC-HPC decks are needed to evaluate long-term durability of concrete with excess IC water. Ongoing research at KU will examine the effects of varying the amount of IC water on shrinkage and durability for a series of concrete mixtures.

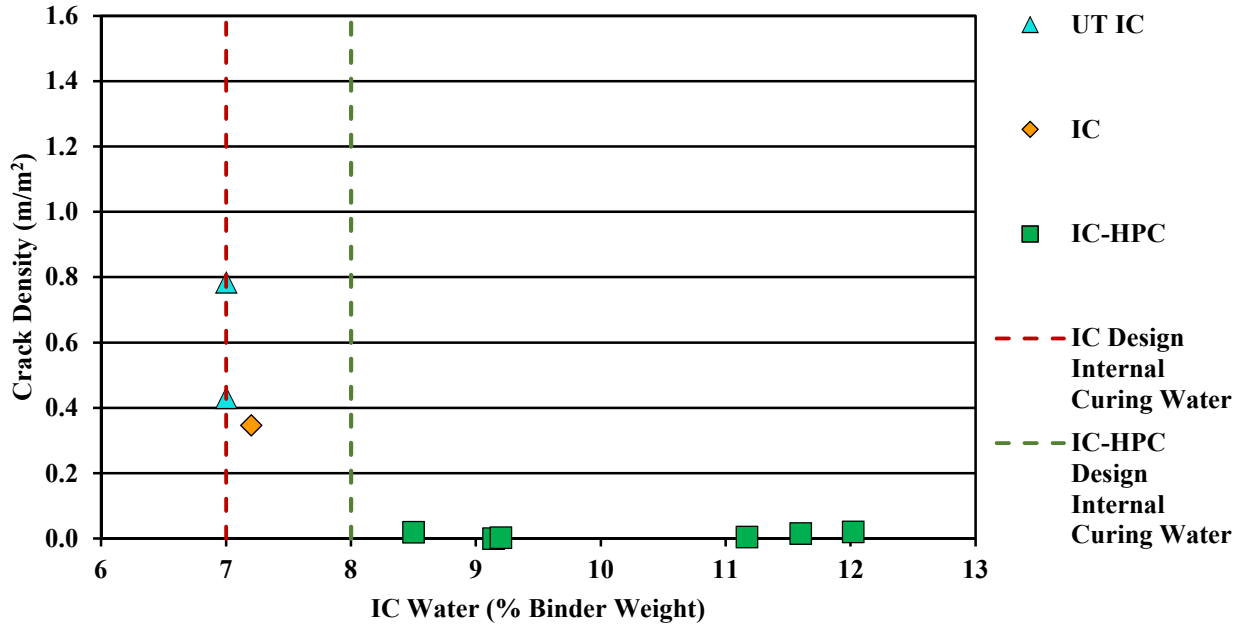


Fig. 9—Crack density vs. actual IC water for Indiana and Utah IC bridge decks

SUMMARY AND CONCLUSIONS

To determine the effect of IC and SCMs on bridge deck cracking, crack surveys were performed on six decks in Indiana; crack surveys by BYU researchers of two Utah bridges with deck toppings (UT-IC) were also used for comparison. Five of the decks in Indiana had internally cured concrete obtained by replacing a portion of aggregate with pre-wetted fine LWA. One deck, IN-Control, was constructed with plain concrete (no LWA) and is used as a control. Four of the decks surveyed in Indiana are supported by steel girders and two are supported by prestressed concrete box beams. The four decks supported by steel girders had a ternary concrete mixture containing SCMs, slag or Class C fly ash, with silica fume and internal curing (IN-IC-HPC). The two decks supported by prestressed box beams contained 100% portland cement mixtures, including IN-Control and one with internally cured concrete (IN-IC). The two internally cured deck toppings in Utah that were surveyed by BYU are both supported by prestressed concrete girders and precast deck panels. The internally cured decks are compared for cracking performance with low-cracking high-performance (LC-HPC) and control bridge decks in Kansas.

These surveys will serve as a baseline for future surveys and provide the data for some conclusions concerning the early performance of the decks. Future surveys will aid in making additional conclusions on the long-term performance of bridge decks that utilize SCMs and/or IC.

The following conclusions can be drawn from the surveys as well as previous studies:

1. The IN-IC-HPC bridge decks are exhibiting less cracking than the IN-IC and IN-Control decks, the UT-IC toppings, and the Kansas LC-HPC and control decks within the first three years after placement.
2. The Kansas LC-HPC decks exhibit less cracking than the IN-IC and IN-Control decks and the UT-IC deck toppings.
3. Paste content appears to be the dominant factor affecting cracking, with the IN-IC-HPC and LC-HPC decks, with paste contents of 26% or less performing significantly better than the IC decks with paste contents greater than 27% by volume. Even when including IC and an SCM in the UT-IC deck toppings, the high paste content led to more cracking than most of the Kansas control decks.
4. Further research is needed to establish the long-term cracking and durability performance of concrete bridge decks that incorporate internal curing or internal curing and SCMs.

ACKNOWLEDGEMENTS

Funding for this research was provided by the ACI Foundation and sponsoring organizations: ABC Polymers,

the ACI Foundation's Strategic Development Council (SDC), Active Minerals International, the American Society of Concrete Contractors, Baker Concrete Construction, BASF Corporation, FORTA Corporation, the Expanded Shale, Clay and Slate Institute, the Euclid Chemical Company, GPC Applied Technologies, the University of Kansas Transportation Research Institute, PNA Construction Technologies, Inc., Premier Construction Products, Sika Corporation, and Structural Group, Inc. Special thanks are due to Jeremy Hunter, Bill Bristol, Greg Carlton, Tony Zander, and Mike Nelson from Indiana Department of Transportation.

REFERENCES

- Alhmoode, A.; Darwin, D.; and O'Reilly, M., 2015, "Crack Surveys of Low-Cracking High-Performance Concrete Bridge Decks in Kansas 2014-2015," *SL Report* 15-3, University of Kansas Center for Research, Lawrence, KS, 118 pp.
- ASTM C128-15, 2015, "Standard Test Method for Density, Relative Density (Specific Gravity), and Absorption of Fine Aggregate," ASTM International, West Conshohocken, PA, 6 pp.
- Barrett, T.; Miller, A.; and Weiss, J., 2015a, "Documentation of the INDOT Experience and Construction of the Bridge Decks Containing Internal Curing in 2013," *SPR 3752*. Joint Transportation Research Program, *Indiana Department of Transportation*, and Purdue University, West Lafayette, IN, 108 pp.
- Barrett, T., Miller, A., and Weiss, J., 2015b, "Documentation of Bridge Deck Construction Using Industrially Produced Internally Cured, High Performance Concrete," 27th Biennial National Conference of the Concrete Institute of Australia in conjunction with the 69th RILEM Week, Melbourne, Australia.
- Bentz, D., and Weiss, J., 2011, *Internal Curing: A 2010 State-of-the-Art Review*. US Department of Commerce, National Institute of Standards and Technology, 94 pp.
- Browning, J.; Darwin, D.; Reynolds, D.; and Pendergrass, B., 2011, "Lightweight Aggregate as Internal Curing Agent to Limit Concrete Shrinkage," *ACI Materials Journal*, V. 108, No. 6, Nov.-Dec., pp. 638-644.
- Darwin, D.; Browning, J.; and Lindquist, W., 2004, "Control of Cracking in Bridge Decks: Observations from the Field," *Cement, Concrete, and Aggregates*, V. 26, No. 2, December, pp. 148-154.
- Darwin, D.; Browning, J.; Lindquist, W.; McLeod, H.; Yuan, J.; Toledo, M.; and Reynolds, D., 2010, "Low-Cracking, High-Performance Concrete Bridge Decks: Case Studies Over First 6 Years," *Transportation Research Record* 2202, Dec. pp. 61-69.
- Darwin, D.; Browning, J.; McLeod, H. A. K.; Lindquist, W.; and Yuan, J., 2012, "Implementing Lessons Learned From Twenty Years of Bridge-Deck Crack Surveys," *Andy Scanlon Symposium on Serviceability and Safety of Concrete Structures: From Research to Practice*, SP-284, American Concrete Institute, Farmington Hills, MI, pp. 1-18.
- Darwin, D.; Khajehdehi, R.; Alhmoode, A.; Feng, M.; Lafikes, J.; Ibrahim, E.; O'Reilly, M., 2016, "Construction of Crack-Free Bridge Decks: Final Report," SM Report No. 121, University of Kansas Center for Research, Lawrence, KS, 160 pp.
- De la Varga, I.; Castro, J.; Bentz, D.; and Weiss, J., 2012, "Application of Internal Curing for Mixtures Containing High Volumes of Fly Ash," *Journal of Cement & Concrete Composites*, V. 34, No. 9, pp. 1001-1008.
- Di Bella, C.; Schlitter, J.; Carboneau, N.; and Weiss, J., 2012, "Documenting the Construction of a Plain Concrete Bridge Deck and an Internally Cured Bridge Deck" Indiana LTAP Center, TR-1-2012.
- Durability of Concrete Bridge Decks-A Cooperative Study, Final Report*, 1970. The state highway departments of California, Illinois, Kansas, Michigan, Minnesota, Missouri, New Jersey, Ohio, Texas, and Virginia; the Bureau of Public Roads; and Portland Cement Association, 35 pp.
- Guthrie, W. S.; Yaede, J. M.; and Bitnoff, A. C., 2014, *Comparison of Conventional and Internally Cured Concrete Bridge Decks in Utah: Mountain View Corridor Project*, Report No. UT-15.02. Utah Department of Transportation, Salt Lake City, UT, Dec. 2014.

- Henkensiefken, R.; Castro J.; Bentz D.; Nantung, T.; and Weiss J., 2009, “Water Absorption in Internally Cured Mortar Made with Water-Filled Lightweight Aggregate,” *Cement and Concrete Research*, V. 29, No. 10, pp. 883-892.
- Jones, W.; House, M.; and Weiss, J., 2014, “Internal Curing of High-Performance Concrete Using Lightweight Aggregates and other Techniques,” *Technical Report* No. CDOT-2014-3, Colorado Department of Transportation Applied Research and Innovation Branch, Feb. 129 pp.
- Kansas Department of Transportation, 2014a, “Low-Cracking High-Performance Concrete - Aggregates,” Standard Specifications for State Road and Bridge Construction, Topeka, KS.
- Kansas Department of Transportation, 2014b, “Low-Cracking High-Performance Concrete,” Standard Specifications for State Road and Bridge Construction, Topeka, KS.
- Kansas Department of Transportation, 2011, “Low-Cracking High-Performance Concrete - Construction,” Standard Specifications for State Road and Bridge Construction, Topeka, KS.
- Krauss, P. D., and Rogalla, E. A., 1996, “Transverse Cracking in Newly Constructed Bridge Decks,” *National Cooperative Highway Research Program Report* 380, Transportation Research Board, Washington, D.C., 126 pp.
- Lindquist, W.; Darwin, D.; and Browning, J., 2005, “Cracking and Chloride Contents in Reinforced Concrete Bridge Decks,” *SM Report* No. 78, University of Kansas Center for Research, Lawrence, KS, Feb., 453 pp.
- Lindquist, W.; Darwin, D.; and Browning, J., 2008, “Development and Construction of Low-Cracking High-Performance Concrete (LC-HPC) Bridge Decks: Free Shrinkage, Mixture Optimization, and Concrete Production” *SM Report* No. 92, University of Kansas Center for Research, Lawrence, KS, Nov., 540 pp.
- Lindquist, W.; Darwin, D.; Browning, J.; McLeod, H. A. K.; Yuan, J.; and Reynolds, D., 2015, “Implementation of Concrete Aggregate Optimization,” *Construction & Building Materials*, V. 74, Jan., pp. 49-56.
- McLeod, H. A. K.; Darwin, D.; and Browning, J., 2009, “Development and Construction of Low-Cracking High-Performance Concrete (LC-HPC) Bridge Decks: Construction Methods, Specifications, and Resistance to Chloride Ion Penetration,” *SM Report* No. 94, University of Kansas Center for Research, Lawrence, KS, Sep., 815 pp.
- Menkulasi, F.; Nelson, D.; Roberts Wollmann, C.; and Cousin, T., 2015, “Reducing Deck Cracking in Composite Bridges by Controlling Long Term Properties,” *Sustainable Performance of Concrete Bridges and Elements Subjected to Aggressive Environments: Monitoring, Evaluation and Rehabilitation at ACI Fall Convention*, ACI SP-304, American Concrete Institute, Farmington Hills, MI, pp. 21-40.
- Miller, A.; Albert, E.; Spragg, R.; Antico, F. C.; Ashraf, W.; Barrett, T.; Behnood, A.; Bu, Y.; Chiu, Y.; Desta, B.; Farnam, Y.; Jeong, H.; Jones, W.; Lucero, C.; Luo, D.; Nickel, C.; Panchmatia, P.; Pin, K.; Qiang, S.; Qiao, C.; Shagerdi, H.; Tokpatayeva, R.; Villani, C.; Wiese, A.; Woodard, S.; and Weiss, J., 2014, “Determining the Moisture Content of Pre-Wetted Lightweight Aggregate: Assessing the Variability of the Paper Towel and Centrifuge Methods,” *4th International Conference on the Durability of Concrete Structures*, Purdue University, West Lafayette, IN, 5 pp.
- Miller, G. and Darwin, D., 2000, “Performance and Constructability of Silica Fume Bridge Deck Overlays,” *SM Report* No. 57, University of Kansas Center for Research, Lawrence, KS, 444 pp.
- Miller, T.; Barrett, A.; Weiss, J., 2015, “Documentation of Bridge Deck Construction Using Industrially Produced Internally Cured, High Performance Concrete” Concrete Institute of Australia Conference, Melbourne, Australia, 10 pp.
- Pendergrass, B. and Darwin, D., 2014, "Low-Cracking High-Performance Concrete (LC-HPC) Bridge Decks: Shrinkage-Reducing Admixtures, Internal Curing, and Cracking Performance," *SM Report* No. 107, The University of Kansas Center for Research, Lawrence, KS, 665 pp.
- Powers, T., 1975, “Freezing Effects in Concrete,” *Durability of Concrete*, SP 47—1, American Concrete Institute, Farmington Hills, MI, pp. 1-12.

Schmitt, T. R. and Darwin, D., 1995, "Cracking in Concrete Bridge Decks," *SM Report No. 39*, University of Kansas Center for Research, Lawrence, KS, 151 pp.

Schmitt, T. R. and Darwin, D., 1999, "Effect of Material Properties on Cracking in Bridge Decks," *Journal of Bridge Engineering*, ASCE, V. 4, No. 1, Feb., pp. 8-13.

Shilstone, J. M., Sr., 1990, "Concrete Mixture Optimization," *Concrete International*, V. 12, No. 6, June, pp. 33-39.

Shrestha, P., Harley, A., Pendergrass, B., Darwin, D., and Browning, J. 2013, "Use of Innovative Concrete Mixes for Improved Constructability and Sustainability of Bridge Decks 2010-2013," *SL Report 13-3*, University of Kansas Center for Research, Lawrence, KS, May, 104 pp.

Streeter, D.; Wolfe, W.; and Vaughn, R., 2012, "Field Performance of Internally Cured Concrete Bridge Decks in New York State," *The Economics, Performance, and Sustainability of Internally Cured Concrete*, SP-290—7. American Concrete Institute, Farmington Hills, MI, pp. 69-84.

Tazawa, E.; Yonekura, A.; and Tanaka, S., 1989, "Drying Shrinkage and Creep of Concrete Containing Granulated Blast Furnace Slag," *Fly Ash, Silica Fume, Slag and Natural Pozzolans in Concrete*, SP-114—64, American Concrete Institute, Farmington Hills, MI, pp. 1325-1343.

Yuan, J.; Darwin D.; and Browning, J., 2011, "Development and Construction of Low-Cracking High-Performance Concrete (LC-HPC) Bridge Decks: Free Shrinkage Tests, Restrained Ring Tests, Construction Experience, and Crack Survey Results," *SM Report No. 103*, University of Kansas Center for Research, Lawrence, KS, June, 505 pp.

AUTHOR BIOS

ACI member **James Lafikes** is a Graduate Research Assistant at the University of Kansas. He received his MS in civil engineering from the University of Kansas, Lawrence, KS.

ACI member **Rouzbeh Khajehdehi** is a Graduate Research Assistant at the University of Kansas. He received his MS in civil engineering from the Southern Illinois University, Edwardsville, IL.

ACI member **Muzai Feng** is a Graduate Research Assistant at the University of Kansas. He received his MS in civil engineering from the University of Kansas, Lawrence, KS.

ACI member **Matthew O'Reilly** is an Assistant Professor at the University of Kansas. He received his Ph.D. in civil engineering from the University of Kansas, Lawrence, KS.

ACI Honorary Member **David Darwin** is the Deane E. Ackers Distinguished Professor and Chair of the Department of Civil, Environmental, and Architectural Engineering at the University of Kansas and a Past President of ACI.

Zeolite Based Concrete- Durable Solution for Nation's Infrastructure

Nidhi M Modha and Pratanu Ghosh

Abstract: In this research, a natural pozzolanic cementitious material known as zeolite is being utilized to investigate the performance of High-Performance Concrete (HPC). Several binary (cement+zeolite) and ternary (cement+zeolite+other supplementary cementitious material) based concrete mixtures including a control mixture of Ordinary Portland Cement (OPC) with water - cementitious (*w/cm*) ratios of 0.40 and 0.44 are cast by replacing cement with different percentage level of zeolite material. The purpose of this study is to investigate effectiveness of zeolite material by means of long term compressive strength (7 to 91 days), tensile strength, modulus of elasticity and corrosion resistance in several concrete mixtures from 7 to 28 days. The compressometer is utilized for the measurement of the modulus of elasticity and Universal Testing Machine (UTM) is utilized to measure the compressive and tensile strength of concrete. In addition, a 4-point Wenner Probe resistivity meter is tested to determine the surface electrical resistivity of concrete, which provides an indirect indication of permeability and in turn, chloride induced corrosion durability in reinforced concrete structures. Overall, zeolite based concrete mixtures with 0.40 *w/cm* ratio and ¾ inch aggregate size provide promising results in terms of compressive strength, tensile strength and remarkable improvement on corrosion resistance in terms of achievement of surface resistivity data.

Keywords: Natural zeolite, High Performance Concrete (HPC), durability, modulus of elasticity, compressive strength, tensile strength, corrosion

ACI member **Nidhi M Modha** was an undergraduate student in the Department of Civil and Environmental Engineering at California State University, Fullerton.

Dr. Pratnu Ghosh is currently an Associate Professor of Civil and Environmental Engineering Department at CSUF. He obtained a Ph.D. degree in Structural Engineering at the University of Utah. His research expertise includes durability and sustainability investigation of concrete structures and service life modeling of reinforced concrete structures using emerging non-destructive testing and advanced numerical methodologies. He also serves as national committee member and research coordinator of AFN 10 and AFN 20 for Transportation Research Board (TRB).

INTRODUCTION

The most widely used material in the construction around the world is concrete, due to its durability and mechanical properties, ability to form into various shapes and sizes, and its low cost. However, depending on the severity of the environmental effects on the concrete structures, the embedded reinforcement in the concrete can be susceptible to corroded and structures can be damaged before reaching its expected service life [1]. Initially, moisture and chloride ions can penetrate the concrete and start attacking the passive layers of the hydrated iron oxide which protects the reinforced concrete against corrosion [2]. Due to the chemical oxidation reaction, the metallic iron starts turning into the rust and the volume of the corrosion byproduct increases. As a result, this increase in the volume exerts tensile stresses into the concrete and can cause cracks and delaminates. If this process is allowed to continue, the load capacity of the structure will eventually be compromised. [1-2].

To overcome this challenge, it has become very important to develop High-Performance Concrete (HPC). HPC generally increases the durability of reinforced concrete against the chloride-induced corrosion and can extend the service life along with better long-term compressive and tensile strength. Hence, a natural cementitious material known as zeolite is being used to enhancing the performance of HPC. Natural zeolite, a crystalline hydrated alumino-silicate processed (volcanic ash) mineral, is a highly effective pozzolan due to natural occurrence of aluminum silicate [3]. Natural zeolite is widely used as a cementitious material since it prevents the expansion of concrete in alkali silica reaction and enhances the performance of HPC [4].

Different binary and ternary based HPC mixtures using supplementary cementitious material such as ground granulated blast furnace slag (GGBFS or slag cement), silica fume, Class F and C fly ash, pumice, and metakaolin with OPC are often made. The main natural pozzolan that being investigated for this study is zeolite. In this study, the use of natural zeolite in HPC as supplementary cementitious material is being investigated for corrosion resistance and strength. Electrical resistivity testing is performed under the durability investigation against the chloride induced corrosion in concrete structures.

Chan et al (1999) conducted a study on replacement of cement with zeolite, Fly ash (FA), and silica fume at levels from 5% to 30% to increase the compressive strength of concrete. As w/cm ratio increased to 0.45 the compressive strength was lower than the control mixture [5]. Tanijaya et al. (2008) studied the modulus of elasticity, compressive and tensile strength for zeolite based mixtures and concluded that increasing natural zeolites content, the mechanical properties, namely modulus of elasticity, compressive and tensile strength, are decreasing over time [6].

The primary cementitious material in concrete is portland cement, but this constituent releases more than 6% of total carbon dioxide (CO_2) into the environment during manufacturing [7]. Consequently, replacing the amount of cement in concrete mixtures with natural pozzolanic material is found to be an effective solution to reduce carbon dioxide (CO_2) emission and promotes sustainability. Valipour et al (2014) completed a study on environmental effect of zeolite based concrete and ordinary Portland cement (OPC) concrete. Based on this study, it was concluded that replacing 10%, 20% and 30% of cement with zeolite will reduce the potential of CO_2 emission by 60.3%, 69.7% and 64.3%, respectively, and that zeolite is an environmental friendly cementitious material [8].

EXPERIMENTAL METHOD

Different types of binary and ternary-based zeolite mixtures including the OPC mixture with w/cm ratios of 0.44 and 0.40 are prepared to investigate chloride induced corrosion resistance and engineering properties of concrete. These ranges of w/cm ratio are typical for reinforced concrete bridge decks and pavements. In addition, feasible w/cm ratio will ensure higher strength and less voids in concrete. Concrete with w/cm ratios higher than 0.5 generally result in lower compressive strength and a more permeable pore structure, which can lead to poor durability. All mixtures contain 564 lb/yd³ (334 kg/m³) of cementitious materials with Coarse Aggregate Factor (CAF) of 0.67. Two different maximum size aggregates (MSAs) for the coarse aggregate are utilized and they are ¾ in. (19 mm) and ½ in. (12.5 mm). River sand is used as the fine aggregate meeting ASTM C33 standard. All cementitious materials are replaced by mass. Different tests are performed on each concrete mixture using the following materials. Table 1 shows all concrete mixtures composition.

- Type II-V Portland cement (TII-V) in California due to high sulfate attack problem
- Supplementary cementitious materials (SCMs):
- Zeolite
- Ground granulated blast furnace slag of Grade 120 & 100 (G120S and G100S)
- Class C Fly Ash (C)
- Class F Fly Ash (F)
- Silica Fume (SF)
- Metakaolin (M)
- Pumice (P)
- Water reducing and air entraining admixtures (target air-content 4%-5%) satisfying ASTM C494 specifications.

Cylinders consisting of 4 in. (100 mm) diameter by 8 in. (200 mm) long, are cast in accordance with the ASTM C192 practice and are demolded after 24 hours and cured in a saturated lime water tank. Target compressive strength is 4000 psi (27 MPa) at 28 days as recommended by most Department of Transportations (DOTs).

Research Significance

The research presented in this study focuses on identifying the effectiveness of zeolite material in binary and ternary based HPC mixtures including the control OPC mixture with variation of w/cm ratio and different aggregate sizes. The emphasis of the paper is to investigate surface electrical resistivity and various important mechanical properties, namely compressive strength, tensile strength and modulus of elasticity in short term period. In order to maintain structural integrity and longevity over intended service life of a structure, reinforced concrete structures must meet both strength and durability requirements. For this reason, the other purpose of this study is to identify mixture proportions including zeolite based cementitious mixtures that results in high compressive strength and durability against chloride induced corrosion.

Mechanical Properties Testing

Modulus of elasticity is related to stiffness and strength of concrete and it is widely used in the design of reinforced concrete structures. In this study, the compressometer is utilized for the measurement of the modulus of elasticity indirectly by evaluating concrete sample deformation and strain as per ASTM C496 standard. Figure 1 shows picture of modulus of elasticity testing. Then, the experimental modulus of elasticity is compared with theoretically one. The theoretical modulus of elasticity was computed utilizing the following formula:

$$E_c = 57,000\sqrt{f'_c} \quad \text{(Equation 1)}$$

A Universal Testing Machine (UTM) is used for testing the compressive and tensile strength of the concrete cylinders in accordance with the ASTM C39 and ASTM C496 standards. Cylinders are placed in a UTM (Figure 2) using a rubber capping and continuous load was applied until it breaks. For tensile strength, cylinder is placed in horizontal direction, as shown in Figure 2, with wooden strips to hold it in place and monotonic compressive load is applied. Data is digitally recorded and stored in table and graphs. The maximum split tensile strength of each sample is obtained using the following formula:

$$\left(\frac{2P}{\pi * D * L} \right) \quad \text{(Equation 2)}$$

where P = Maximum applied load indicated by the testing machine (lb or N), D = Diameter (in. or mm), L = Length (in. or mm).

For compressive strength, tensile strength and modulus of elasticity measurement, two specimens are tested at each designated age and average values are computed for analysis purposes.

4-Point Wenner Probe for Surface Electrical Resistivity

This device measures the surface electrical resistivity of cylindrical concrete specimens following FDOT (FM5-578) method. Figure 3 illustrates the Wenner Probe meter and the calibration procedure before the testing. This instrument measures the surface resistivity when the probes are placed properly on the surface of the cylindrical samples. Before starting surface resistivity test, the cylinder samples are taken out from the lime water tank and dried using paper towels. The cylinders are then tested at surface saturated dry (SSD) condition except the edges, which are in a dry condition. Two readings are taken around the perimeter of the cylinder at 0, 90, 180 and 270 degrees. Three cylinders are tested each day and average values are presented in the results section.

RESULTS/DISCUSSIONS

Modulus of Elasticity:

Figures 4 through 7 compare the theoretical values to experimental values of modulus of elasticity for 0.44 and 0.40 w/cm ratio and ½ in. and ¾ in. (12.5 mm and 19 mm) aggregate size at 28 days. It is evident from the graphs that zeolite based ternary and binary mixtures are performing better than the OPC mixture. Especially, 75TII-V/25Z and 85TII-V/ 15Z mix designs are the optimum mixtures which can be implemented in the future concrete mixture design since their values are higher compared to other zeolite based mixtures. From Figure 7, it can be observed that ternary mixtures namely 60TII-V/20Z/20P, 60TII-V/20Z/20F, and 50TII-/15Z/35G100S with w/cm ratio 0.40 and ¾ in aggregate size have a higher modulus of elasticity compared to the other zeolite based ternary mixtures.

Compressive Strength:

Figures 8 through 11 summarize the compressive strength of the zeolite based mixtures and the results show that the mixtures with 0.40 w/cm and with ¾ in aggregate size achieved higher compressive strength from 7 to 91 days. In addition, most ternary mixtures with w/cm of 0.40 have higher compressive strength compared to the control mixture. As per Figure 11, compressive strength of concrete sample with 0.40 w/cm and ¾ in. (19mm) aggregate was tested to have higher compressive strength and it satisfied the recommended strength requirement of 4000 psi (27 MPa) at 28 days suggested by most Department of Transportations (DOTs), with the exception 10% zeolite replacement in OPC. Based on Figures 8 through 11, it is noticeable that mixtures with partial replacements of Portland cement with zeolite material also indicated this well-established trend that lowering the w/cm ratio and increasing the aggregate size resulted in higher compressive strengths. It is to be noted the dashed red line in Figures 8-11 indicates the suggested minimum compressive strength requirement set by most Department of Transportations (DOT).

Tensile Strength:

Figures 12 through 15 show the comparison of tensile strength test results for zeolite based mixtures at 7 and 28 days. Per Figure 14, binary mixtures like 80TII-V/20Z and 75TII-V/25Z with 0.40 w/cm and ¾ in. (19mm) aggregate size have higher tensile strengths at 7 and 28 days compared to other mixtures. Based on the Figure 15, for ternary based zeolite mixtures 75TII-V/20Z/5SF and 55TII-V/10Z/35G120S attained higher tensile strengths at 7 days and 70TII-V/20Z/10M and 55TII-V/10Z/35G100S at 28 days. Zeolite based concrete mixtures with 0.40 w/cm ratio performed better than mixtures with 0.44 w/cm ratio in terms of tensile strength measurement. Further, ternary based zeolite mixtures had considerable higher tensile strength at 0.40 w/cm ratio. In general, 30% replacement of zeolite in binary mixtures performed worse in tensile strength development. It can be reasonably concluded zeolite performs better up to 20-25% replacement in binary

mixtures. In addition, increasing the coarse aggregate size has great impact on the tensile strength of the concrete.

Electrical Surface Resistivity Data:

Figures 16-19 show the frequency distribution of surface electrical resistivity of OPC, zeolite based binary and ternary mixtures with two different w/cm ratio (0.40 and 0.44) and two different aggregate sizes ($\frac{1}{2}$ and $\frac{3}{4}$ in.) at 28 days. For each mixture, 24 data points from 3 cylinders ($3 \times 8 = 24$) were collected for surface resistivity measurement and it was included in frequency distribution graph. Based on Figures 16 through 19 and the Florida Department of Transportation (FDOT) FM5- 578 specification of surface electrical resistivity, it should be noted that the majority of the concrete mixtures fall in-between moderate to low chloride ion permeability classifications as shown in Table 2. Table 2 depicts the relationship between surface resistivity data and chloride ion permeability class in accordance with FDOT specification. In addition, zeolite based binary and ternary mixtures obtained significantly higher electrical resistivity compared to OPC mixture. Further, as expected, zeolite based ternary mixtures obtained higher surface electrical resistivity compared to binary mixtures except the ternary cementitious mixture which is blended with zeolite and Class C Fly Ash (55TII-V/20Z/25C). In particular, the mixtures with 0.40 w/cm ratio and $\frac{1}{2}$ in aggregate size showed remarkable improvement in terms of electrical resistivity data and they mostly range in between low to very low permeability class. Figure 19-part 2 shows overall distribution of SR data for all zeolite based ternary mixtures instead of single ternary mixture due to limitation of page limit of the manuscript. These mixtures are promising indicators for potential future implementation future reinforced concrete bridges and pavements.

CONCLUSION

This comprehensive study shows that High Performance Concrete (HPC) mixtures with zeolite, enhances the chloride ion resistance against corrosion by significant achievement of the surface electrical resistivity by 28 days. Further, mechanical properties of zeolite based concrete has been remarkably improved in terms of modulus of elasticity, compressive and tensile strength compared to the OPC mixture. In addition, zeolite based concrete mixtures with water to total cementitious materials (w/cm) ratios of 0.40 and $\frac{1}{2}$ in (12.5mm) and $\frac{3}{4}$ in (19mm) aggregates yield promising results in terms of surface electrical resistivity, modulus of elasticity, compressive and tensile strength. Based on the experimental results, it can be reasonably concluded that zeolite as a supplementary cementitious material is highly sensitive to high w/cm ratios. In summary, this study will help to understand the effectiveness and proper replacement level of zeolite material in various binary and ternary mixtures for future implementation in concrete bridges and pavements.

ACKNOWLEDGMENT

The authors would like to acknowledge Headwaters Resources (Fly Ash), BASF (Silica fume and Chemical admixtures like MBVR and Glenium 3030) and CalPortland Cement (Type II-V) for providing the necessary materials to perform this research.

REFERENCES

- [1]. Mehta, N. K., and Monteiro, P. J. M, “Concrete: Microstructure, Properties, and Materials,” McGraw-Hill, ISBN-13: 978-0071797870, New York, NY, 2006.
- [2]. Kung, P., “Fiber optic sensors to monitor reinforced concrete corrosion.,” SPIE Newsroom, 2014.
- [3]. Najimi, M., Sobhani, J., Ahmadi, B., and Shekarchi, M., “An Experimental Study on Durability Properties of Concrete Containing Zeolite as a Highly Reactive Natural Pozzolan,” *Construction and Building Materials*, Vol. 35, 2012, pp. 1023–1033.
- [4]. Ahmadi, B., and Shekarchi, M., “Use of Natural Zeolite as a Supplementary Cementitious Material,” *Cement and Concrete Composites*, Vol. 32, No.2, 2010, pp. 134–141.
- [5]. Chan, S. Y., and Ji, X., “Comparative Study of the Initial Surface Absorption and Chloride Diffusion of High Performance Zeolite, Silica Fume and PFA Concretes,” *Cement and Concrete Composites*, Vol. 21, No.4, 1999, pp. 293–300.

- [6]. Tanijaya, J., And Hardjito, D., “Experimental Study on the Use of Natural Zeolites as Partial Replacement for Cement in Concrete,” Eleventh East Asia-Pacific Conference on Structural Engineering & Construction (EASEC-11) “Building A Sustainable Environment,” 2008.
- [7]. Valipour, M., Pargar, F., Shekarchi, M., and Khani, S., “Comparing A Natural Pozzolan, Zeolite, to Metakaolin and Silica Fume in Terms of their Effect on the Durability Characteristics of Concrete: A Laboratory Study,” *Construction and Building Materials*, Vol. 41, 2013, pp. 879–888.
- [8]. Valipour, M., Yekkalar, M., Shekarchi, M., and Panahi, S., “Environmental Assessment of Green Concrete Containing Natural Zeolite on the Global Warming Index in Marine Environments,” *Journal of Cleaner Production*, Vol. 65, 2014, pp. 418–423.
- [9]. FM 5-578., “Florida Method of Test for Concrete Resistivity as an Electrical Indicator of its Permeability,” Florida Department of Transportation, 2004, pp. 1-4.

Table 1- Concrete Mixtures Composition

Mix ID	Cement (TII-V)	Zeolite (Z)	Silica Fume (SF)	Metakaolin (M)	Pumice (P)	Class F Fly Ash (F)	Class C Fly Ash (C)	Slag 120 (G120S)
100TII-V	100							
90TII-V/10Z	90	10						
85TII-V/15Z	85	15						
80TII-V/20Z	80	20						
75TII-V/25Z	75	25						
70TII-V/30Z	70	30						
70TII-V/20Z/10SF	70	20	10					
70TII-V/20Z/10M	70	20		10				
60TII-V/20Z/20F	60	20				20		
55TII-V/20Z/25C	55	20					25	
55TII-V/20Z/25P	55	20			25			
75TII-V/15Z/10SF	75	15	10					
55TII-V/10Z/G120S	55	10						35

Table 2- Surface Resistivity – Permeability Class from FDOT [9]

Chloride Ion Permeability	Surface Resistivity data kΩ-cm
High	< 12
Moderate	12 – 21
Low	21 – 37
Very Low	37 – 254
Negligible	> 254

[1 cm = 0.3937 in]



Figure 1 – Measurement of Modulus of Elasticity

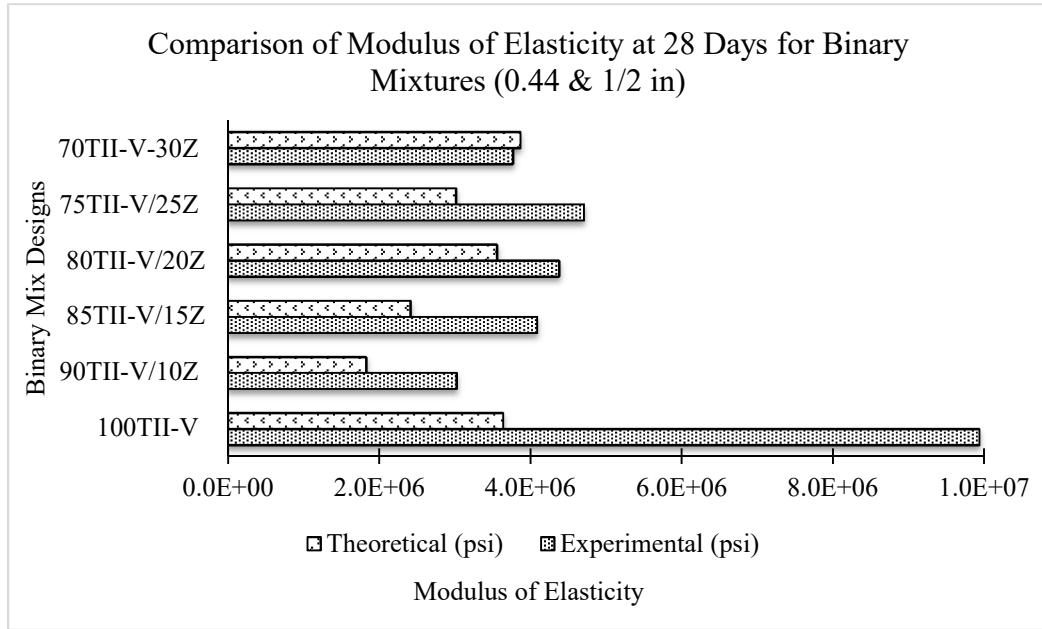


Figure 2- Measurement of Compressive and Tensile Strength

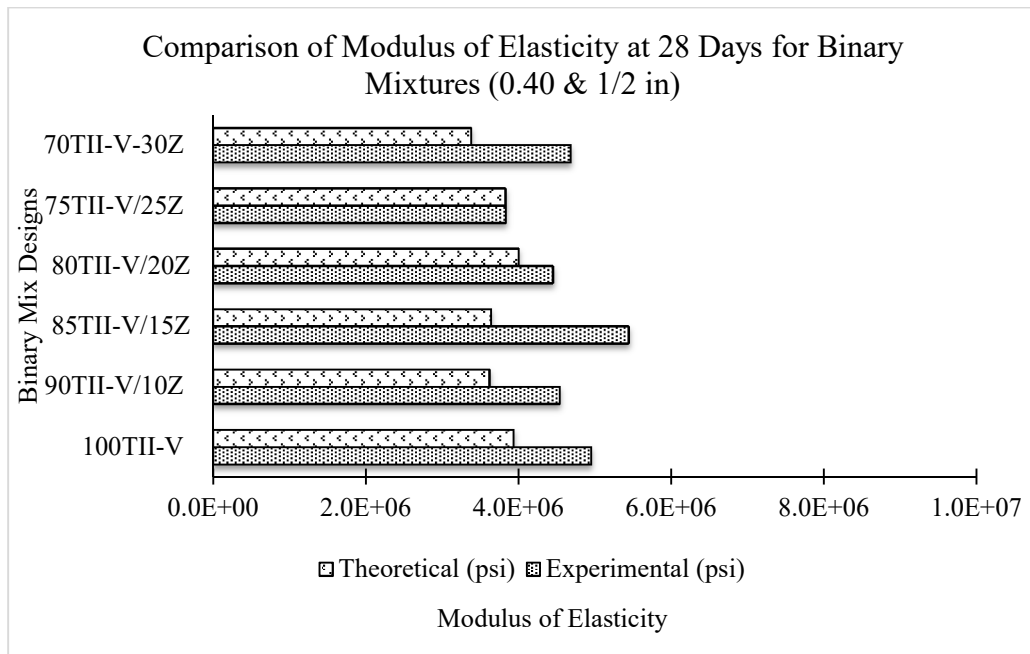


Figure 3- Measurement of Surface Electrical Resistivity by 4-Point Wenner Probe

Modulus of Elasticity:

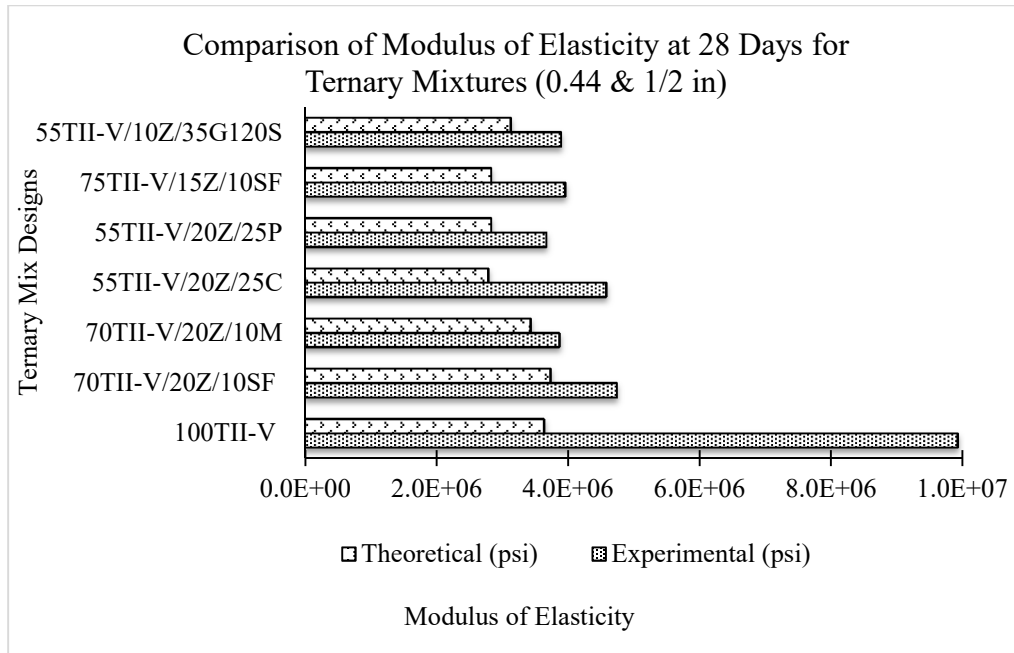


(a)

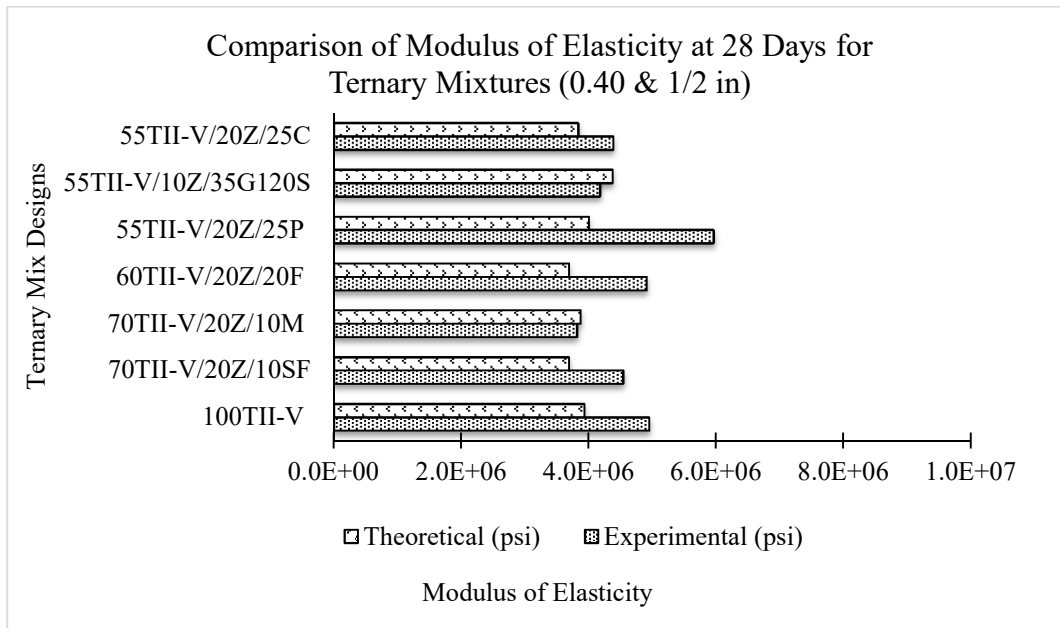


(b)

Figure 4- Comparison of experimental to theoretical modulus of elasticity for binary mixtures for 1/2 in aggregate with (a) 0.44 and (b) 0.40 w/cm ratio
[1 psi = 0.0068 MPa]

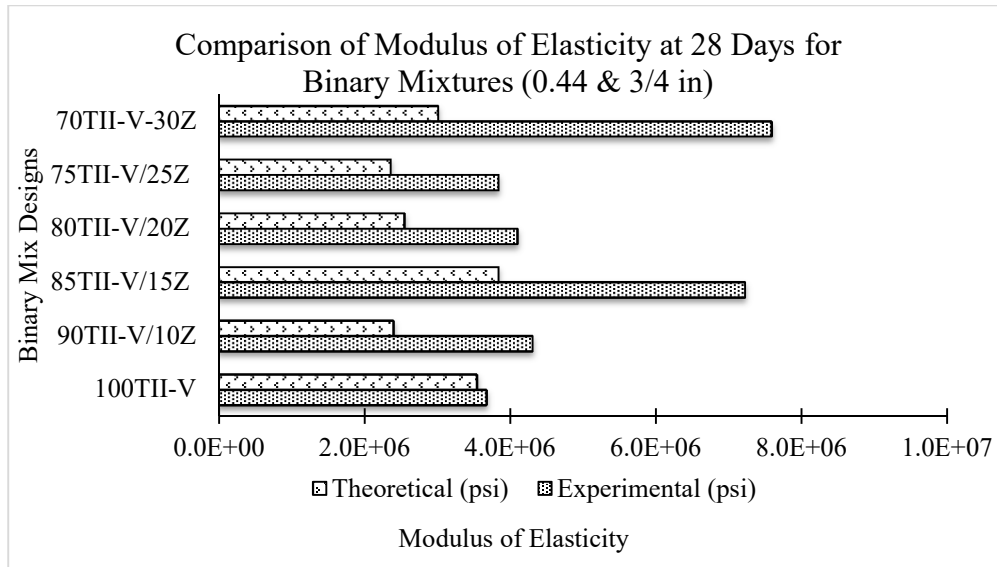


(a)

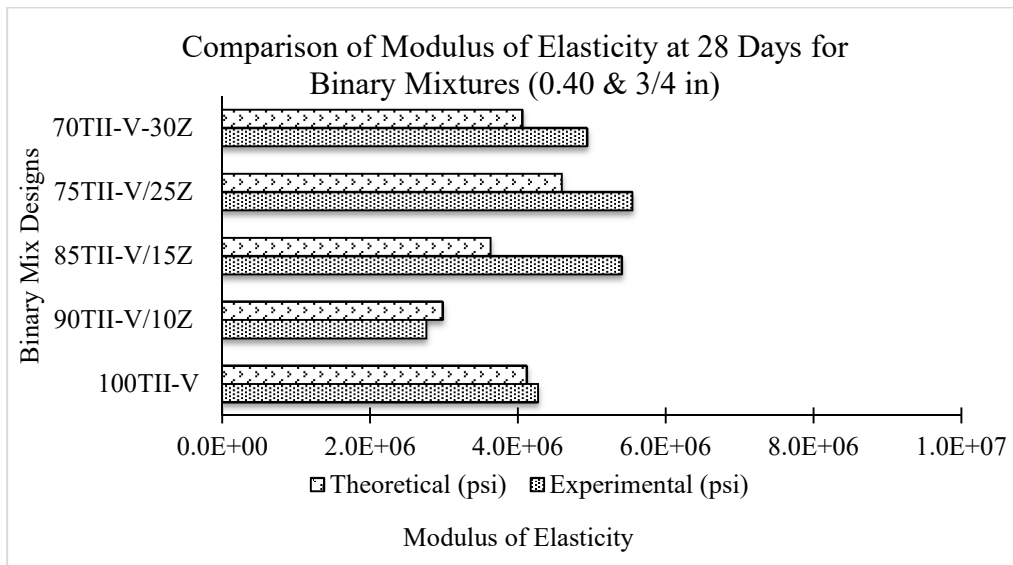


(b)

Figure 5- Comparison of experimental to theoretical modulus of elasticity for ternary mixtures of 1/2 in aggregate with (a) 0.44 and (b) 0.40 w/cm ratio
[1 psi = 0.0068 MPa]



(a)



(b)

Figure 6-Comparison of experimental to theoretical modulus of elasticity for 3/4 inch aggregate size binary mixtures with (a) 0.44 and (b) 0.40 w/cm ratio
[1 psi = 0.0068 MPa]

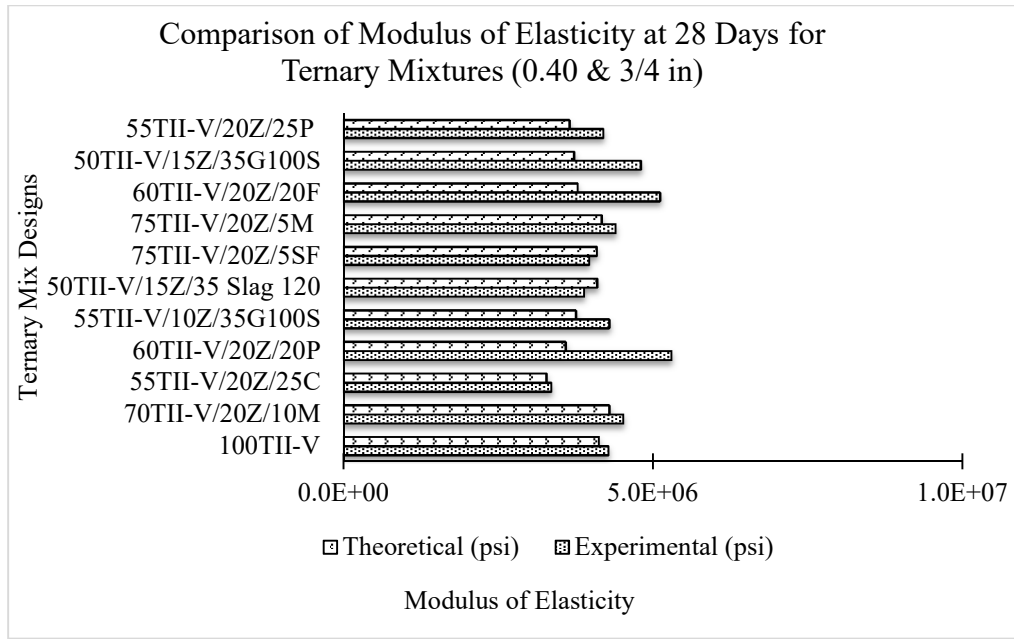
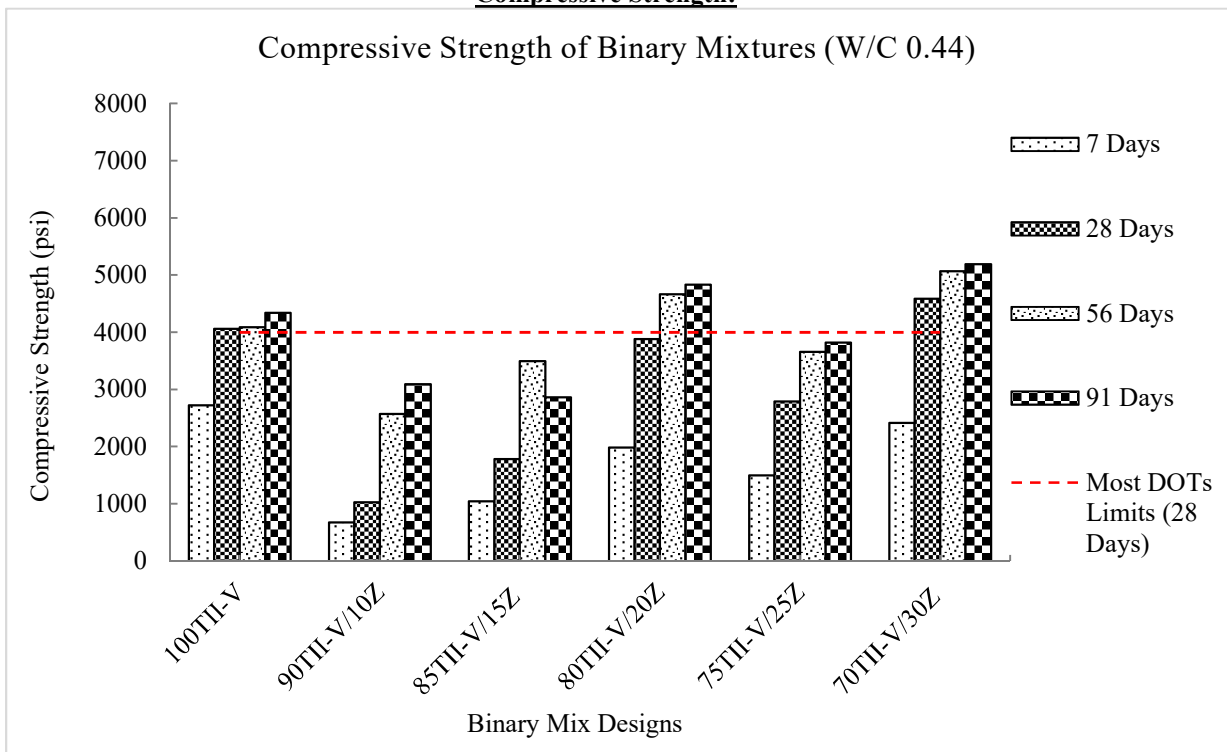
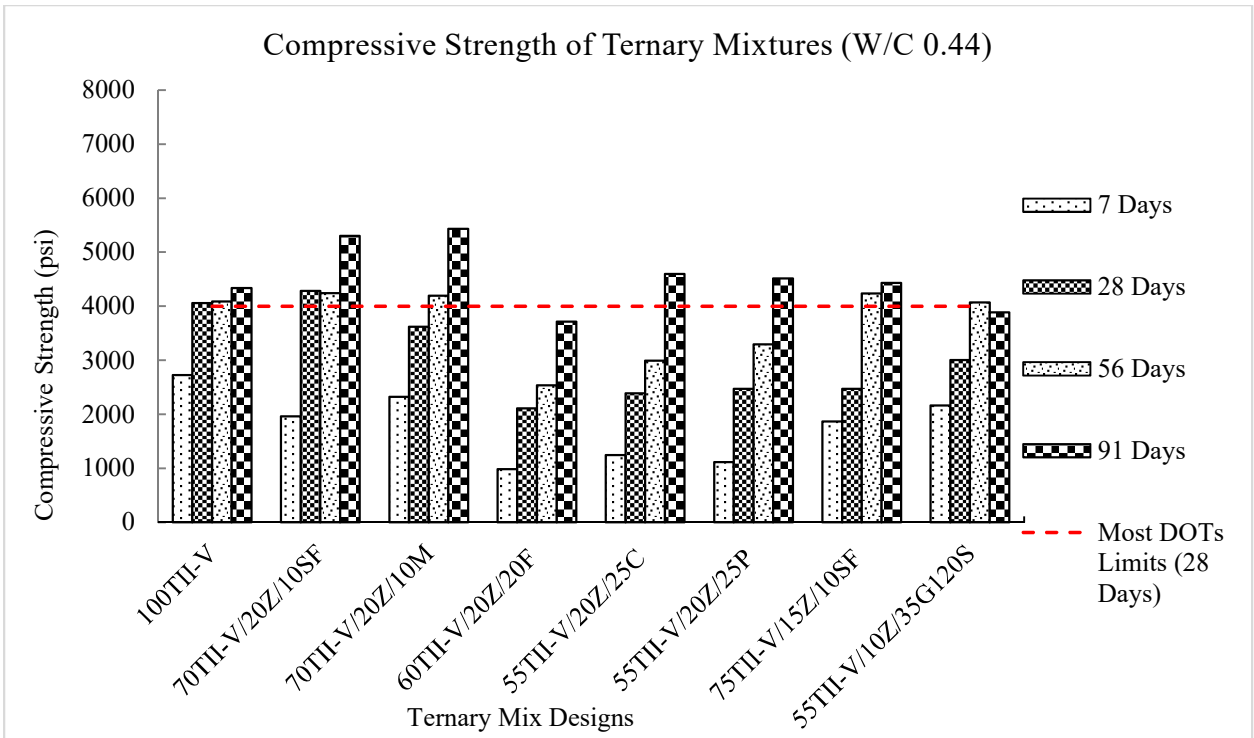


Figure 7- Comparison of experimental to theoretical modulus of elasticity for ternary mixtures with 3/4 in aggregate
 [1 psi = 0.0068 MPa]

Compressive Strength:

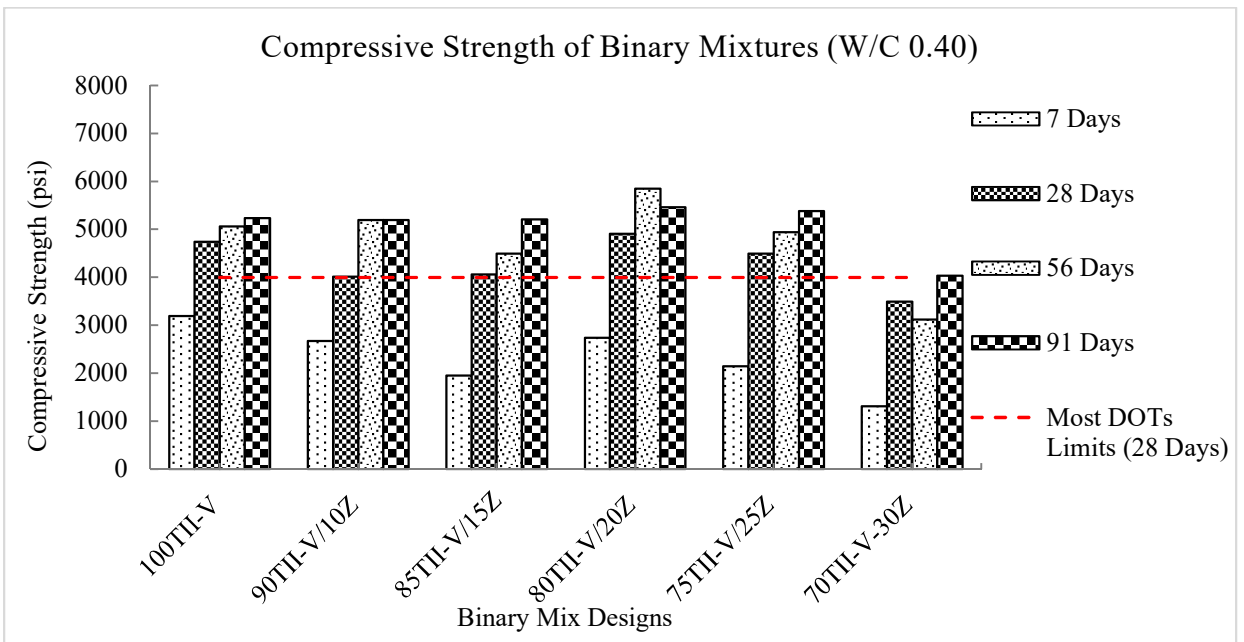


(a)

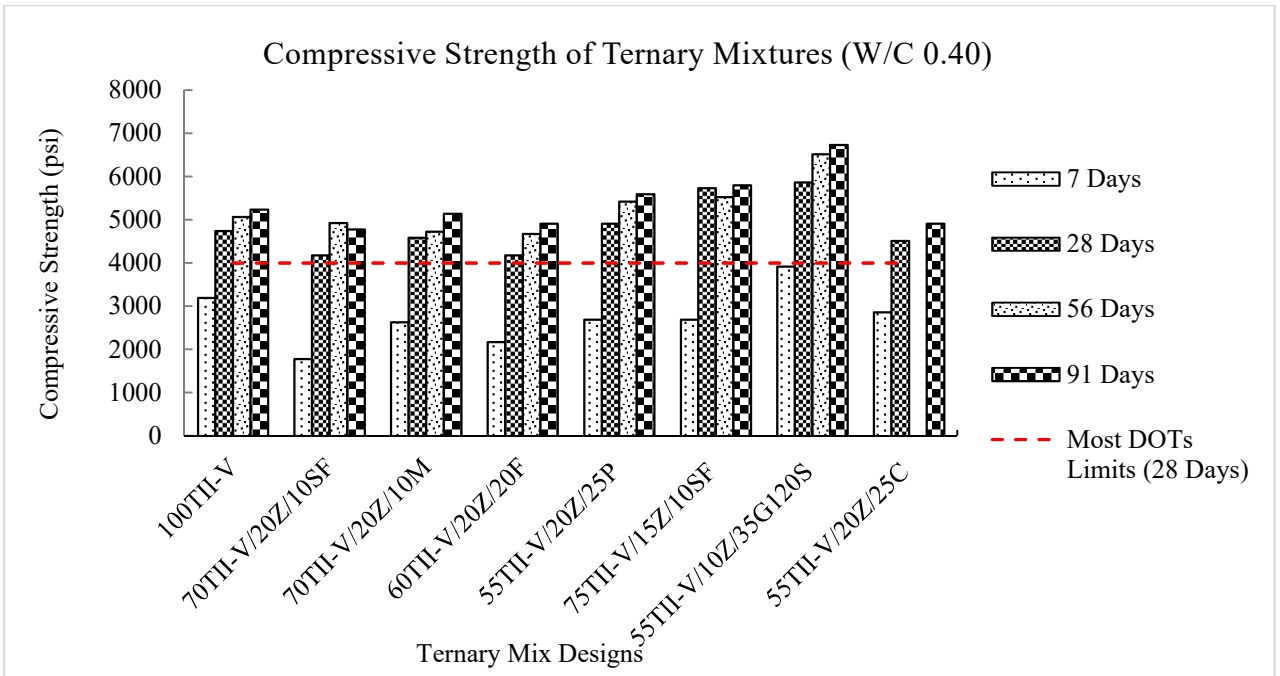


(b)

Figure 8- Compressive strength of (a) binary and (b) ternary mixtures with ½ in. aggregate size (0.44 w/cm ratio)
[1 psi = 0.0068 MPa]



(a)



(b)

Figure 9- Compressive strength of (a) binary and (b) ternary mixtures with 1/2 in aggregate size (0.40 w/cm ratio)

[1 psi = 0.0068 MPa]

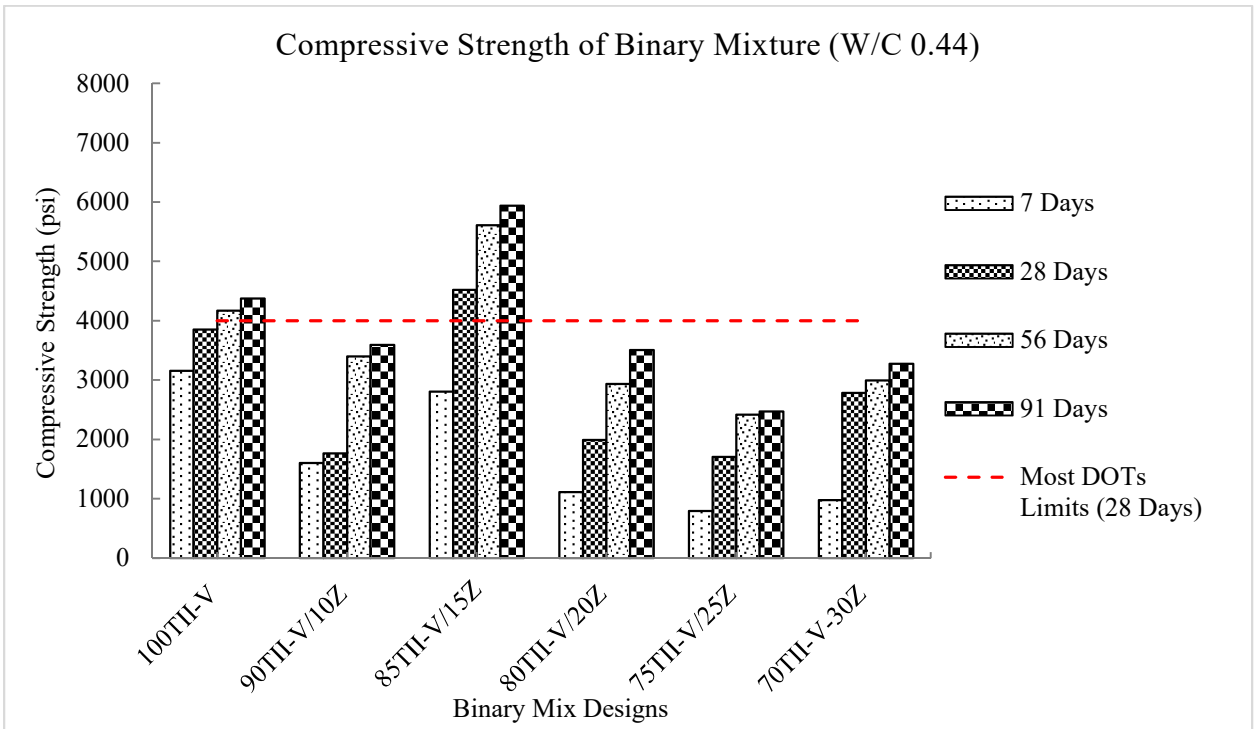
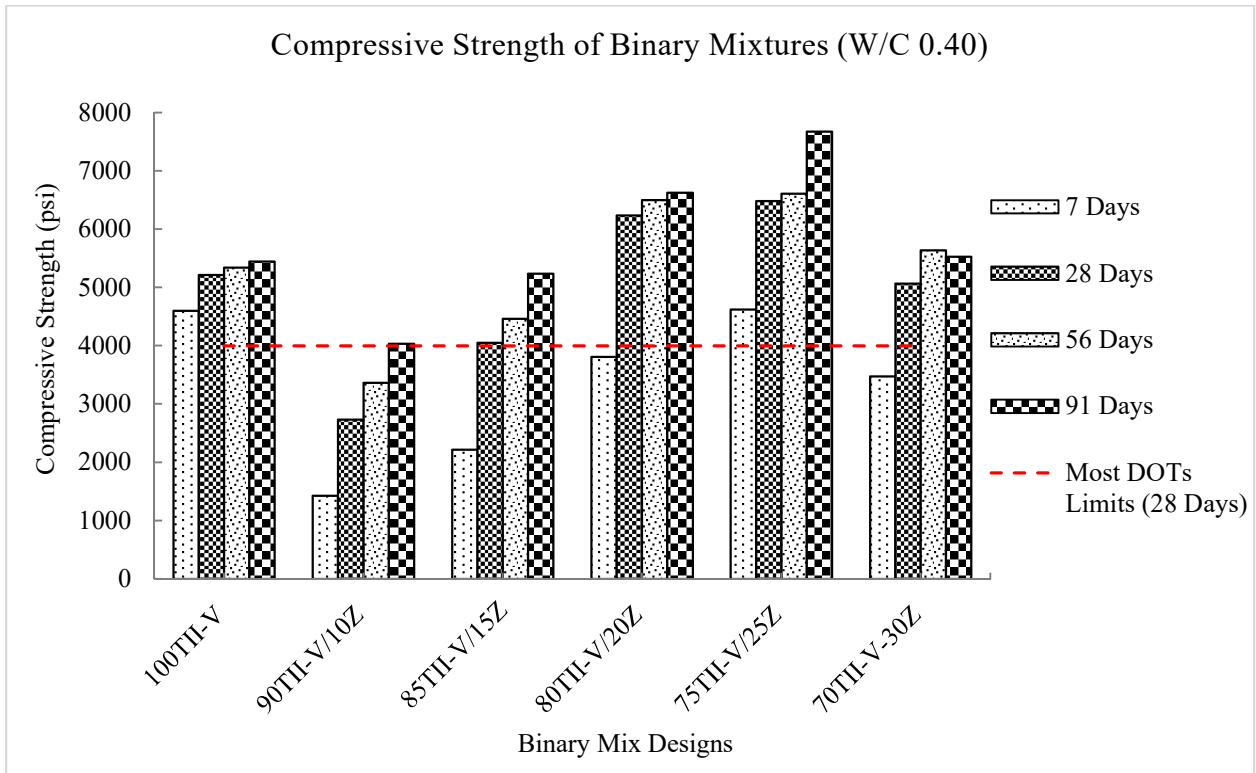
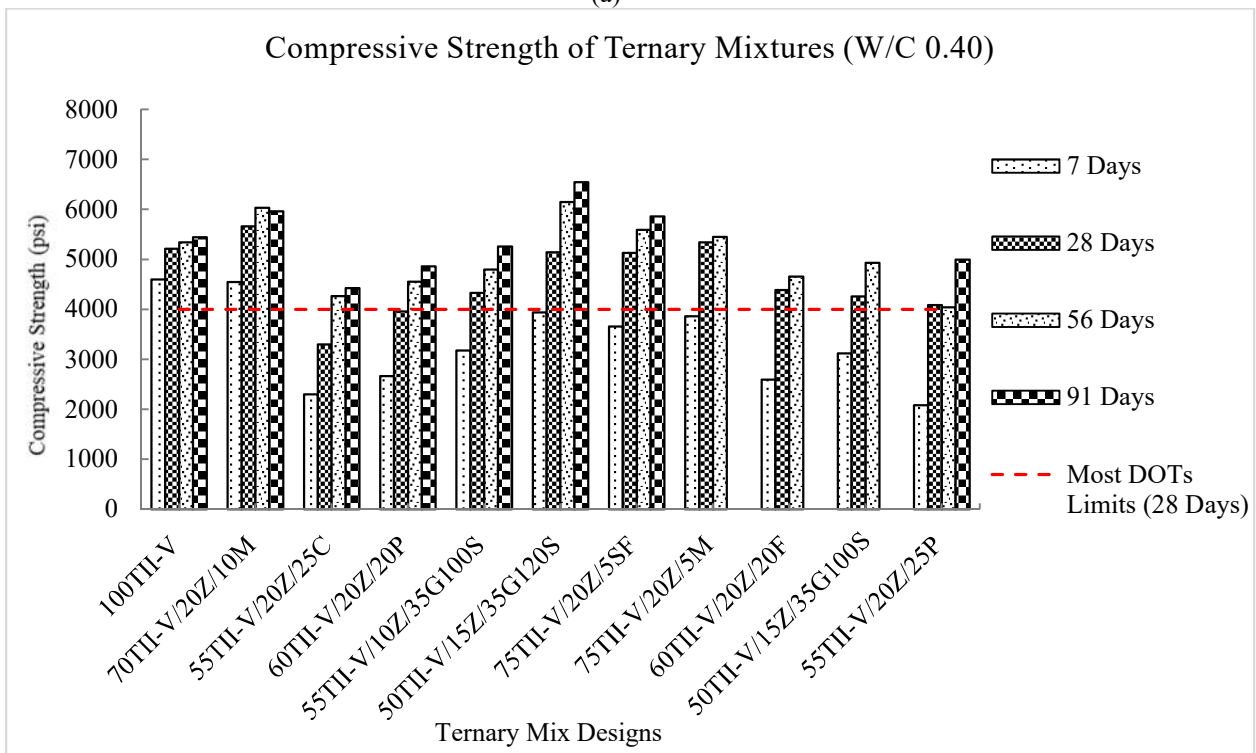


Figure 10- Compressive strength of binary mixtures with 3/4 in aggregate size (0.44 w/cm ratio)

[1 psi = 0.0068 MPa]



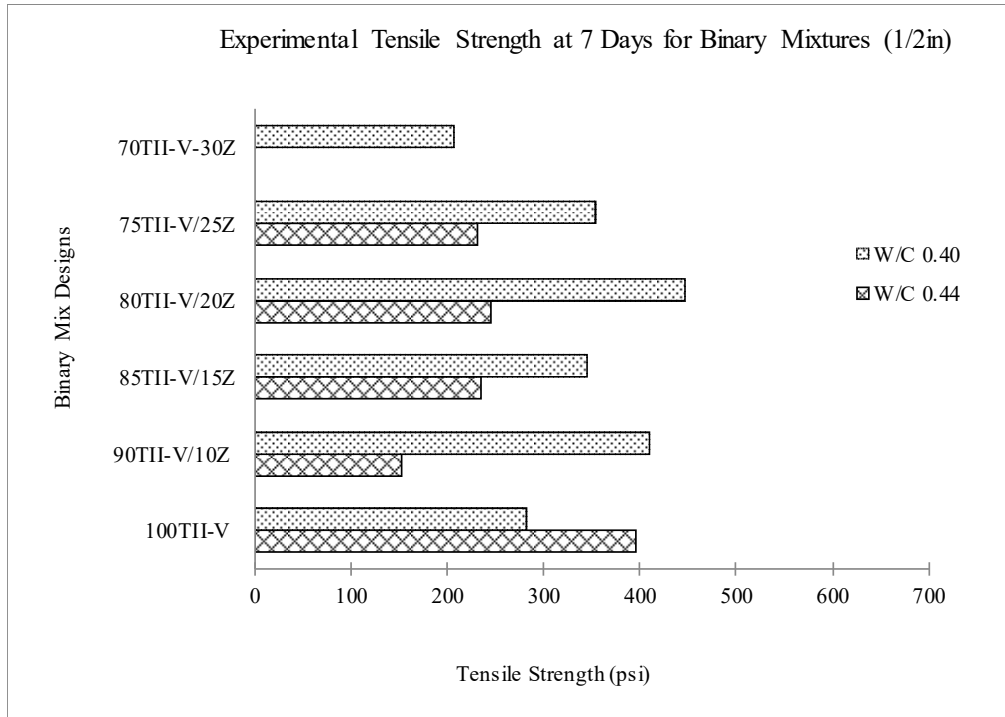
(a)



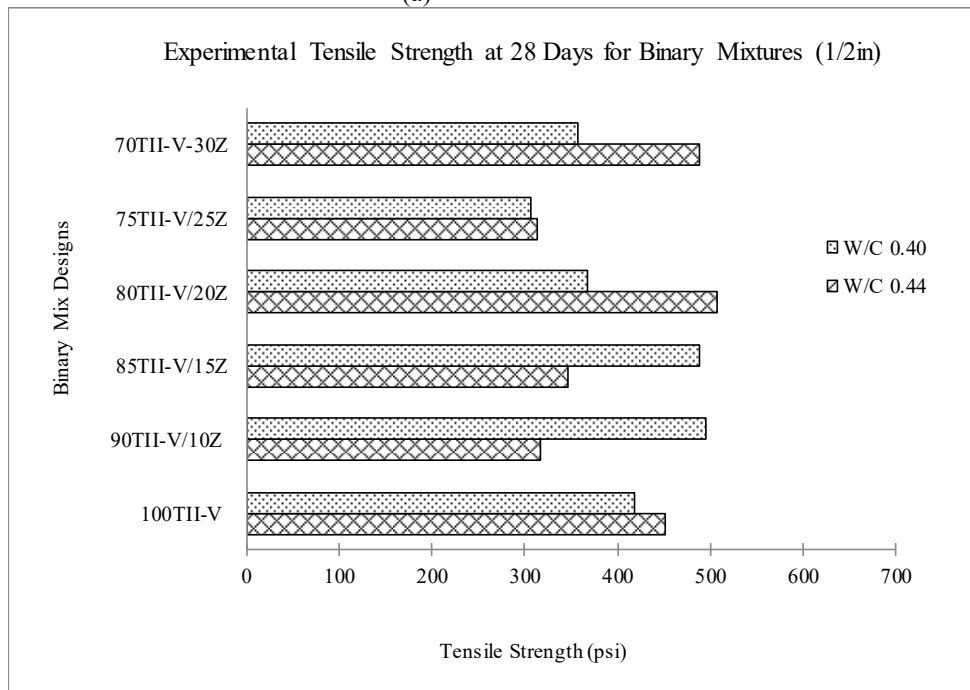
(b)

Figure 11- Compressive strength of (a) binary and (b) ternary mixtures with 3/4 in aggregate size (0.40 w/cm ratio)

Tensile Strength:

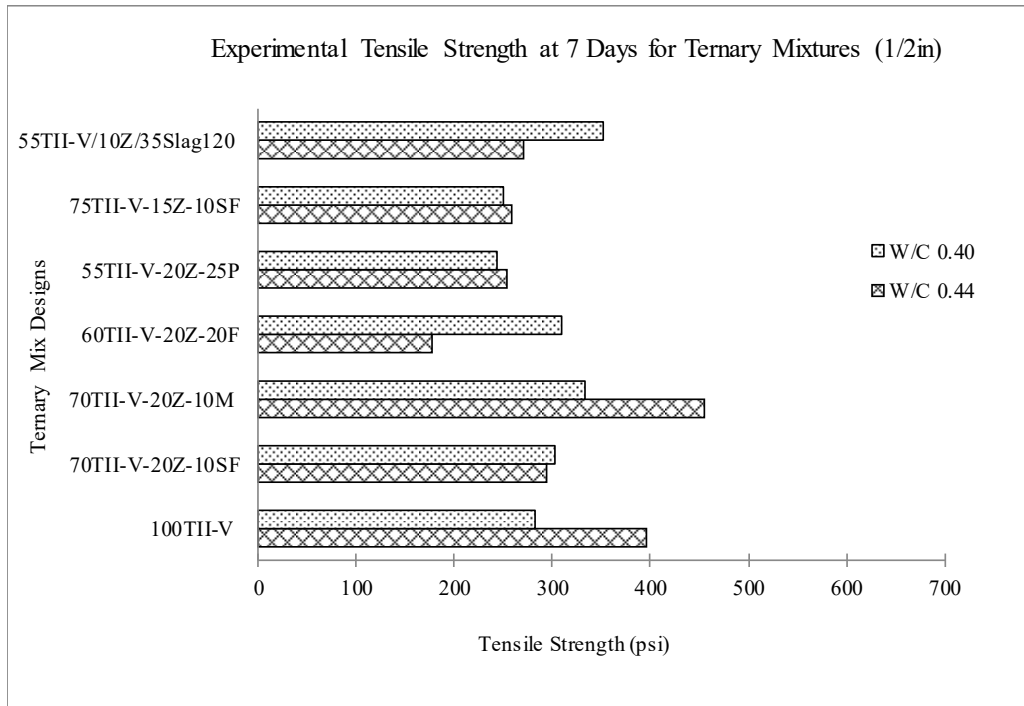


(a)

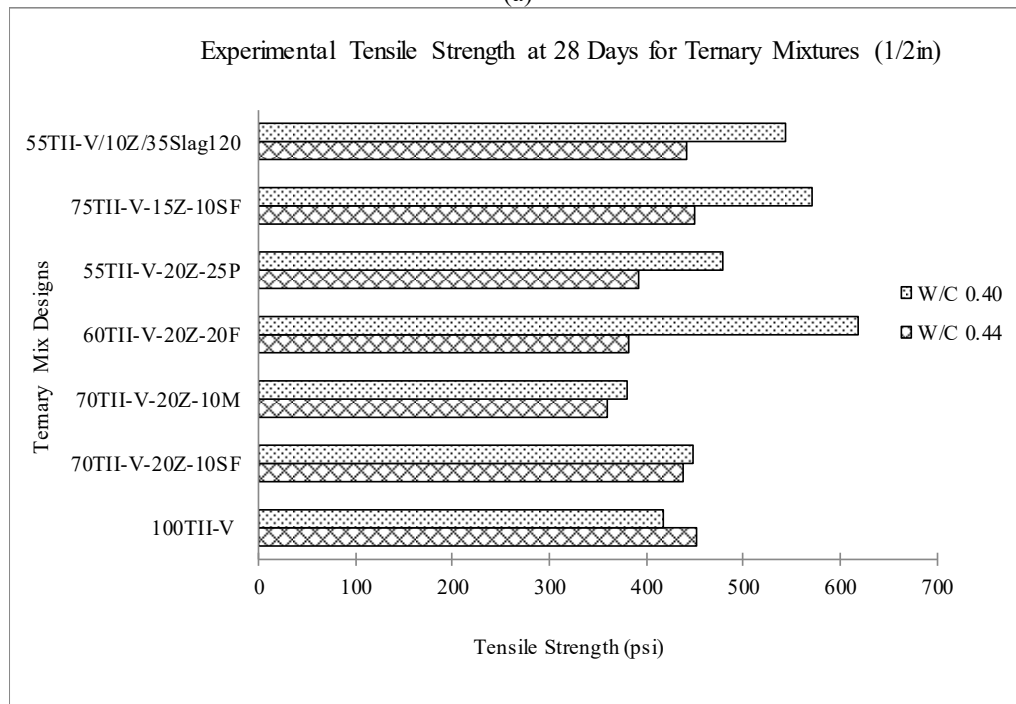


(b)

Figure 12- Experimental tensile strength of binary mixtures at (a) 7 and (b) 28 days for 1/2 in aggregate size [1 psi = 0.0068 MPa]

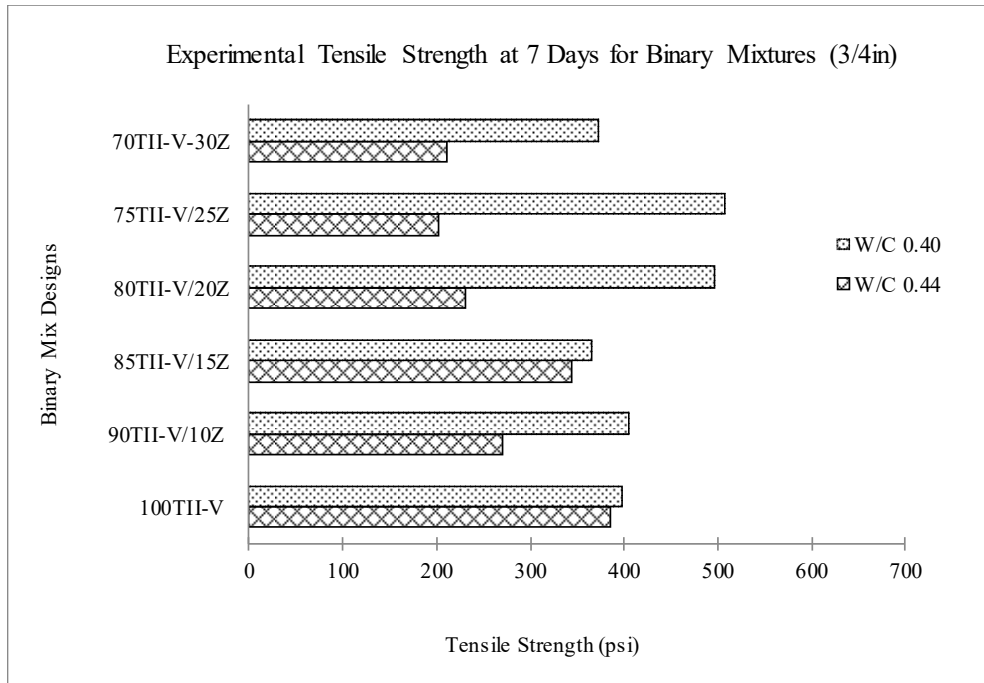


(a)

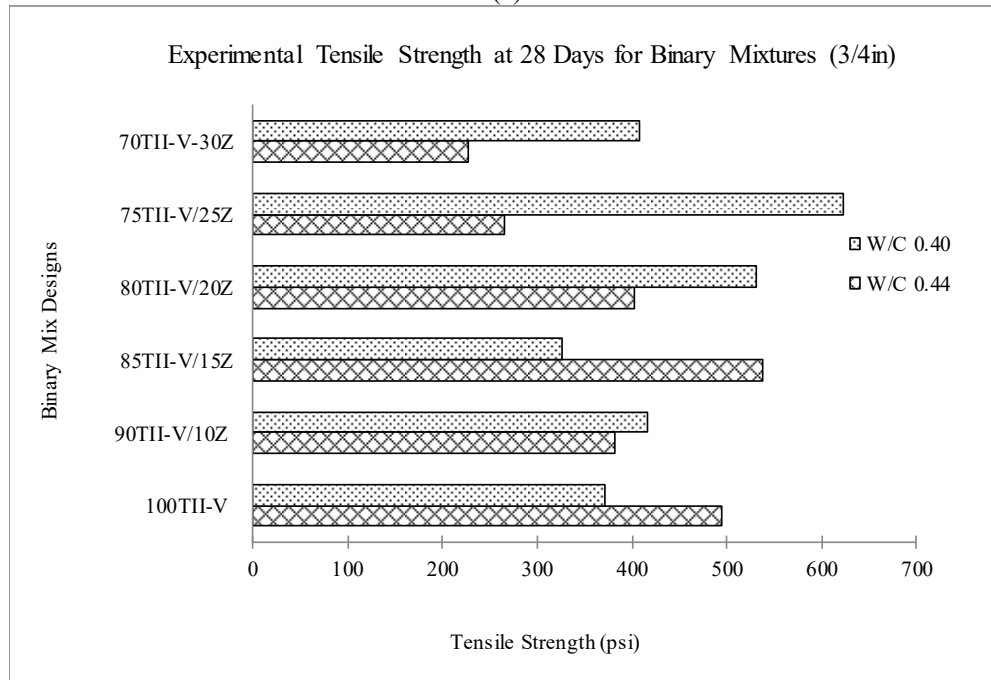


(b)

Figure 13- Experimental tensile strength of ternary mixtures at (a) 7 and (b) 28 days for 1/2 in aggregate size [1 psi = 0.0068 MPa]

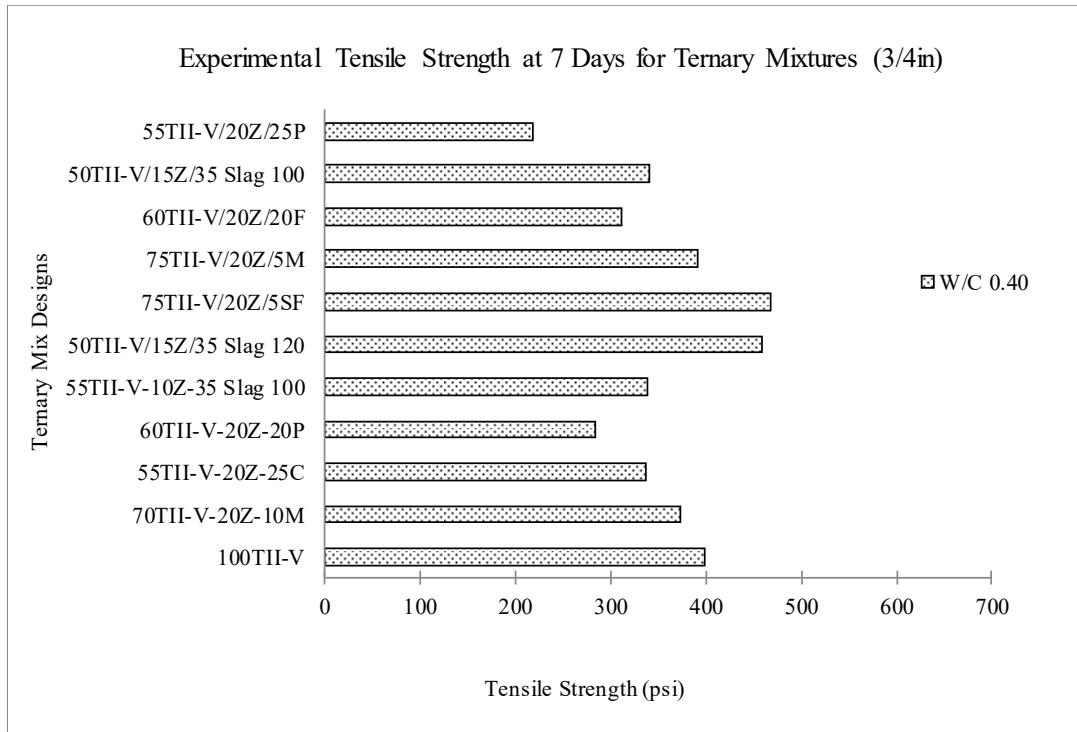


(a)

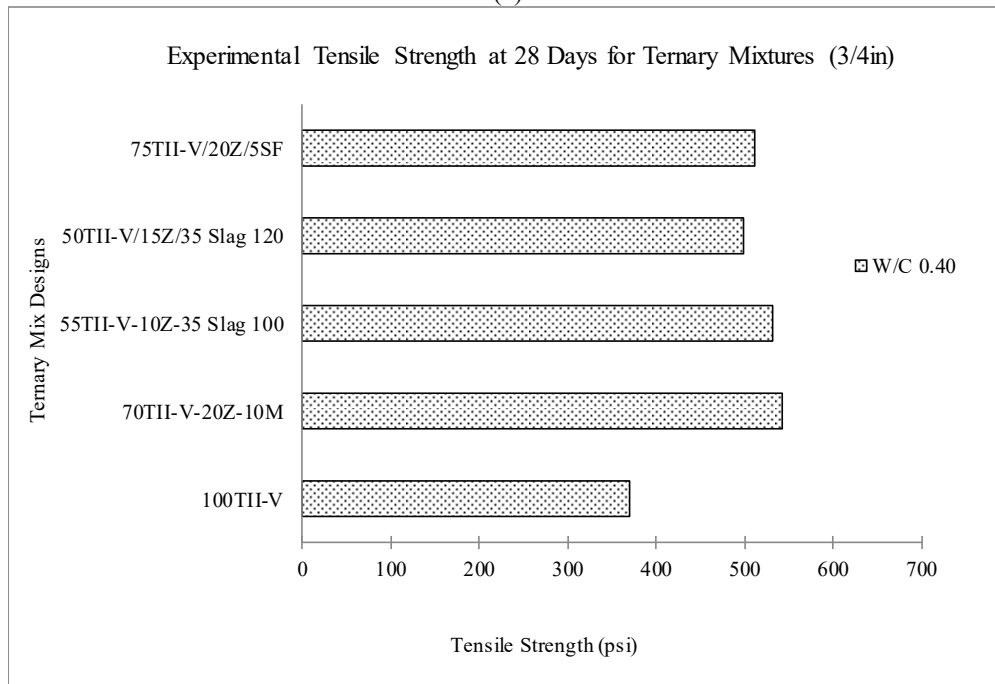


(b)

Figure 14- Experimental tensile strength of binary mixtures at (a) 7 and (b) 28 days for $\frac{3}{4}$ in aggregate size [1 psi = 0.0068 MPa]



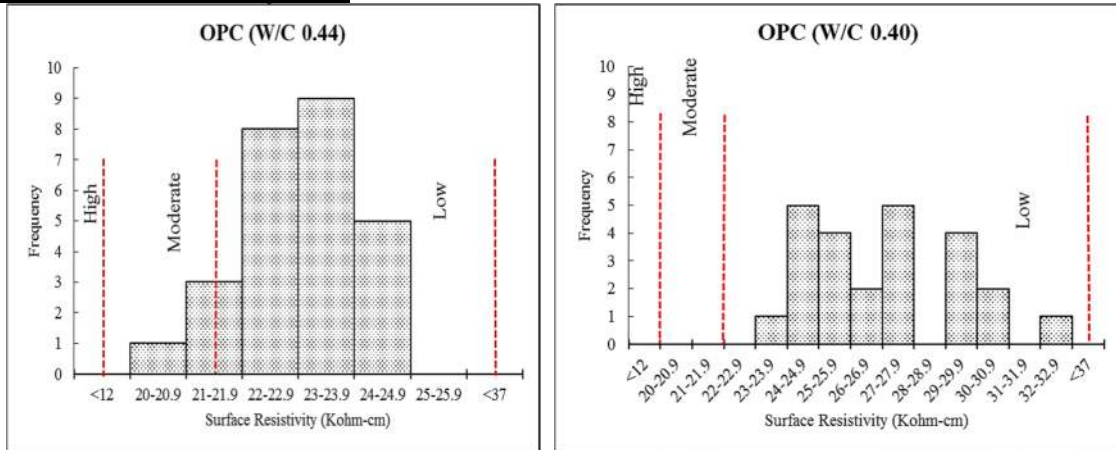
(a)



(b)

Figure 15- Experimental tensile strength of ternary mixtures at (a) 7 and (b) 28 days for $\frac{3}{4}$ in aggregate size [1 psi = 0.0068 MPa]

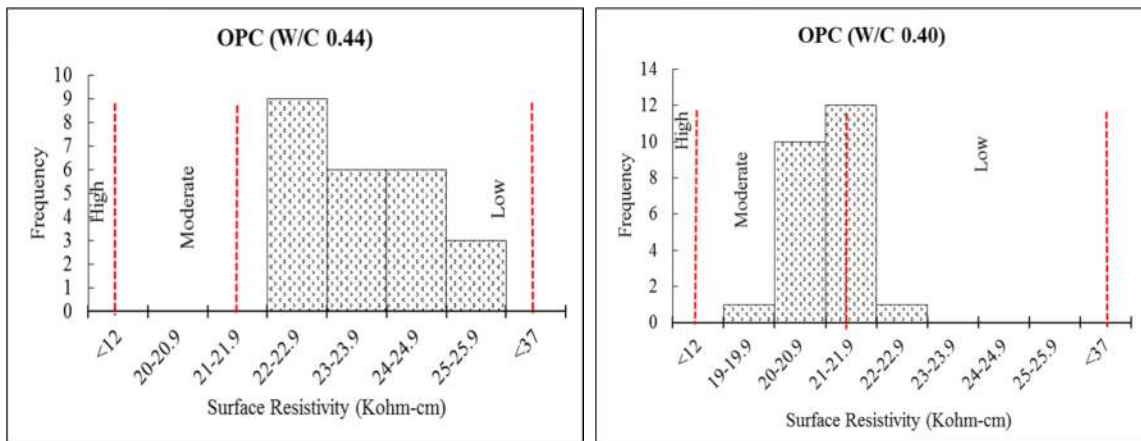
Electrical Surface Resistivity Data:



(a)

(b)

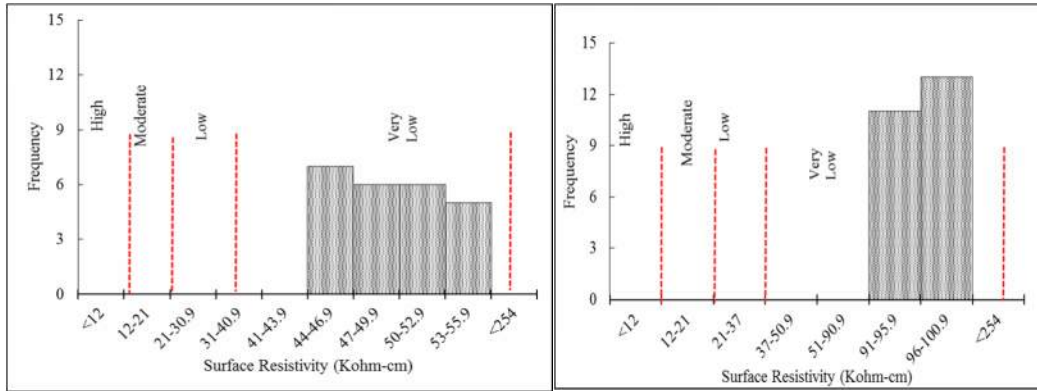
Figure 16- Comparison of surface electrical resistivity of (OPC) to (a) 0.44 with (b) 0.40 w/cm for 1/2" aggregate size at 28 Days
[1 cm = 0.3937 in]



(a)

(b)

Figure 17- Comparison of surface electrical resistivity of (OPC) to (a) 0.44 with (b).40 w/cm for 3/4" aggregate size at 28 days
[1 cm = 0.3937 in]



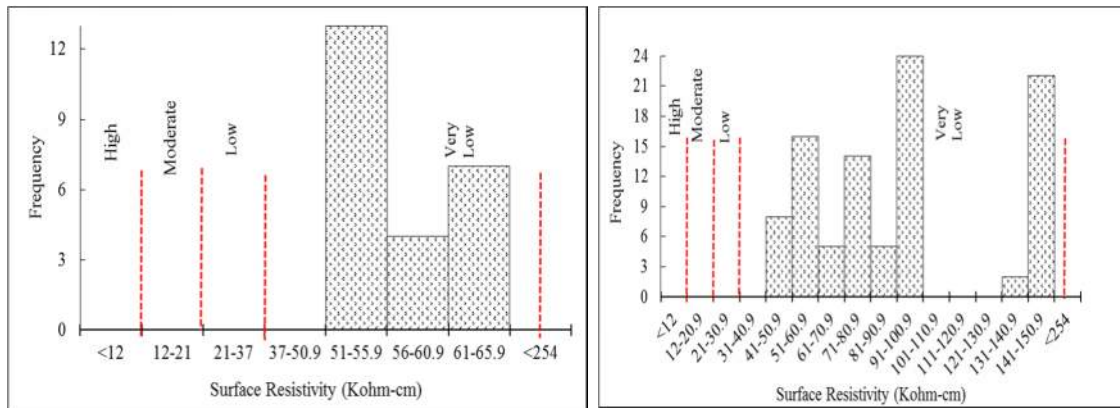
Mixture Design
85TII-V/15Z

Mixture Design
75TII-V/15Z/10SF

(a)

(b)

Figure 18- Comparison of surface electrical resistivity of (a) binary to (b) ternary mixture for 0.40 w/cm and ½ in aggregate size at 28 Days
[1 cm = 0.3937 in]



Mixture Design:
80TII-V/20Z

Mixture Design:
60TII-V/20Z/20F
70TII-V/20Z/10M
55TII-V/20Z/25C
55TII-V/20Z/25P

(a)

(b)

Figure 19- Comparison of surface electrical resistivity of (a) binary to (b) ternary mixtures for 0.40 w/cm and ½ in aggregate size at 28 Days
[1 cm = 0.3937 in]

Freeze-Thaw and Salt Resistance of a Fly Ash Based Pervious Concrete

Gang Xu, Luis Gerardo Navarro, Kafung Wong, and Xianming Shi

Synopsis: In this work, the freeze/thaw resistance and ambient-temperature salt resistance of fly ash geopolymer pervious concrete specimens were investigated separately, to isolate the physical and chemical phenomena underlying their deterioration during “salt scaling”. The laboratory investigation examined four groups of samples, with portland cement or activated fly ash as the sole binder, with or without graphene oxide (GO) modification, respectively. The incorporation of GO significantly improved the resistance of pervious concrete to freeze/thaw cycles and ambient-temperature salt attack, regardless of the binder type. The specimens were then examined by using X-ray Diffraction (XRD) method, which revealed that the mineralogy and chemical composition of fly ash pastes differed significantly from those of cement pastes. Nuclear magnetic resonance (NMR) was also employed to study the chemical structure and ordering of different hydrates. This work provides an enhanced understanding into the freeze/thaw and salt scaling resistance of fly ash pervious concrete and the role of GO.

Keywords: pervious concrete, fly ash, geopolymer, freeze-thaw, salt attack, wet-dry, X-ray diffraction (XRD), nuclear magnetic resonance (NMR)

ACI student member **Gang Xu** has earned his Ph.D. in Structural Engineering (2018), at the Department of Civil and Environmental Engineering, Washington State University. His research interests include sustainable and innovative concrete materials, nanotechnology application in building materials, structural engineering and bridge health monitoring.

Luis Gerardo Navarro is an Undergraduate Student in the Department of Civil and Environmental Engineering at Washington State University, Pullman, WA.

Kafung Wong is an Undergraduate Student in the Department of Chemical Engineering at Washington State University, Pullman, WA.

ACI member **Xianming Shi** is an Associate Professor in the Department of Civil and Environmental Engineering, Washington State University. Dr. Shi holds his Ph.D. in Chemistry from the Chinese Academy of Sciences and a 2nd M.Sc. in Industrial & Management Engineering from Montana State University. His research interests include sustainable infrastructure materials, infrastructure preservation and rehabilitation, multiscale characterization and modification, corrosion protection, and infrastructure durability.

INTRODUCTION

Pervious concrete is a special type of concrete, featuring a high porosity that allows water from precipitation and other sources to pass through directly into the base/subbase and underlying soil. The infiltration effect provided by pervious concrete pavements can recharge the groundwater and reduce the amounts of total suspended solids, total phosphorus, total nitrogen and metals in the ground water [1]. A typical pervious concrete mix design contains portland cement, the environmental footprint of which raises some concerns such as the high-energy consumption and the release of air pollutants (NO_x and SO₂) and greenhouse gases (CO₂). To make the pervious concrete environmentally friendly and sustainable, fly ash, a by-product of coal fired power plant, has been chosen in this study to fully replace portland cement in the pervious concrete since it has been used as a partial cement replacement in the concrete for years [2][3][4][5].

Significant quantities of fly ash are generated every year. In 2013, the United States produced 115 million tons of coal ashes. While only 45 percent were used beneficially, nearly 64 million tons were disposed of [6]. Based on the analytical CaO content, fly ash can be divided into high-calcium fly ash (CaO content > 10%) and low-calcium fly ash (CaO Content < 10%) [7]. Recent years have seen increasing use of younger lignite or sub-bituminous coal at power plants, which increased the availability of high-calcium fly ashes [8]. Berry et al. [9] has demonstrated that it is possible to use the high-calcium fly ash as the sole cementitious binder to make concrete with moderate strength.

One significant barrier that hinders the implementation of pervious concrete pavement is its lack of durability in cold climates. Specifically, the use of chemical deicers in cold regions tends to exacerbate the susceptibility of exterior concrete structures to freeze/thaw (F/T) cycles [10–12]. Relative to impervious concrete, pervious concrete is more prone to the ingress of water and deicer solution and is thus more vulnerable to premature failure due to salt scaling damage. Previous studies [13,14] found that pervious concrete features a weak resistance to F/T cycles.

In this work, the freeze-thaw resistance and ambient-temperature salt resistance of pervious concrete specimens were investigated separately, to isolate the physical and chemical phenomena underlying their deterioration during the “salt scaling” test featuring the combined effects of freeze/thaw cycling and deicer attack. Sustainable pervious concrete with fly ash as the sole binder was developed with alkali activation at room temperature. Graphene oxide (GO) was also used to facilitate the polymerization of reaction products from alkali activation. Previous studies [15][16][17] indicated that GO can improve the overall performance of cement mix significantly by regulating cement hydration, providing crack branching and bridging mechanism and acting as nanofillers. Therefore, GO has significant potential for the application in fly ash-based pervious concrete of high strength and durability.

The following sections detail the material preparation, fabrication, freeze-thaw testing and wet-dry (with salt solutions) testing of pervious concrete. The microstructural characterization of GO-modified fly ash concrete was also carried out through X-ray powder diffraction (XRD) analysis and nuclear magnetic resonance (NMR) spectroscopy.

RESEARCH SIGNIFICANCE

This work investigates the physical and chemical phenomena underlying the deterioration of a fly ash geopolymer pervious concrete in cold-climate service conditions. Pervious concrete is a type of sustainable concrete and the replacement of cement by an ambiently cured fly ash geopolymer binder aimed to further reduce its CO₂ and energy footprints. The NMR study reveals the hydrate structure of GO-modified fly ash and cement pervious concrete, which sheds light on the fundamental difference in performance between fly ash and cement hydrates at the molecular level.

EXPERIMENTAL STUDY

Material

The class C *high-calcium* fly ash used in this study was obtained from a power plant in Oregon, U.S. Fly ash compositions were examined by X-ray fluorescence (XRF) analysis and are presented in Table 1. Loss on ignition was acquired through thermogravimetric analysis.

Table 1—Physical and chemical properties of the fly ash and glass powder (% wt.)

	Glass powder	Fly ash
Specific gravity	2.6	2.5
Bulk Density (lbs/ft ³) [kg/m ³]	43 [689]	54 [860]
d98 top size (μm)	40	--
D50 median size (μm)	8-9	--
SiO ₂ (wt. %)	50-55%	23.5%
CaO (wt. %)	20-25%	23.2%
Al ₂ O ₃ (wt. %)	14-20%	13.8%
Fe ₂ O ₃ (wt. %)	<1%	4.8%
MgO (wt. %)	<2%	4.2%
Na ₂ O+K ₂ O (wt. %)	8-14%	6.7%
Loss on Ignition (wt. %)	<0.5%	≈ 0.8%

The amount of chemical activators designed to facilitate dissolution of fly ash and polymerization of hydration products are listed as follows.

- Water glass, i.e., sodium Silicate (Na₂SiO₃·9H₂O): 7% by weight of fly ash
- Sodium Sulfate (Na₂SO₄·10H₂O): 1% by weight of fly ash
- Quicklime (CaO): 5% by weight of fly ash
- Calcium Chloride (CaCl₂·2H₂O): 0.5% by weight of fly ash

GO used in this study were produced by using a modified Hummer's method, which mainly involves chemical oxidation of the graphite [18]. The as-produced GO was pasty, which was diluted with deionized water first and then sonicated for 45 minutes by using a Branson digital sonifier (S-450D, 400 W, 50% amplitude) to produce stable GO suspension (Fig. 1). The major elements of GO were C = 71 wt.% and O = 26 wt.%. Note that currently the cost of using GO is much higher than the use of other reinforcing materials such as fibers; however, the cost of GO is anticipated to drop exponentially over time as this novel nano-material is increasingly used by various industries. Furthermore, the GO works as a multifunctional admixture in the chemically activated fly ash [19], instead of simply a type of nano-filler or nano-fiber.



Fig. 1—Ultrasonication of GO suspension.

One type of single-sized coarse aggregate, crushed limestone in 3/8-inch size was used as coarse aggregate meeting the ASTM C33 standard specification. One commercially available glass powder recycled from industrial feedstocks was used as a micro-filler in the pervious concrete mix design to improve workability and sustainability, the properties of this glass powder was also listed in Table 1. A Type I/II cement was used in the mix design of control groups.

Mix Proportions

Four groups of pervious concretes were designed to investigate the performance of fly ash based pervious concrete under freeze-thaw and wet-dry cycles. The proportions of four mixes are shown in Table 2. Triethanolamine (TEA) was used to improve early-age strength of pervious concrete. Air-entraining (AE) agent, MB-AE 90, and high-range water reducer (HRWR), MasterGlenium 7920, were used to improve the workability and freeze-thaw resistance of pervious concrete. Note that the AE agent was needed to improve the freeze-thaw resistance of the mortar phase, despite of the highly connected air void characteristics of the pervious concrete matrix.

Prismatic test specimens (3 x 4 x 16 in. [76 x 102 x 406 mm]) were used according to ASTM C666 [20]. The concrete was mixed and cast in steel molds in accordance with ASTM C192 [21]. The specimens were demolded after 24 hours, and cured for 14 days before the testing. Six fly ash based specimens were also cured for 28 days to test the effects of longer curing time.

Table 2—Pervious concrete material proportions

Mix Design	Agg. Size (mm) [inch]	Agg. (kg/m ³) [lb/ft ³]	Cement (kg/m ³) [lb/ft ³]	Fly ash (kg/m ³) [lb/ft ³]	Water (kg/m ³) [lb/ft ³]	GO (g/100kg binder)*	TEA (ml/100kg binder)*	HRWR (ml/100kg binder)*
Cement	9.5 [3/8]	1425 [89]	320 [20]	--	80 [5]	--	40	300
Cement + GO	9.5 [3/8]	1425 [89]	320 [20]	--	80 [5]	30	40	300
Fly ash	9.5 [3/8]	1425 [89]	--	320 [20]	80 [5]	--	40	1000
Fly ash + GO	9.5 [3/8]	1425 [89]	--	320 [20]	80 [5]	30	40	1000

* 2% (by weight of fly ash) glass powder used

* Air entraining agent dosage = 30ml/100kg binder for all mix designs

* 1 fl oz/cwt = 65.2 mL/100 kg, 1 oz/cwt = 62.5 g/100kg

* Fly ash weight includes the designed amount of chemical activators

Test Procedures

Freeze/thaw test

The freeze/thaw tests were carried out according to ASTM C666 Procedure A [20]. By design, this test protocol investigates the resistance of pervious concretes to freeze/thaw damage in an accelerated manner, as pervious concrete

features a weak resistance to F/T cycles when tested under fully saturated (i.e., undrained) condition [13,14] (Fig. 2), which is usually not representative of properly designed and constructed pervious concrete pavements in the field service environment. The freeze/thaw damage was also evaluated based on changes in dynamic modulus of elasticity (E) in accordance to ASTM C215 [22]. Mass loss of the samples was measured, with 15% loss considered as failure [23]. P_{ft} is referred to as the relative dynamic E for freeze/thaw testing.



Fig. 2—Pervious concrete specimens in freezing-and-thawing chamber (undrained).

Wetting and drying in solutions of NaCl

The wet/dry exposure test adopted procedures used in a previous study [24], where pervious concrete specimens were exposed to weekly cycles of wetting and drying in a 3 wt% solution of NaCl. Three specimens were used for each of the mix designs in Table 2, which were submerged in the NaCl solution for 4 days at a temperature of 72 ± 4 °F (22 ± 2 °C). Then, they were removed from the solution and dried in air at the same temperature for 3 days. The deicer solutions were replaced every 5 weeks.

Similar to the freeze-thaw test in ASTM C666 [20], the effects of wet-dry cycles were evaluated based on changes in the dynamic modulus of elasticity in accordance to ASTM C215 [22]. The fundamental transverse resonance frequency of each specimen was measured before the test and every two weeks thereafter, the dynamic E was calculated based on the mass, dimensions and fundamental frequency of the specimen according to ASTM C215 [22]. The ratio (P_{wd}) of the dynamic E at the given number of cycles to the initial dynamic E is referred to as the relative dynamic E for wet/dry testing.

NMR and XRD tests

^{29}Si , and ^{27}Al Magic Angle Spinning (MAS) NMR spectroscopy was performed on the freshly ground paste samples at 56-day, using a Bruker solid-state NMR instrument with a magnetic field strength of 7.05 T, packed in 4 mm ZrO_4 rotors and spun at 5 or 12 kHz at ambient temperature. ^{29}Si spectra (operating frequency of 59.5 MHz) were acquired between 1000 and 7500 scans using a pulse recycle delay of 15 seconds, a pulse width 1.2 μs and an acquisition time of 80 ms. ^{29}Si chemical shifts were referenced to tetramethylsilane (TMS) at 0 parts per million (ppm). The samples were spun for no longer than 60 minutes to avoid dehydration of the sample and loss in the intensity of peaks [25]. Powder XRD patterns were collected for the paste samples after failure in the NaCl solutions, using an X-ray diffractometer with an incident beam of Cu-K α radiation ($\lambda = 1.5418$ Å) for a 2θ scanning range of 5° to 70° .

EXPERIMENTAL RESULTS AND DISCUSSION

Specimens in the freeze/thaw test

To evaluate the freeze/thaw resistance of pervious concrete, the change of fundamental transverse resonance frequency over the freeze/thaw cycles were measured and recorded in Table 3. The variation of relative dynamic E (calculated based on Table 3 as P_{ft}) with respect to the number of freeze/thaw cycles was presented in Fig. 3, which provides a good indication of the deterioration of pervious concrete over the entire duration of freezing and thawing cycles. Fig. 3 includes the resistance to freeze/thaw cycles of five groups: Portland cement pervious concrete cured for 14 days (“Cement-14d”), GO-modified cement pervious concrete cured for 14 days (“Cement+GO_14d”), fly ash pervious concrete cured for 14 days (“Fly Ash_14d”), fly ash pervious concrete cured for 28 days (“Fly Ash_28d”), and GO-modified fly ash pervious concrete cured for 28 days (“Fly Ash+GO_28d”). The specimens after failure were shown in Fig. 4.

As shown in Fig. 3, the fly ash pervious concrete specimens cured for 14 days before testing experienced a total failure at 36 cycles, whereas those cured for 28 days before testing had a total failure at 60 cycles, indicating fly ash hydration

was a slow process and fly ash pervious concrete presented a better resistance to the freeze/thaw test at later ages. After adding GO, the fly ash pervious concrete (cured for 28 days) experienced a total failure at 144 cycles, showing equal durability characteristics compared to that of the conventional cement pervious concrete (cured for 14 days), which also had a total failure at 144 cycles. After adding GO, the total failure of cement pervious concrete was also delayed from 144 cycles to 162 cycles.

Overall, GO showed the ability to improve the resistance to freeze/thaw cycles for both cement and fly ash pervious concretes. Due to the slow hydration of fly ash (chemically activated hydration in fly ash versus spontaneous hydration in cement), the freeze/thaw resistance of GO-modified fly ash pervious concrete cured for 28 days can only be comparable to the cement pervious concrete cured for 14 days.

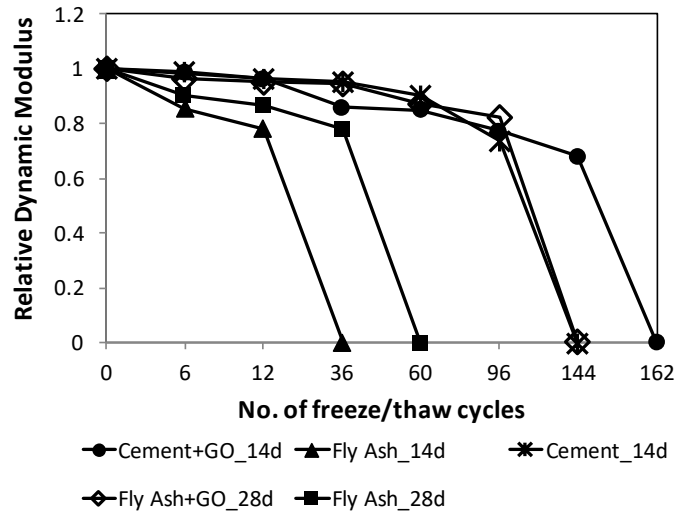


Fig. 3—Relative dynamic modulus of elasticity (P_{ft}) versus number of freeze/thaw cycles.

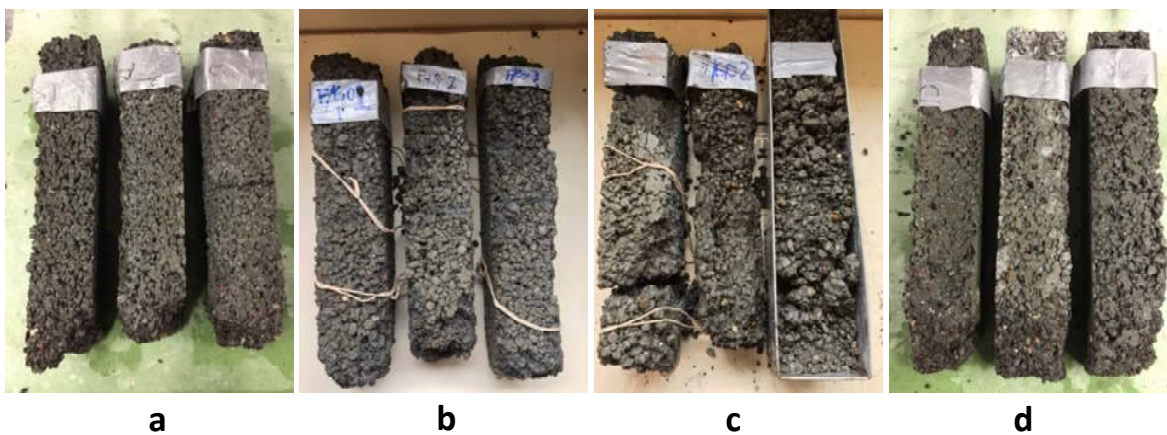


Fig. 4—Failed specimens after the freeze/thaw test, (a) Fly Ash_28d group; (b) Fly Ash+GO_28d group; (c) Cement+GO_14d group; (d) Cement_14d group.

Table 3—Average transverse resonance frequency (Hz) and coefficients of variation for specimens in freeze/thaw cycles

	Cement_14d	Cement+GO_14d	Fly Ash_28d	Fly Ash+GO_28d
--	------------	---------------	-------------	----------------

Cycles	Average	COV	Average	COV	Average	COV	Average	COV
0	1832	0.015	1806	0.032	1452	0.039	1733	0.035
6	1823	0.016	1791	0.031	1379	0.044	1701	0.027
12	1800	0.028	1772	0.027	1349	0.013	1691	0.030
36	1789	0.005	1672	0.015	1283	0.019	1683	0.032
60	1737	0.047	1662	0.066	24	0.062	1619	0.029
96	1571	0.057	1586	0.081	failed	--	1570	0.039
144	30	0.057	1488	0.084	--	--	30	0.023
162	failed	--	30	0.039	--	--	failed	--

Specimens in the wet/dry test with NaCl solutions

To evaluate the negative impact of NaCl on the pervious concrete in wet/dry cycles, the change of fundamental transverse resonance frequency was measured and recorded in Table 4. The variation of relative dynamic E (calculated based on Table 4 as P_{wd}) with respect to the number of wet/dry cycles was presented in Fig. 5, which provides a good indication of the deterioration of pervious concrete with NaCl solutions. Fig. 5 includes the resistance to wet/dry cycles of four groups: cement pervious concrete cured for 14 days (“Cement_14d”), GO-modified cement pervious concrete cured for 14 days (“Cement+GO_14d”), fly ash pervious concrete cured for 14 days (“Fly Ash_14d”) and GO-modified fly ash pervious concrete cured for 14 days (“Fly Ash+GO_14d”).

As shown in Fig. 5, the P_{wd} of cement pervious concrete generally decreased as the cycle increased. The P_{wd} of fly ash specimens decreased after the first cycles, however it showed an increasing trend afterwards. After adding GO, the resistance to wet/dry cycles in NaCl solutions was improved for both cement and fly ash pervious concretes. Previous studies [26,27] indicated that salts can affect the chemistry of cement paste, as chloride solutions caused the formation of calcium chloride hydrate and calcium oxychloride. The decrease of P_{wd} in cement pervious concretes can be related the formation of these phases. The increase of P_{wd} in fly ash pervious concretes can be attributed to both the slow strength gain and the different chemistry of fly ash pastes, which was examined by XRD and NMR methods later.

Overall, GO showed the ability to improve the resistance to NaCl attack for both cement and fly ash pervious concretes. Fly ash pervious concretes also exhibited a better resistance to NaCl than their cement counterparts. While the freeze/thaw test caused a rapid physical damage to pervious concrete, the salt attack caused the specimens to deteriorate slowly.

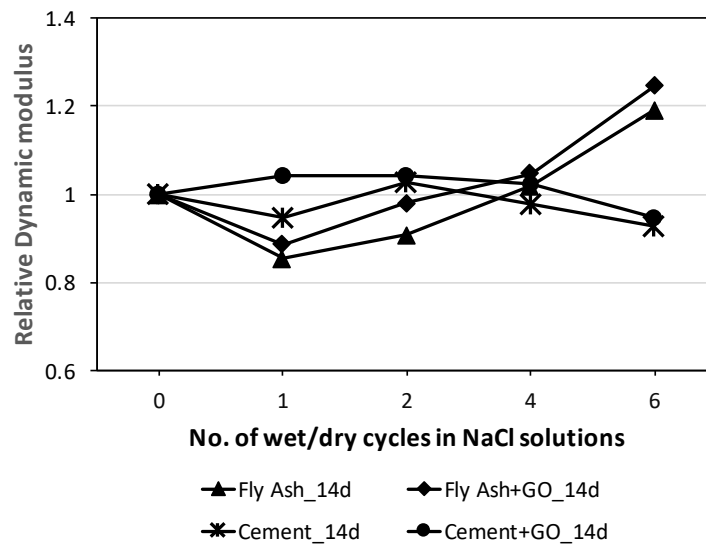


Fig. 5—Relative dynamic modulus of elasticity (P_{wd}) versus number of wet/dry cycles in NaCl solutions.

Table 4—Average transverse resonance frequency (Hz) and coefficients of variation for specimens in wet/dry cycles

Cycles	Cement 14d		Cement+GO 14d		Fly Ash 14d		Fly Ash+GO 14d	
	Average	COV	Average	COV	Average	COV	Average	COV
0	1816	0.046	1720	0.051	1398	0.163	1547	0.111
1	1769	0.039	1755	0.057	1292	0.190	1456	0.110
2	1841	0.041	1757	0.059	1331	0.165	1531	0.082
4	1798	0.034	1741	0.047	1411	0.166	1584	0.084
6	1749	0.039	1675	0.065	1525	0.140	1726	0.040

XRD analysis

The residual of pastes after salt attack was further examined by the XRD analysis. Fig. 6 shows the XRD patterns of the different pastes. A wide band is observed between 25° and 35° (2 theta) for all patterns, indicating the presence of amorphous C-S-H around 30° [28]. For the residuals of ordinary fly ash and cement pervious concrete, the XRD patterns suggest the presence of Calcite (at 23.1° , 29.4° , 36.1° , 39.6° , 43.2° , 47.6° and 48.5°) as the main crystalline compound because the salt scaling damage is caused by NaCl along with carbonation which results in paste decalcification [12]. Important decreasing of Calcite peaks and increasing of Portlandite peaks (at 18.2° , 28.9° , 34.3° , 47.4° , 50.1° and 54.5°) are observed in the pastes of Cement+GO and Fly Ash+GO groups, suggesting that GO improved the resistance of pastes to carbonation in salt solutions, which is likely related to the formation of more compact and ordered hydrates. Taking into account the carbonation of Ettringite which forms calcium carbonate and gypsum, the absence of Gypsum peak (at 45.5°) in the Fly Ash+GO and Cement+GO pastes is another evidence of GO-improved resistance to carbonation. Hatrurite (also known as Alite) at 32.4° , 41.5° and 52.0° and Larnite (also known as Belite) at 32.7° were overserved as non-hydrated mineral parts of fly ash and cement [29]. Quartz was also detected as a minor compound in the cement pastes.

Peak at 31.8° is assigned to semi-crystalline C-S-H (I) which can be considered as a structurally imperfect tobermorite [30], this semi-crystalline C-S-H (I) showed a better resistance to the salt attack, as its peak stands out in the patterns of residuals of Fly Ash and Cement pervious concrete. Peaks related to pozzolanic products, Margarite ($\text{CaAl}_4\text{Si}_2\text{O}_{11}\cdot\text{H}_2\text{O}$) at 22.2° and Clinotobermorite ($\text{Ca}_5\text{Si}_6\text{O}_{17}\cdot 5\text{H}_2\text{O}$) at 29.7° , were only detected in the Fly Ash+GO group. Merlion et al. [31] mentioned that Clinotobermorite, a typical CSH mineral, has a condensed molecular structure which contributes to a better salt scaling resistance. Ismail et al. [32] found that a denser Al-substituted calcium silicate hydrate (C-A-S-H) mineral (analogy to Margarite) contributes to a higher durability under chloride exposure. This explains the fact that Fly Ash+GO showed the best performance in the wet/dry cycles, because GO activated the formation of these two pozzolanic hydrates to provide better resistance [33] to the salt attack.

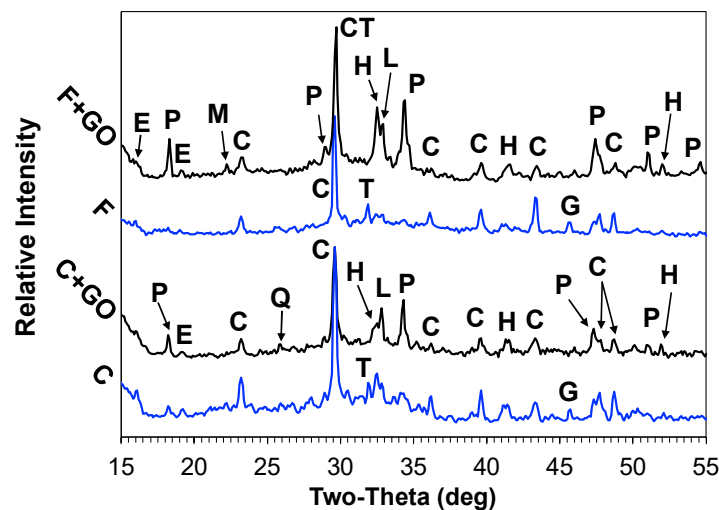


Fig. 6—XRD patterns of pervious concrete pastes after the deicer salt scaling test. C: calcite, CT: clinotobermorite, E: ettringite, G: gypsum, H: hatrurite, L: larnite, M: margarite, P: portlandite, Q: quartz, T: tobermorite.

NMR spectroscopic observation of different pastes

The chemical structure and ordering of hydration products are also important to elucidate the performance of fly ash and cement concrete during freeze/thaw and wet/dry tests. As such, ^{29}Si MAS NMR spectroscopy for pervious concrete samples at 56-day were performed and results are presented in Fig. 7. $\text{Q}^n(\text{mAl})$ notation ($n = 0-4$, $m = 0-n$) was used to describe the chemical bonding conditions of Si nuclei in the pastes, where n represents the number of adjacent Si linked directly to one Si-tetrahedron and m indicates the number of Al substitutions to the adjacent Si [28]. In Fig. 7, each spectrum was semi-quantitatively deconvoluted using a Gaussian function, the difference between experimental spectra and the sum of components was also provided at the bottom of figures as red lines. Table 5 provides the peak assignment, integrated area for each deconvoluted component and references used for the peak assignment. The structure example of each component was also provided in Table 5.

As shown in Fig. 7, after adding GO, the peak area of amorphous Q^4 in fly ash (around -113 ppm) decreased from 13.2% to 6.3%, suggesting GO promoted the dissolution of fly ash, which could provide more precursors for the formation of hydrates. Decrease of Q^2 at -85.5 ppm indicated the decrease of C-S-H gels since Q^2 Si mainly existed in C-S-H chains. Important increases of $\text{Q}^1(\text{J})$ (around -81.5 ppm) and Q^4 in Low Quartz (semi-crystalline quartz) [34] at -107.4 ppm were also marked in Fig. 7, indicating that GO promoted the formation of Jennite-like C-S-H [35,36] (containing a higher Ca-content than normal C-S-H) and Low Quartz phase. Overall, GO increased the total peak area of Q^3 and Q^4 from 47.0% to 54.6%, as such the polymerization degree of fly ash hydrates was increased by GO, therefore the GO-modified fly ash pervious concrete showed a better resistance to freeze/thaw and wet/dry cycles (in Fig. 3&5) than the ordinary fly ash pervious concrete.

NMR spectra of fly ash hydrates were also compared with that of cement hydrates to understand the difference in their resistance to the freeze/thaw and wet/dry cycles. As shown in Fig. 8a, 47% peak area of fly ash hydrates was on the network structure (Q^3 and Q^4) side, so fly ash hydrates were essentially Geopolymer. But more than 90% peak area of cement hydrates was on the chain structure (Q^1 and Q^2) side in Fig. 8b, as such cement hydrates were totally different from fly ash hydrates. Due to the cross-linking 3-D network in fly ash hydrates, its structure should be more stable than the linear chain structure of cement hydrates theoretically, which could explain why fly ash pervious concretes had a better resistance in the salt attack with respect to the chemical structure and ordering.

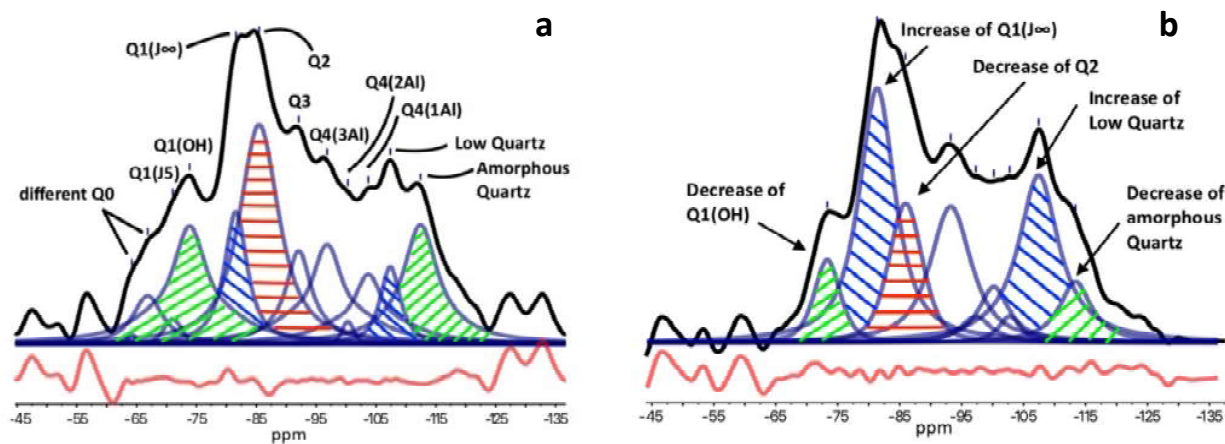


Fig. 7— ^{29}Si MAS NMR Spectra at 56-d for (a) Fly Ash paste; (b) Fly Ash + GO paste; X-axis unit: ppm.

a

b

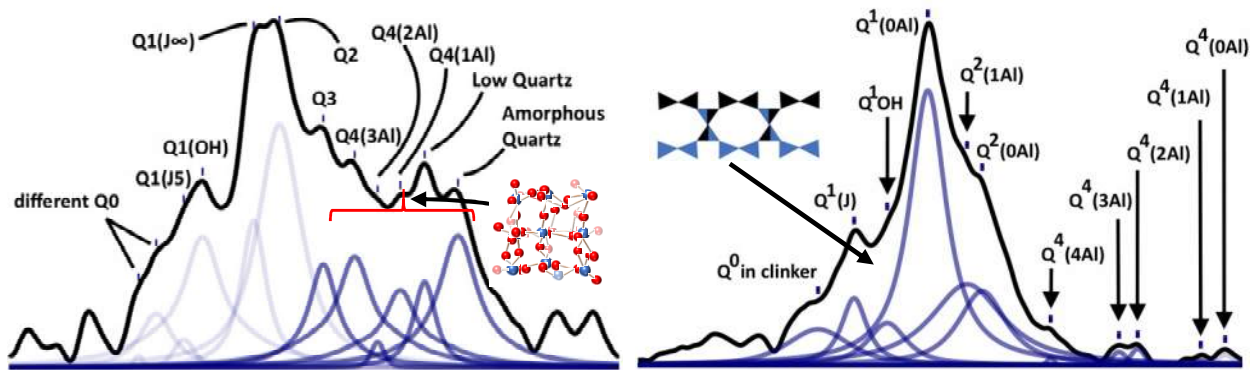


Fig. 8—²⁹Si MAS NMR Spectra comparison between (a) Fly Ash paste; (b) Cement paste.

Table 5—Integrated area percentage of de-convoluted NMR spectrum components in fly ash pastes

	Structure	Q ⁿ type	Fly Ash		Fly Ash+GO		Ref.
			ppm	area %	ppm	area %	
Q ⁴	3-D network	amorphous Q ⁴ in fly ash	-112.4	13.2	-113.4	6.3	[25,28,37,38]
		Q ⁴ (0Al) in low quartz	-107.4	4.3	-107.4	21.8	
		Q ⁴ (1Al)	-103.7	8.7	-102.7	1.8	
		Q ⁴ (2Al)	-100.3	0.6	-100.2	5.5	
		Q ⁴ (3Al)	-96.8	12.6	-97.3	2.6	
		Sum		39.4		38.0	
Q ³		Q ³	-92.1	7.6	-93.2	16.6	
		Sum		7.6		16.6	
Q ²		Q ² (0Al)	-85.5	23.6	-86.0	12.0	
		Sum		23.6		12.0	
Q ¹		Q ¹ (J∞)	-81.5	8.6	-81.4	27.6	[25,28,39]
		Q ¹ (OH)	-73.9	15.5	-73.3	5.8	
		Q ¹ (J5)	-71.0	1.0	-	-	
		Sum		25.1		33.4	
Q ⁰		Different Q ⁰ units	-66.9	4.1	-	-	[25,40]
			-64.2	0.2	-	-	
		Sum		4.3			
Total Qⁿ sum				100		100	

SUMMARY AND CONCLUSIONS

Fly ash and cement pervious concrete specimens were exposed to the freeze/thaw cycles and wet/dry cycles in NaCl solutions. The effects of exposure were evaluated based on the changes in the dynamic modulus of elasticity. XRD and NMR were employed to explain the difference in their performance in terms of mineralogy and chemical structure. The following conclusions are based on the test results and analyses presented in this work.

1. Due to the slow hydration of fly ash, the freeze/thaw resistance of GO-modified fly ash pervious concrete cured for 28 days was comparable to the cement pervious concrete cured for 14 days. GO improved the resistance to freeze/thaw cycles for both cement and fly ash pervious concretes.

2. Fly ash pervious concretes showed a better resistance to NaCl comparing with cement ones. Compared to the freeze/thaw test causing a rapid physical damage to pervious concrete, the salt attack caused specimens to deteriorate slowly. GO also improved the resistance to the NaCl attack for both cement and fly ash pervious concretes.
3. GO promoted the formation of semi-crystalline C–S–H (I) and C-A-S-H gels in fly ash hydrates, which provided a better resistance to the salt attack.
4. NMR is very useful to study the chemical structure and ordering of hydration products. The fly ash hydrates showed the network structure different from the chain structure of cement hydrates, which could explain why fly ash pervious concretes had a better resistance in the salt attack. GO also increased the polymerization degree of fly ash hydrates.
5. This laboratory study has demonstrated the feasibility of a more sustainable pervious concrete material made from mainly activated Class C fly ash (without the use of NaOH) and cured under ambient conditions.

ACKNOWLEDGMENTS

The funding support was provided by the USDOT Center for Environmentally Sustainable Transportation in Cold Climates (CESTiCC). The authors owe their thanks to Prof. Pizhong Qiao and Zhidong Zhou at WSU for help on freeze-thaw tests and Prof. Canxiong Guo at Beijing University of Chemical Technology for assistance in the use of NMR spectrometer. Boral, Lafarge, BASF and W.R. Grace kindly donated sample materials for this study. The technology reported has been protected by a non-provisional patent filed by Washington State University.

REFERENCES

- [1] V.R. Schaefer, M.T. Suleiman, K. Wang, J.T. Keavern, P. Wiegand, An overview of pervious concrete applications in stormwater management and pavement systems, *Civ. Constr. Environ. Eng.* Iowa State Univ. Ames IA. 50011 (2006). <http://www.rmc-foundation.org/images/PCRC%20Files/Hydrological%20%26%20Environmental%20Design/An%20Overvie w%20of%20Pervious%20Concrete%20Applications%20in%20Stormwater%20Management%20and%20Pav ement%20Systems.pdf> (accessed February 17, 2015).
- [2] C. Roskos, *Building Green: Development and evaluation of an environmentally friendly concrete*, Masters of Science, Montana State University, 2011.
- [3] A. Harwalkar, S. Awanti, Laboratory and Field Investigations on High-Volume Fly Ash Concrete for Rigid Pavement, *Transp. Res. Rec. J. Transp. Res. Board.* 2441 (2014) 121–127. doi:10.3141/2441-16.
- [4] Alkali-activated fly ashes A cement for the future, (n.d.).
- [5] M. Schneider, M. Romer, M. Tschudin, H. Bolio, Sustainable cement production—present and future, *Cem. Concr. Res.* 41 (2011) 642–650. doi:10.1016/j.cemconres.2011.03.019.
- [6] R. Minkara, *Beneficial Use of Ash in Concrete*, (2015).
- [7] W.-J. Fan, X.-Y. Wang, K.-B. Park, Evaluation of the Chemical and Mechanical Properties of Hardening High-Calcium Fly Ash Blended Concrete, *Materials.* 8 (2015) 5933–5952. doi:10.3390/ma8095282.
- [8] X. Guo, H. Shi, W.A. Dick, Compressive strength and microstructural characteristics of class C fly ash geopolymer, *Cem. Concr. Compos.* 32 (2010) 142–147. doi:10.1016/j.cemconcomp.2009.11.003.
- [9] M. Berry, J. Stephens, D. Cross, Performance of 100% fly ash concrete with recycled glass aggregate, *ACI Mater. J.* 108 (2011) 378–384.
- [10] I. Anderson, M.M. Dewoolkar, Laboratory Freezing-and-Thawing Durability of Fly Ash Pervious Concrete in a Simulated Field Environment, *ACI Mater. J.* 112 (2015). doi:10.14359/51687921.
- [11] X. Shi, M. Akin, T. Pan, L. Fay, Y. Liu, Z. Yang, Deicer Impacts on Pavement Materials: Introduction and Recent Developments, *Open Civ. Eng. J.* 3 (2009) 16–27. doi:10.2174/1874149500903010016.
- [12] J.J. Valenza, G.W. Scherer, A review of salt scaling: II. Mechanisms, *Cem. Concr. Res.* 37 (2007) 1022–1034. doi:10.1016/j.cemconres.2007.03.003.
- [13] A.M. Amde, S. Rogge, *Development of High Quality Pervious Concrete Specifications for Maryland Conditions*, 2013. <http://trid.trb.org/view.aspx?id=1244634> (accessed December 25, 2015).
- [14] Z. Yang, H. Brown, A. Cheney, Influence of Moisture Conditions on Freeze and Thaw Durability of Portland Cement Pervious Concrete, in: *Concr. Technol. Forum Focus Pervious Concr.*, Citeseer, 2006: pp. 24–25. <http://citeseerx.ist.psu.edu/viewdoc/download?doi=10.1.1.579.27&rep=rep1&type=pdf> (accessed August 27, 2016).
- [15] S. Lv, S. Ting, J. Liu, Q. Zhou, Use of graphene oxide nanosheets to regulate the microstructure of hardened cement paste to increase its strength and toughness, *CrystEngComm.* 16 (2014) 8508–8516. doi:10.1039/C4CE00684D.

- [16] K. Gong, Z. Pan, A.H. Korayem, L. Qiu, D. Li, F. Collins, C.M. Wang, W.H. Duan, Reinforcing Effects of Graphene Oxide on Portland Cement Paste, *J. Mater. Civ. Eng.* 27 (2015). doi:10.1061/(ASCE)MT.1943-5533.0001125.
- [17] N. Ranjbar, M. Mehrali, M. Mehrali, U.J. Alengaram, M.Z. Jumaat, Graphene nanoplatelet-fly ash based geopolymer composites, *Cem. Concr. Res.* 76 (2015) 222–231. doi:10.1016/j.cemconres.2015.06.003.
- [18] D. Li, M.B. Mueller, S. Gilje, R.B. Kaner, G.G. Wallace, Processable aqueous dispersions of graphene nanosheets, *Nat. Nanotechnol.* 3 (2008) 101–105.
- [19] G. Xu, J. Zhong, X. Shi, Influence of graphene oxide in a chemically activated fly ash, *Fuel* 226 (2018) 644–657.
- [20] ASTM C666 / C666M-15, Standard Test Method for Resistance of Concrete to Rapid Freezing and Thawing, ASTM International, West Conshohocken, PA, 2015.
- [21] ASTM C192/C192M, Standard Practice for Making and Curing Concrete Test Specimens in the Laboratory, ASTM International, West Conshohocken, PA, 2016.
- [22] ASTM C215-14, Standard Test Method for Fundamental Transverse, Longitudinal, and Torsional Resonant Frequencies of Concrete Specimens, ASTM International, West Conshohocken, PA, 2014.
- [23] V.R. Schaefer, K. Wang, M.T. Suleiman, J.T. Kevern, Mix Design Development for Pervious Concrete In Cold Weather Climates, Iowa State University, 2006.
- [24] D. Darwin, J. Browning, L. Gong, S.R. Hughes, Effects of deicers on concrete deterioration, *ACI Mater. J.* 105 (2008) 622–627.
- [25] I.G. Richardson, A.V. Girão, R. Taylor, S. Jia, Hydration of water- and alkali-activated white Portland cement pastes and blends with low-calcium pulverized fuel ash, *Cem. Concr. Res.* 83 (2016) 1–18. doi:10.1016/j.cemconres.2016.01.008.
- [26] H. Lee, R.D. Cody, A.M. Cody, P.G. Spry, Effects of various deicing chemicals on pavement concrete deterioration, in: -Cont. Transp. Symp. Proc., 2000: pp. 151–155. <http://www.ctre.iastate.edu/pubs/midcon/Lee.pdf> (accessed August 15, 2017).
- [27] Thomas Telford Bookshop - Civil Engineering Publications, (n.d.). http://www.thomastelford.com/books/bookshop_main.asp?ISBN=9780727725929 (accessed August 15, 2017).
- [28] D. Jeon, Y. Jun, Y. Jeong, J.E. Oh, Microstructural and strength improvements through the use of Na₂CO₃ in a cementless Ca(OH)₂-activated Class F fly ash system, *Cem. Concr. Res.* 67 (2015) 215–225. doi:10.1016/j.cemconres.2014.10.001.
- [29] M. Schmidt, E. Fehling, Christoph Glotzbach, Ultra-High Performance Concrete and Nanotechnology in Construction. Proceedings of Hipermat 2012. 3rd International Symposium on UHPC and Nanotechnology for High Performance Construction Materials, kassel university press GmbH, 2012.
- [30] I.G. Richardson, Model structures for C-(A)-S-H(I), *Acta Crystallogr. Sect. B Struct. Sci. Cryst. Eng. Mater.* 70 (2014) 903–923. doi:10.1107/S2052520614021982.
- [31] S. Merlino, E. Bonaccorsi, T. Armbruster, Tobermorites: Their real structure and order-disorder (OD) character, *Am. Mineral.* 84 (1999) 1613–1621.
- [32] I. Ismail, S.A. Bernal, J.L. Provis, R. San Nicolas, D.G. Brice, A.R. Kilcullen, S. Hamdan, J.S.J. van Deventer, Influence of fly ash on the water and chloride permeability of alkali-activated slag mortars and concretes, *Constr. Build. Mater.* 48 (2013) 1187–1201. doi:10.1016/j.conbuildmat.2013.07.106.
- [33] B. Lothenbach, K. Scrivener, R.D. Hooton, Supplementary cementitious materials, *Cem. Concr. Res.* 41 (2011) 1244–1256. doi:10.1016/j.cemconres.2010.12.001.
- [34] G.E. Kowalczyk, Quantitative determination of crystalline silica utilizing solid state silicon-29 NMR, (1992). <http://preserve.lehigh.edu/cgi/viewcontent.cgi?article=1121&context=etd> (accessed April 29, 2017).
- [35] P. Rejmak, J.S. Dolado, M.J. Stott, A. Ayuela, ²⁹Si NMR in Cement: A Theoretical Study on Calcium Silicate Hydrates, *J. Phys. Chem. C* 116 (2012) 9755–9761. doi:10.1021/jp302218j.
- [36] I.G. Richardson, Tobermorite/jennite- and tobermorite/calcium hydroxide-based models for the structure of C-S-H: applicability to hardened pastes of tricalcium silicate, β-dicalcium silicate, Portland cement, and blends of Portland cement with blast-furnace slag, metakaolin, or silica fume, *Cem. Concr. Res.* 34 (2004) 1733–1777. doi:10.1016/j.cemconres.2004.05.034.
- [37] Z. Peng, K. Vance, A. Dakhane, R. Marzke, N. Neithalath, Microstructural and ²⁹Si MAS NMR spectroscopic evaluations of alkali cationic effects on fly ash activation, *Cem. Concr. Compos.* 57 (2015) 34–43. doi:10.1016/j.cemconcomp.2014.12.005.

- [38] M. Criado, A. Fernández-Jiménez, A. Palomo, I. Sobrados, J. Sanz, Effect of the SiO₂/Na₂O ratio on the alkali activation of fly ash. Part II: ²⁹Si MAS-NMR Survey, Microporous Mesoporous Mater. 109 (2008) 525–534. doi:10.1016/j.micromeso.2007.05.062.
- [39] J. Moon, M.M.R. Taha, K.-S. Youm, J.J. Kim, Investigation of Pozzolanic Reaction in Nanosilica-Cement Blended Pastes Based on Solid-State Kinetic Models and ²⁹Si MAS NMR, Materials. 9 (2016) 99. doi:10.3390/ma9020099.
- [40] LE SAOUT Gwenn, Nuclear Magnetic Resonance, (2010).

LIST OF NOTATIONS

E: modulus of elasticity.
P_{ft}: the relative dynamic *E* for freeze/thaw testing.
P_{wd}: the relative dynamic *E* for wet/dry testing.

LIST OF CAPTIONS FOR TABLES AND FIGURES

- Table 1**—Physical and chemical properties of the fly ash and glass powder (% wt.)
- Table 2**—Pervious concrete material proportions
- Table 3**—Average transverse resonance frequency (Hz) and coefficients of variation for specimens in freeze/thaw cycles
- Table 4**—Average transverse resonance frequency (Hz) and coefficients of variation for specimens in wet/dry cycles
- Table 5**—Integrated area percentage of de-convoluted NMR spectrum components in fly ash pastes
- Fig. 1**—Ultrasonication of GO suspension.
- Fig. 2**—Pervious concrete specimens in freezing-and-thawing chamber (undrained).
- Fig. 3**—Relative dynamic modulus of elasticity (*P_{ft}*) versus number of freeze/thaw cycles.
- Fig. 4**—Failed specimens after the freeze/thaw test, (a) Fly Ash_28d group; (b) Fly Ash+GO_28d group; (c) Cement+GO_14d group; (b) Cement_14d group.
- Fig. 5**—Relative dynamic modulus of elasticity (*P_{wd}*) versus number of wet/dry cycles in NaCl solutions.
- Fig. 6**—XRD patterns of pervious concrete pastes after the deicer salt scaling test. C: calcite, CT: clinotobermorite, E: ettringite, G: gypsum, H: hatrurite, L: larnite, M: margarite, P: portlandite, Q: quartz, T: tobermorite.
- Fig. 7**—²⁹Si MAS NMR Spectra at 56-d for (a) Fly Ash paste; (b) Fly Ash + GO paste; X-axis unit: ppm.
- Fig. 8**—²⁹Si MAS NMR Spectra comparison between (a) Fly Ash paste; (b) Cement paste.

SP-336-4

Multifunction Green Corrosion Inhibiting Admixtures for Mortar under Chloride Environment

Yu Jiang, Gang Xu, Zhipeng Li, and Xianming Shi

Synopsis: In this study, we tested compressive strength, rheology, initial setting time and transport properties of mortar samples mixed with green corrosion-inhibiting admixtures were tested. Four types of green corrosion inhibitors were adopted, which were extracted from peony leave, Kentucky blue grass, sugar beet leave and dandelion. All of them affected the compressive strength adversely, but improved other properties of mortar samples. Resistance of mortar to chloride induced corrosion was evaluated using open circuit potential (OCP), electrochemical impedance spectroscopy (EIS) and linear polarization resistance (LPR) techniques. The results indicated that these green corrosion-inhibiting admixtures provided promising inhibiting performance under chloride environment. The results also suggested these green corrosion-inhibitors have the potential to be used as multifunction corrosion inhibitors for concrete, such as serving as water reducer and set retarder. Future work would focus on chemical mechanism of green corrosion inhibitors and the comparative evaluation of these green corrosion inhibitors with other commercially available corrosion inhibitors.

Keywords: green corrosion inhibitor, chloride induced corrosion, setting time, flowability, water absorption, gas permeability, EIS, LPR

ACI student member **Yu Jiang** is a M.S. Candidate in the Department of Civil and Environmental Engineering, Washington State University. His research interests include sustainable advances for reinforced concrete structure under chloride environment, nanotechnology application in civil engineering and structural engineering.

ACI student member **Gang Xu** has earned his Ph.D. in Structural Engineering (2018), at the Department of Civil and Environmental Engineering, Washington State University. His research interests include sustainable and innovative concrete materials, nanotechnology application in building materials, structural engineering and bridge health monitoring.

ACI student member **Zhipeng Li** is a Ph.D. student in the Department of Civil and Environmental Engineering, Washington State University. His research interests include sustainable approaches to ultrahigh performance concrete, the use of nanotechnology to enable waste utilization in concrete, and durability of reinforced concrete structures.

ACI member **Xianming Shi** is an Associate Professor in the Department of Civil and Environmental Engineering, Washington State University. Dr. Shi holds his Ph.D. in Chemistry from the Chinese Academy of Sciences and a 2nd M.Sc. in Industrial & Management Engineering from Montana State University. His research interests include sustainable infrastructure materials, infrastructure preservation and rehabilitation, multiscale characterization and modification, corrosion protection, and infrastructure durability.

INTRODUCTION

Concrete provides a passive corrosion protection for the embedded steel rebars on account of the high-alkaline environment [1]. However, improper design, an aggressive service environment and other facts may accelerate the ingress of chloride ions or other corrosion-causing substance and thus lead to the corrosion of reinforcement steel [2], [3]. Chloride ions from marine environment, deicers and other sources may lead to severe corrosion on reinforced concrete (RC) bridges and RC pavements [4]. After corrosion has been initiated, the volume expansion of corrosion products may induce cracks, and thus reduce the service life and load capacity of the reinforced concrete. Furthermore, these cracks will increase the diffusion of chloride ions into the concrete. As a result, corrosion may propagate even faster [5]. On the other hand, corrosion also can result in loss of the steel reinforcement cross sectional area, which in turn reduce the load capacity of RC structures. Therefore, premature failure of RC structures may occur due to these facts.

The addition of a corrosion inhibiting admixture is a preferred method to prevent chloride-induced rebar corrosion in RC structures [6]. It has the advantages including easy application, cost effectiveness and less side effects compared to other traditional corrosion prevention and protection methods. For instance, the epoxy coatings for rebar are prone to aging, damage and degradation; the use of stainless steel or galvanized reinforcement in concrete results in substantial environmental footprints such as air pollution during their production period [7].

One challenge is that many corrosion inhibitors are toxic and thus may induce harmful health effects and cause environmental concerns [8],[9],[10]. For example, some corrosion inhibiting admixtures will cause temporal or

permanent damage to human organs like kidney and liver [11]. Efforts have been made to use green corrosion inhibiting admixtures, such as inhibitors extracted from plants, to mitigate this problem.

Recent studies on green corrosion inhibitors have shown that they are highly effective and environmentally friendly compared to organic and inorganic inhibitors. Nazari et al. [12] developed a green corrosion inhibitor from waste peony leaves which has a good inhibition effect to protect carbon steel from NaCl. Raja et al. [9] reviewed recent studies of natural corrosion inhibitors, including opuntia ficus indica, arghel extract, bambusa arundinacea, rhizophora mangle and vernonia amygdalina. Besides the inhibitors extracted from natural plants, other green corrosion inhibiting admixtures were also studied. For instance, an eco-friendly biopolymer corrosion inhibiting admixture was investigated and proved to be effective [13],[14].

Based on the successful development of peony-leave based corrosion inhibitors [12], this study further investigated four types of liquid admixtures as green corrosion inhibitors, which were extracted from peony leave, Kentucky blue grass, sugar beet leave and dandelion, respectively. The influence of these four green admixtures on mortar properties were evaluated. Test methods including 7, 14, 28, and 56 days compressive strength test, rheology test, setting time test, water absorption test, gas permeability test and rapid chloride migration (RCM) test were employed. Furthermore, the inhibiting efficiency of the corrosion inhibitors were measured using electrochemical methods (open circuit potential (OCP) [15], electrochemical impedance spectroscopy (EIS) [16] and linear polarization resistance (LPR) [17]).

EXPERIMENTAL

Materials

An ASTM C150-07 [18] Type I/II low-alkali Portland cement was used in this study. Siliceous sand, complying with ASTM C144 [19], was used as fine aggregates. Steel rebar in 3/8 in. (9.5 mm) diameter, complying with ASTM A1035 [20], was used as concrete reinforcement. Four types of liquid corrosion inhibitors were extracted from peony leave (PL), Kentucky blue grass (KG), sugar beet leave (SL) and dandelion (D), respectively, through a zero-waste chemical/biological process [12].

Sample Preparation

Table 1 listed the material proportion of four groups of mortar mixed with green corrosion inhibiting admixtures and a control group. The cement and sand were mixed first in a concrete mixer for 1.5 minutes. Then green admixtures were added into water before mixing with the cement and sand for another 1.5 minutes. The fresh mixture was cast into 2 in. ×4 in. (5cm ×10cm) cylindrical molds for reinforced mortar specimens and 4 in. ×8 in. (10cm ×20cm) cylindrical molds for Rapid Chloride Migration (RCM) test specimens. All the specimens were demolded after curing at room temperature for 24 hours. They were then cured in a moisture container at 23°C with relative humidity of over 95% for 27 additional days. Mortar samples for corrosion monitoring test had 3/8 in. (9.5mm) diameter steel rebar embedded at the center of cylinder, and 1 in. (25mm) cover was maintained for the embedded rebar.

Measurements

Compressive Strength Test

Mortar cylinders of size 2 in. x 4 in. (5cm ×10cm) were prepared using cement and sand in ratio of 1:2.48, with a water-cementitious material ratio at (w/cm) of 0.4. Inhibitor admixtures in the amount of 1%, 2% and 3% by mass

of cement were added. They were then tested for compressive strength at 3, 7, 14, 28 and 56 days, in accordance with ASTM C109 [21] specification.

Table 1—Mix Proportion of mortar mixed with four green corrosion inhibitor and control sample

	Dosage	Cement kg(lb)	Sand kg(lb)	Water L(gal)	Admixture g(oz)	Water reducer mL(in ³)
Peony Leave	1.00%	1.48 (3.263)	3.68 (8.113)	0.60 (0.159)	14.80 (0.522)	7.42 (0.251)
	2.00%	1.48 (3.263)	3.68 (8.113)	0.54 (0.143)	29.60 (1.044)	7.42 (0.251)
	3.00%	1.48 (3.263)	3.68 (8.113)	0.47 (0.124)	44.40 (1.566)	7.42 (0.251)
Grass	1.00%	1.48 (3.263)	3.68 (8.113)	0.65 (0.172)	14.80 (0.522)	7.42 (0.251)
	2.00%	1.48 (3.263)	3.68 (8.113)	0.63 (0.166)	29.60 (1.044)	7.42 (0.251)
	3.00%	1.48 (3.263)	3.68 (8.113)	0.61 (0.161)	44.40 (1.566)	7.42 (0.251)
Sugar	1.00%	1.48 (3.263)	3.68 (8.113)	0.65 (0.172)	14.80 (0.522)	7.42 (0.251)
	2.00%	1.48 (3.263)	3.68 (8.113)	0.63 (0.166)	29.60 (1.044)	7.42 (0.251)
	3.00%	1.48 (3.263)	3.68 (8.113)	0.61 (0.161)	44.40 (1.566)	7.42 (0.251)
Dandelion	1.00%	1.48 (3.263)	3.68 (8.113)	0.65 (0.172)	14.80 (0.522)	7.42 (0.251)
	2.00%	1.48 (3.263)	3.68 (8.113)	0.64 (0.169)	29.60 (1.044)	7.42 (0.251)
	3.00%	1.48 (3.263)	3.68 (8.113)	0.63 (0.166)	44.40 (1.566)	7.42 (0.251)
Control	-	1.48 (3.263)	3.68 (8.113)	0.67 (0.177)	-	7.42 (0.251)

Rheology Test

The rheology tests were used to characterize the fresh concrete mixtures. The K-slump and workability tests were performed on the samples in accordance with ASTM C1362 [22] to determine the effect of the green admixtures on the flow-ability, workability and the degree of compaction of fresh mortar.

Setting Time Test

The setting times of the cementitious pastes were determined with a concrete penetrometer following the procedure set out in the ASTM C403 [23]. The point of initial set is reached when the penetration value is 500 pounds per square inch (psi).

Water Absorption Test

Water absorption test in accordance with ASTM C1585 [24] was performed to evaluate the water resistance of the mortar specimens with three types of surface treatments. Before testing, all specimens were vacuum oven-dried at 60°C for 72 hours. After that, the specimens were moved to a sealable container at 23°C for 24 hours.

The test was performed by allowing one surface of the specimen to be in contact with water of 0.4 in. (10 mm) depth using a support. Using the supporting frame and keeping the water level at 0.04-0.12 in. (1-3 mm) above the top

of the support allowed continuous contact between the specimen surface and the water without changing the water depth throughout the test. The sides of the test samples were carefully sealed to create unidirectional flow through the samples. The weight of the specimen was recorded at fixed time intervals. The absorption coefficient k_s ($\text{g}/\text{cm}^2 \cdot \text{s}^{1/2}$) was then determined using the following equation:

$$Q/A = k_s \sqrt{t} \quad (1)$$

Where Q is the amount of absorbed water (g), A is the cross-sectional area of the specimen that was in contact with water (cm^2), and t is the time (s).

Gas Permeability Test

Gas permeability test of concrete was conducted to evaluate the impermeability of the three types of surface-treated concrete specimens. The test was performed using liquid methanol as the gas source to determine the gas transport properties. Specimens were vacuum oven-dried at 60°C for 72 hours to remove the moisture within specimen. Subsequently, the specimen was placed and sealed on the top of a cell with epoxy sealant to avoid any leakage of methanol vapor. The initial weight of the whole specimen setup including the cell, methanol liquid, specimen, and epoxy sealant was measured at the beginning of the test.

The values of mass variation versus time due to the vaporization of methanol liquid at a constant 60°C water bath temperature during the test were continuously recorded at each time interval until a steady-state mass loss was reached. The gas permeability coefficient k (m^2) was then calculated using the following equations.

$$pv = 10^{\left(8.0809 - \frac{1582.2}{239.76 + T}\right)} \quad (2)$$

$$\eta = 10^{-7} (4.7169T^{0.618} - 99e^{-8.7593 \cdot 10^{-4}T} + 94e^{-7.916 \cdot 10^{-3}T} + 5) \quad (3)$$

$$Q = \frac{266 \cdot 10^{-3} m'}{10^{\left(8.0809 - \frac{1582.2}{239.76 + T}\right)}} T \quad (4)$$

$$k = \frac{2L\eta P_2 Q}{A(P_1^2 - P_2^2)} \quad (5)$$

where P_v is the absolute pressure of vapor (N/m^2); T is the absolute temperature (K); g is the dynamic viscosity (N/m^2); Q is the volumetric flow rate (m^3/s); m' is the rate of mass loss (g/s); P_1 is the inlet pressure (N/m^2); P_2 is the outlet pressure (N/m^2); L is the length of the sample (m); and A is the cross-sectional area perpendicular to the flow direction (m^2).

Corrosion Monitoring

OCP, EIS and LPR tests were conducted for electrochemical corrosion analysis of green admixtures. The specimens were saturated in a NaCl solution with concentration of 3.5% and under freeze/thaw cycling. The EIS & LPR equipment used included PARSTAT MC multichannel potentiostat, a platinum electrode as counter electrode and an Ag/AgCl electrode as reference. By applying sinusoidal perturbations with a frequency from 100 kHz to 0.005Hz, the working electrode was polarized by ± 10 mV around its OCP and the current response vs. the applied voltage was

recorded to produce the EIS spectrum.

The LPR curves were measured within $E_{ocp} \pm 20$ mV at a scan rate of 0.167 mV/s. Representing the slope of the polarization curve, the polarization resistance, R_p , can be calculated by:

$$R_p = \Delta V / \Delta I \quad (6)$$

Where ΔV and ΔI represent the voltage and current increments, respectively, in the linear portion of the polarization curve at $i = 0$. LPR measurements were used to calculate the corrosion current density by the Stern-Geary equation:

$$i_{corr} = \beta_a \beta_c / [2.303(\beta_a + \beta_c) R_p] = B / R_p \quad (7)$$

Where i_{corr} is the corrosion current density, β_a is the anodic Tafel slope, β_c is the cathodic Tafel slope, and B is a constant related to β_a and β_c . In this study, a tentative value of 26 mV for the B constant was used.

RCM Test

Follow the NT BUILD 492 [25], Two cylindrical samples in size of ϕ 2 in. \times 2 in. (ϕ 50mm \times 50mm) were sliced from the original mortar specimens in size of ϕ 2 in. \times 8 in. (ϕ 50mm \times 200mm) at the age of 27 days for the RCM test (two specimens from each core, 0.4 in.–0.8 in. (10mm–20 mm) of the outermost surfaces of each core were cut off) and stored in water. One day prior to the RCM test, each series of the test samples was saturated with saturated limewater under vacuum conditions. The vacuum-saturation was performed following the procedure described in: surface-dry samples were placed vertically in a desiccator connected to a vacuum-pump and a pressure of 40 mbar was applied for 3 h. Then, with the vacuum pump still running, the desiccator was slowly filled with saturated limewater to immerse all the samples completely. After that, for an additional hour, the vacuum was maintained before allowing air to re-enter the desiccator. The samples were kept in the solution for about 18 h. The RCM test was performed on the saturated samples at the age of 28, 29 and 30 days. Power sources with constant voltage outputs (adjustable in the range of 0–80 V, accuracy of 0.05 V) were used. Four mortar samples were tested at the same time. The used volume of the catholyte (10% NaCl aq. solution) was about 14 L (3.70 gal) while the volume of the anolyte (0.3 M NaOH solution) was approximately 0.3 L (0.08 gal) per test specimen. The electrolytes were refreshed after each series of experiments. After the migration test, three mortar samples were split and sprayed with a 0.1 M AgNO_3 solution to determine the penetration depth of chlorides, while the total chloride concentration profile was measured on the fourth sample.

RESULTS AND DISCUSSION

Compressive Strength test

Compressive strength values of specimens that have been cured for 56 days are given in Fig. 1. The peony leave group had the least side effect on strength, with an approximately 0.2% compressive strength reduction at 28 days when mixed with 1% PL-inhibitor. For both early age strength and long-term strength, the 1% added PL-inhibitor also had the minimum influence, with 8% reduction at 7 days and 4% reduction at 56 days. When more PL-inhibitor (3%) was mixed in the mortar, the strength decreased by 22% at 7 days, 7% at 28 days and 9% at 56 days. However, the dandelion group decreased the compressive strength by nearly 20% at 28 days when 1% D-inhibitor added into the mortar. The 28 days compressive strength of samples with 3% D-inhibitor also dropped 28% compared to the control group, which had the most significant side effect on mortar samples. The other two inhibitors (KG-inhibitor and SL-inhibitor) also reduced the compressive strength, but in an acceptable range. The reduction of compressive strength

caused by different corrosion inhibitors was summarized in Table 2.

Compared to some green corrosion inhibiting admixtures for concrete, four types of inhibitors tested in this study had promising performance. For example, the 3% mixed calcium palmitate inhibitor was reported to reduce 50% compressive strength of concrete at 7 days and 40% at 28 days [26]. However, green corrosion inhibitors made of *Bambusa arundinacea* were proved to be able to improve the compressive strength at both early stage and long-term age [10]. Further studies can focus on the chemical mechanisms that reduce the strength of mortar mixed with these four green corrosion inhibitors, and the method to mitigate this strength reduction.

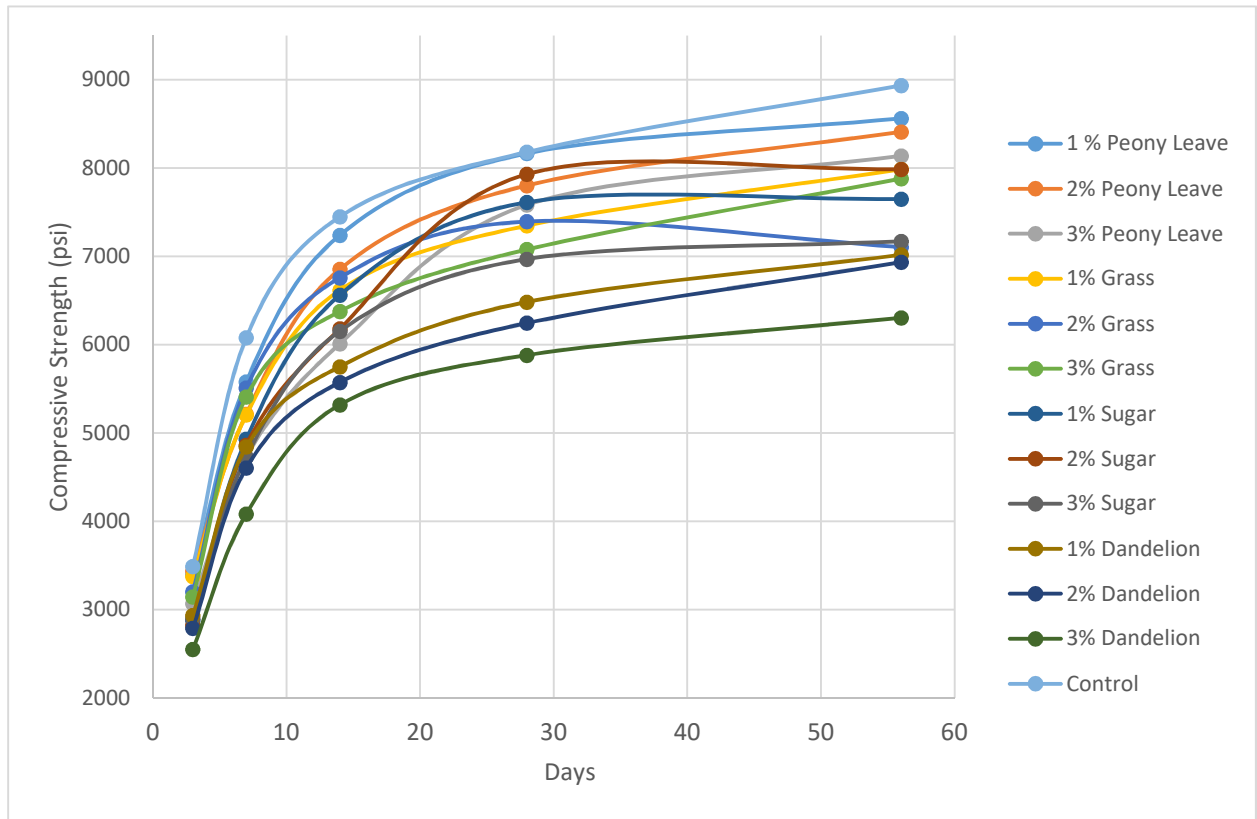


Fig.1—Compressive strength of mortar cylinders

Table 2—Strength reduction of mortar samples

Dosage	Peony Leave			Grass			Sugar Beet			Dandelion		
	1%	2%	3%	1%	2%	3%	1%	2%	3%	1%	2%	3%
3d	2.7	1.5	12.1	3.2	8.2	9.9	17.4	19.0	16.9	15.9	20.1	26.9
7d	8.2	14.2	22.2	14.3	9.3	11.0	18.9	20.0	22.2	20.3	24.3	32.8
14d	2.8	8.0	19.3	11.2	9.3	14.4	11.9	17.0	17.4	22.8	25.2	28.6
28d	0.2	4.6	7.3	10.2	9.6	13.5	7.0	3.1	14.8	20.8	23.7	28.1
56d	4.2	8.1	8.9	11.7	20.5	11.8	14.4	10.6	22.0	21.5	22.4	29.4

Rheology test

Workability change with time is also of significance in practice for transportation and casting of concrete before the initial set. The workability retention may be evaluated by the change in rheological parameters with time. K-slump values can reflect the flowability of fresh mortar or concrete.

The results of rheology properties are shown in Fig. 2 and Fig. 3. The control group had the K-slump value of 5.5 and workability value of 3.75. It shows that PL-inhibitor and KG-inhibitor could significantly increase the flowability and workability of fresh mortar. 3% added PL-inhibitor could increase the workability by approximately 1.5 and K-slump by 5. The 3% KG-inhibitor could improve the workability by 1 and K-slump by 0.8, approximately. However, D-inhibitor had a negative influence and reduced the workability by 40% and K-slump by 20%.

Compared with other admixtures improving the rheology of mortar and concrete, the PL-inhibitor and KG-inhibitor are also competitive. Commercial available water reducer could potentially improve the slump by 40%. The ultrafine fly ash (UFFA), as a kind of mineral admixture which could partially replace the water reducer, was able to increase the slump by 6% maximum [27]. The series of polycarboxylic acid-based copolymers with block and graft groups of polyethylene oxide (PEO) chains could increase the slump by a maximum of 26% [28].

It is well-known that an increase in slump flow signifies greater deformability of fresh concrete and higher slump flow is generally the result of a reduction of the yield stress in fresh concrete [29]. Yield stress results of fresh concrete could be further used to shed light on the improved rheological behavior of mortar samples with the green admixtures incorporated [30]. Also, more experimental groups with different water/binder ratios could be explored to better understand the benefits of green admixtures.

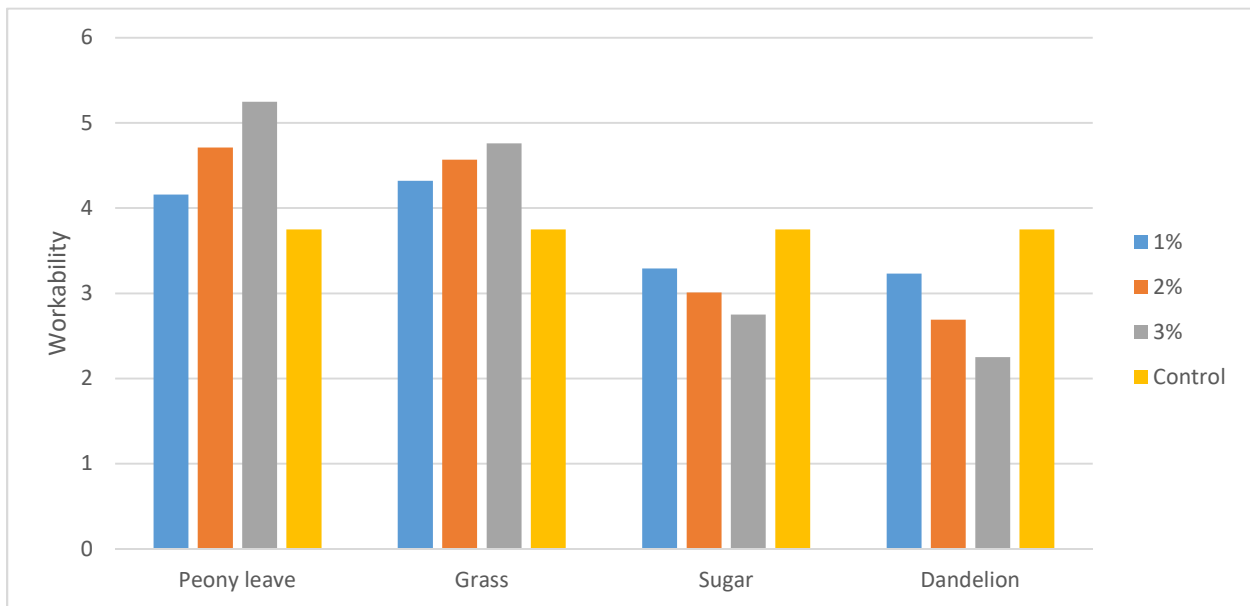


Fig. 2—Workability of mortar samples

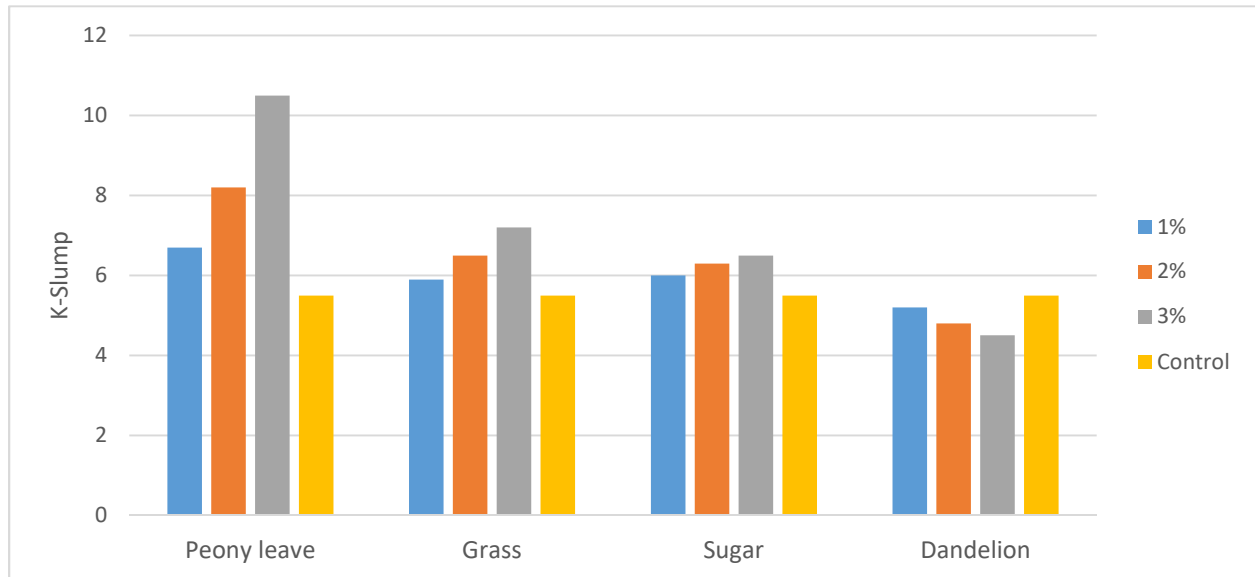


Fig. 3—K-Slump of mortar samples

Initial Setting time test

Initial setting time is a parameter that showing the stiffening of the mortar and concrete. The initial setting time of four types of green admixtures with 1%, 2% and 3% by weight of cement are shown in Fig. 4. The control group's setting time was 357 minutes. Experimental results showed that all four green admixtures could increase the initial setting time of mortar. The sugar beet group had the most significant increase compare to other groups, almost increasing the initial setting time by 47% compared with the control group, when 3% SL-inhibitor. The dandelion group had the least impact on setting time, with only an approximate maximum 11% increase.

As the concentration of the green admixtures increased in the mortar samples, the settings times of mortar with PL-, KG- and SL-inhibitors increased significantly. On the other hand, the D-inhibitor only induced a relatively small increase in the initial setting time (Fig. 4).

The green admixtures used in this study also have the potential to be used as set retarders to slow the hydration of concrete for large or difficult pours in construction. Borogypsum, which is a newly studied set retarder in Portland cement, could increase the initial setting time by 32% [31]. Phosphogypsum, another widely investigated set retarder for cement could potentially triple the setting time of cements [32]. Triethanolamine (TEA), which is commonly used in concrete, has the potential to produce retardation of concrete initial setting by 44% [33]. Thus, green admixtures in this study, such as SL-inhibitor resulting in 47% increase in setting time, could be further developed as a commercial set retarder.

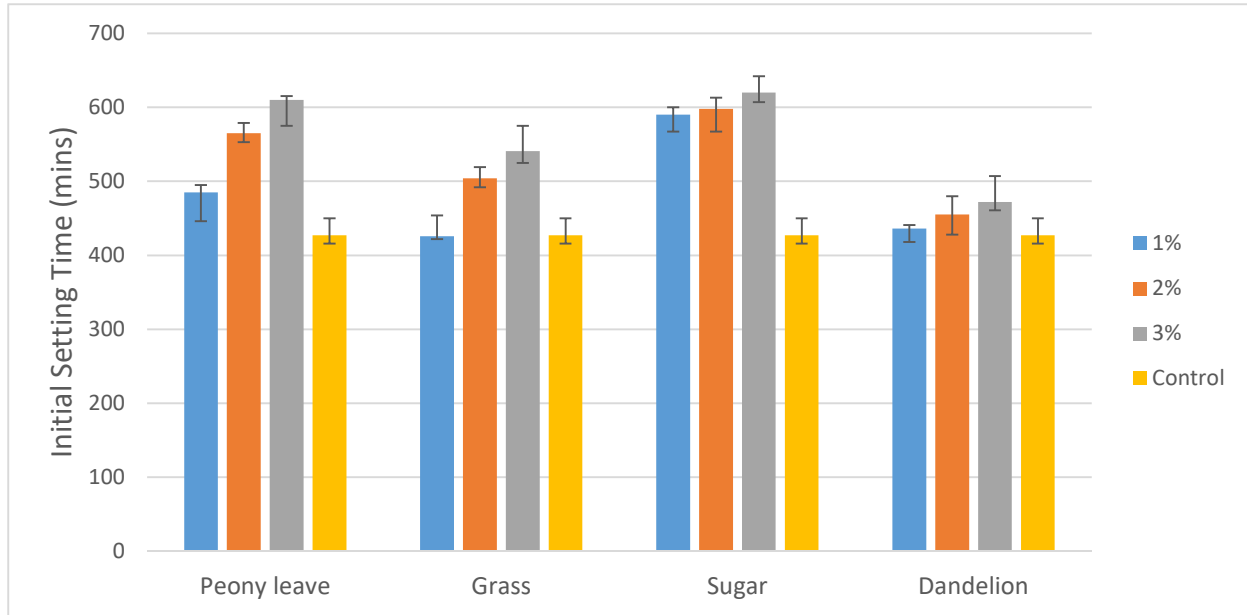


Fig. 4—Initial setting time of mortar samples

Transport Properties

Water absorption and gas permeability are two important transport parameters related to corrosion. The rate of water absorption is closely related to the durability and service life of concrete which often goes through wet/dry cycling in the service. The higher the water absorption rate of the concrete, the more rapidly it is likely to deteriorate. Gas permeability has a close relationship to the chloride diffusion coefficient of concrete, which is an indicator of the risk of rebar corrosion in RC structures. Gas permeability is also related to the resistance of concrete to carbonation.

The water absorption rate and gas permeability coefficient are illustrated in Fig. 5 and Fig. 6. The experimental result indicated that the use of green admixtures had very little influence on these transport properties. Only the KG-inhibitor decreased the water absorption rate by more than 50%. However, the transport properties of mortar were not influenced significantly by other green admixtures, indicating that the samples with PL-, SL- and D-inhibitors added remain good resistance to the ingress of damage sources such as chloride ions or sulphate attacks. Microstructural analysis may be investigated to analyze the influence of green corrosion inhibiting admixtures on mortar samples. Hence, the threats of influence on properties of mortar or concrete could be mitigated.

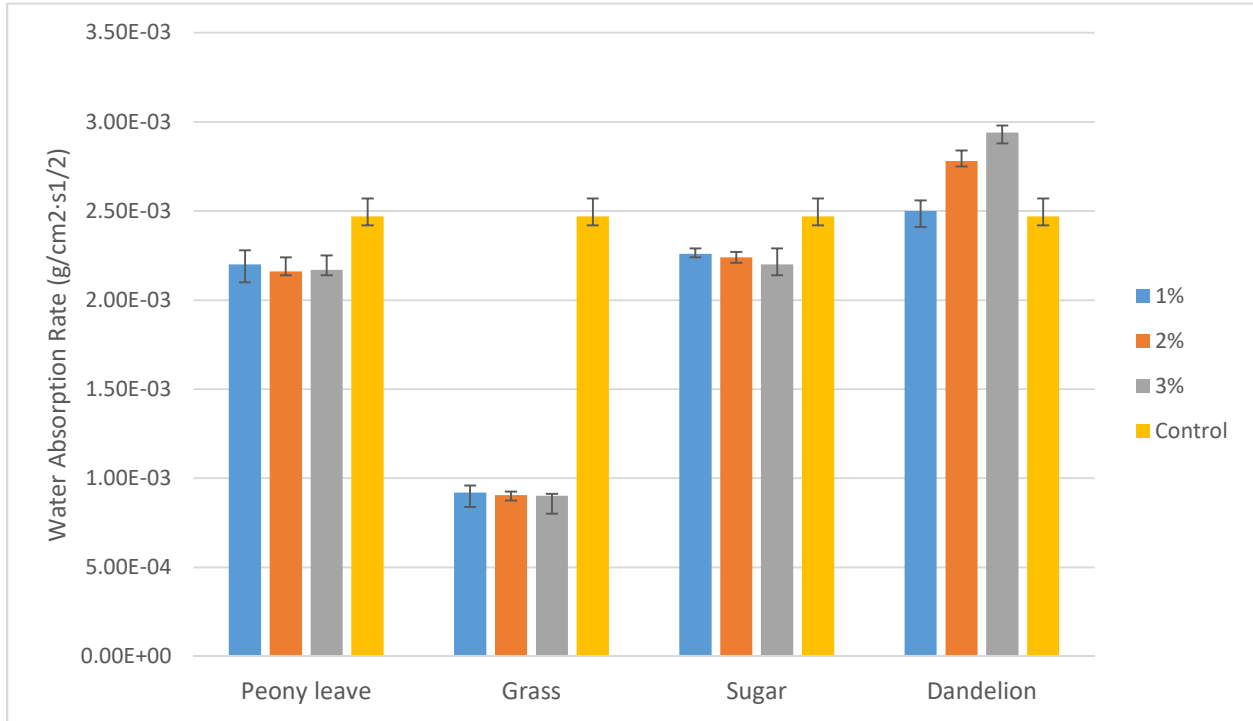


Fig. 5—Water absorption rate of mortar samples

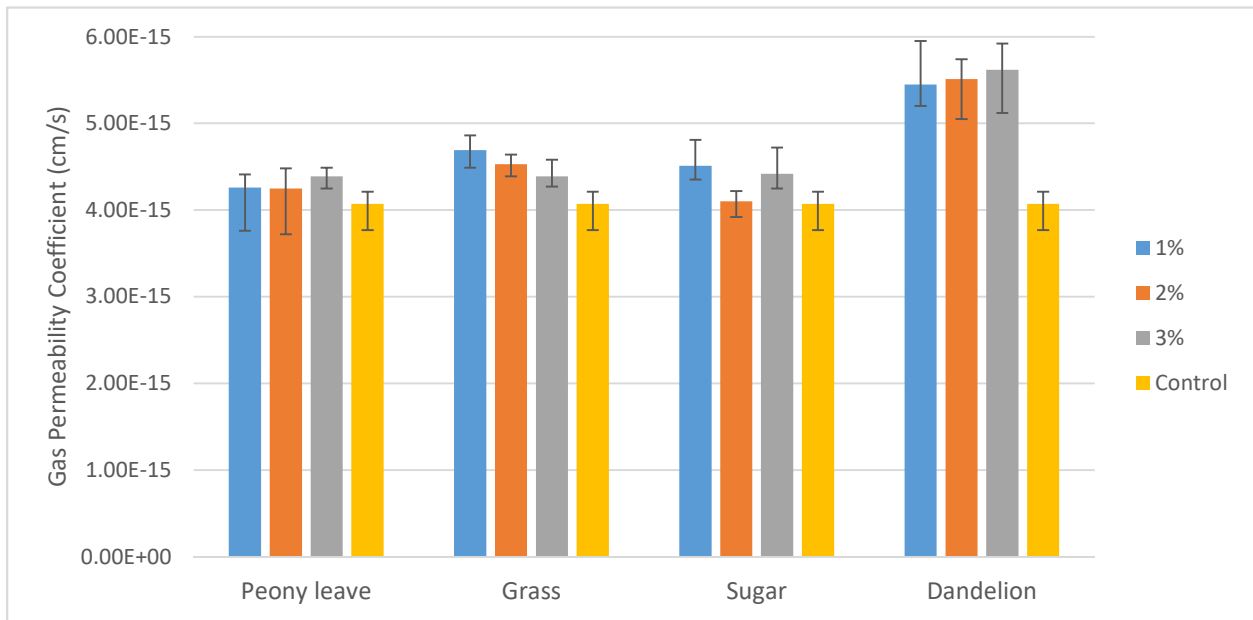


Fig. 6—Gas permeability of mortar samples

Corrosion Monitoring

Fig. 7 shows the open circuit potential versus time of immersion in NaCl solution for the steel reinforcing embedded in the mortar samples mixed with the four types of green admixtures at two different dosages. All the OCP readings started within the low level of risk of corrosion, ranged from -33mV to -87 mV. After 3 days of immersion

with F/T cycles, the OCP value of the control group dropped below -270 mV, which had the medium to high risk of corrosion. The dandelion, peony leave and sugar groups had slightly better performance, and took 3 to 7 days to reach the medium risk level. The grass group had the best performance that the OCP decreased to -270mV after 36 days of immersion. Note that for the 3% dandelion group, OCP readings increased sharply after 7days. The grass groups also had certain regain of OCP value during the immersion.

Compared to OCP readings, current density calculated from EIS or LPR curve is a much more reliable indicator to decide if the corrosion has been initiated. Fig. 8 shows the equivalent circuit model used to fit EIS curves. Fig. 9 gives the EIS spectra for control group and grass group in 7 days as a demonstration. Fig. 10 illustrates the time taken to initiate corrosion of steel rebar when i_{corr} reached $0.1\mu A/cm^2$, calculated from both EIS and LPR value. Corrosion initiated in control group after 7 days of immersion in NaCl. The grass group had the best performance, with 43 days resistance to chloride induced corrosion. The 3% D-inhibitor mixed mortar also had promising inhibition performance, and took 36 days to initiate corrosion of steel reinforcement imbedded in the specimens. To conclude, mortar with 1%, 3% added grass and 3% added dandelion had the best corrosion inhibition efficiency. More experimental study could be taken to compare the inhibition efficiency of green admixtures with other commercial inhibiting admixtures to provide more promising value of the green inhibitors.

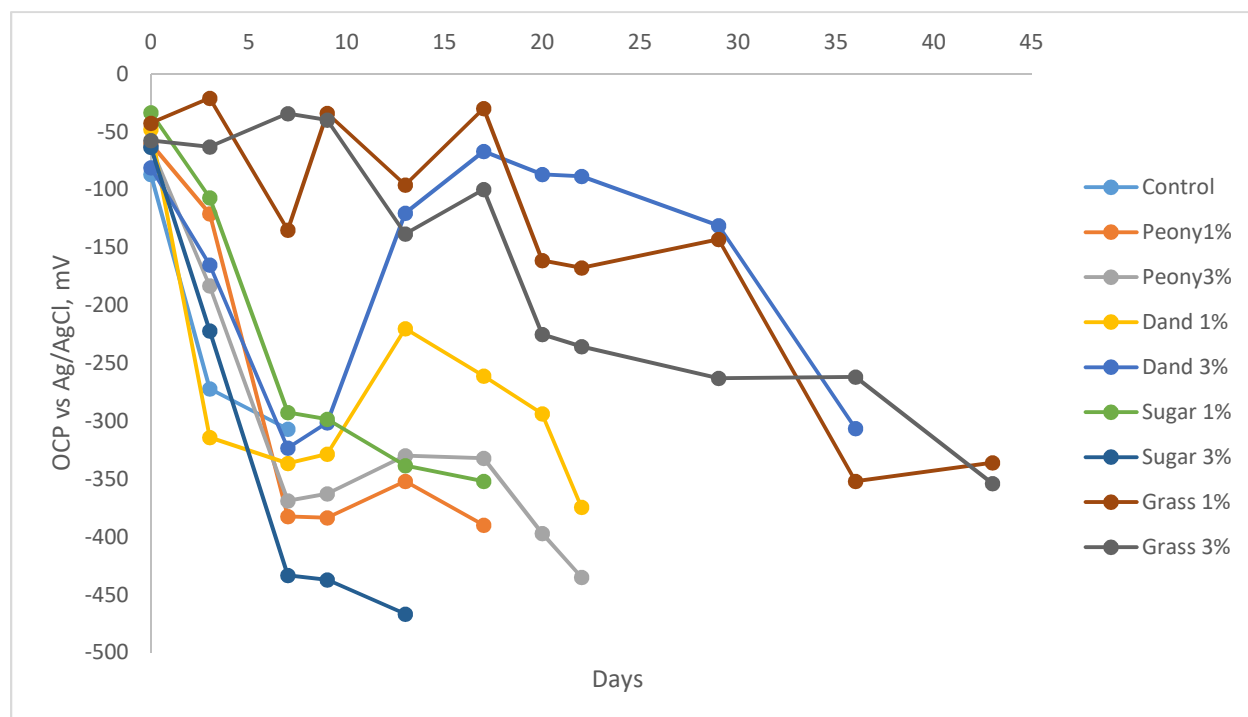


Fig. 7—Open circuit potential of the reinforced mortar samples

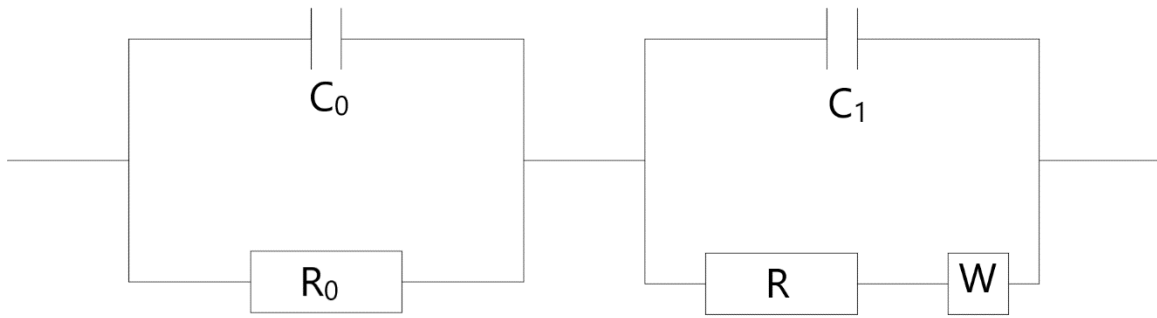


Fig. 8—Equivalent circuit applied to analyze the EIS results

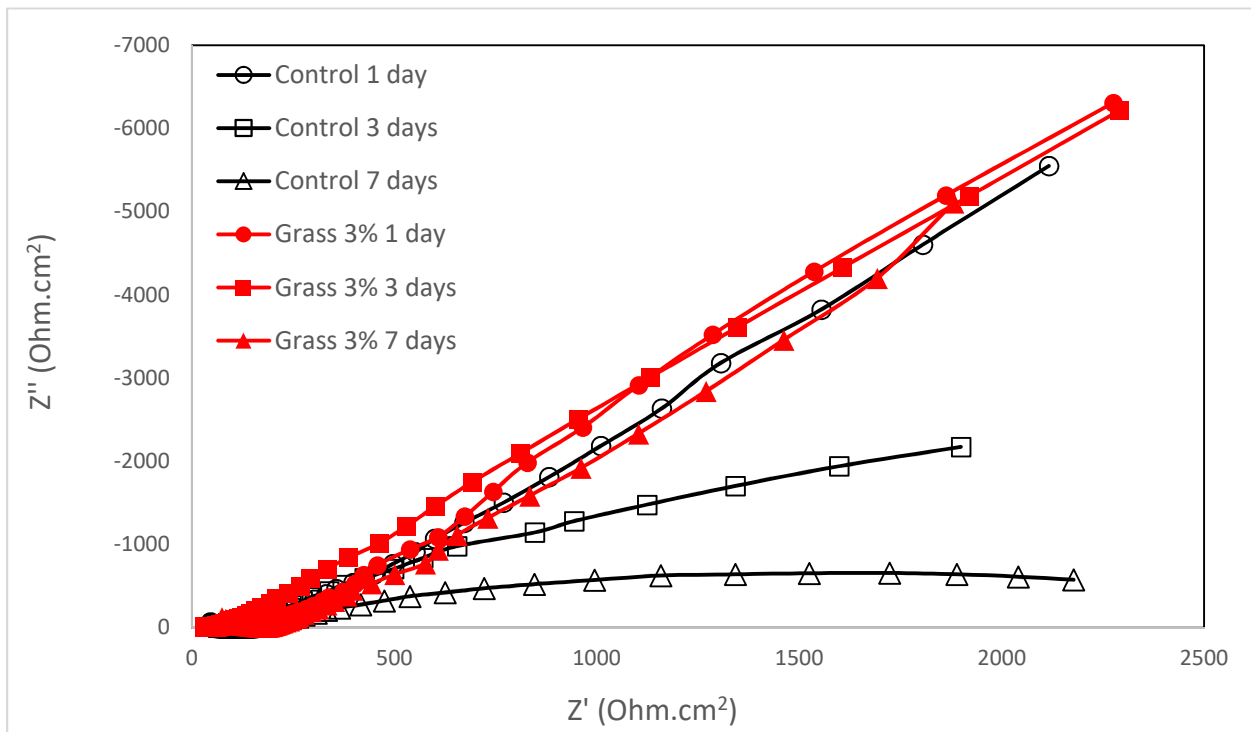


Fig. 9—EIS spectra of control group of reinforced mortar specimen during immersion test

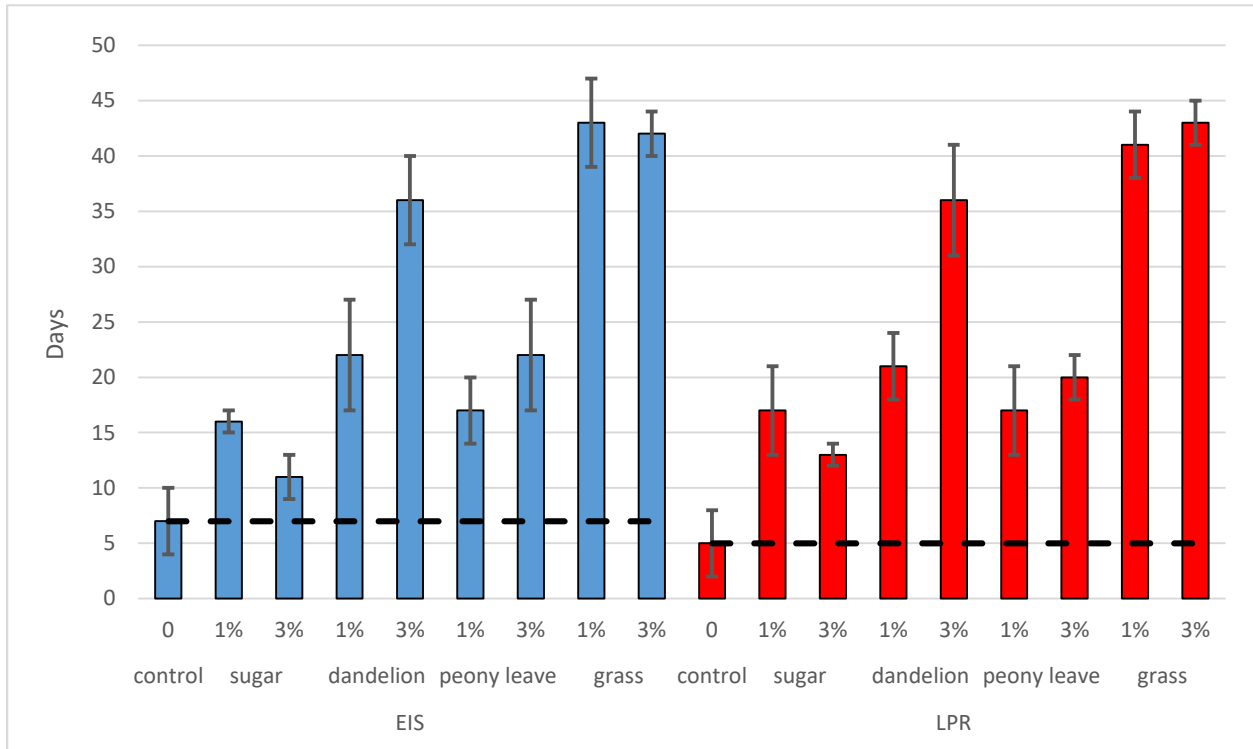


Fig. 10—Time required to initiate corrosion for embedded steel rebar

RCM test

Fig. 11 presents the results of chloride diffusion coefficient determined by the method of RCM [34] in accordance with NT BUILD 492 [25]. In general, the chloride diffusion coefficient of mortar samples mixed with green admixtures was reduced. This reduction can increase the structure service life in a marine environment. However, there were differences in the service life increment efficiency depending on the green admixtures used. Dandelion groups had the least efficiency compared with other groups. This may be due to the higher water absorption ratio and gas permeability of mortar mixed with D-inhibitor.

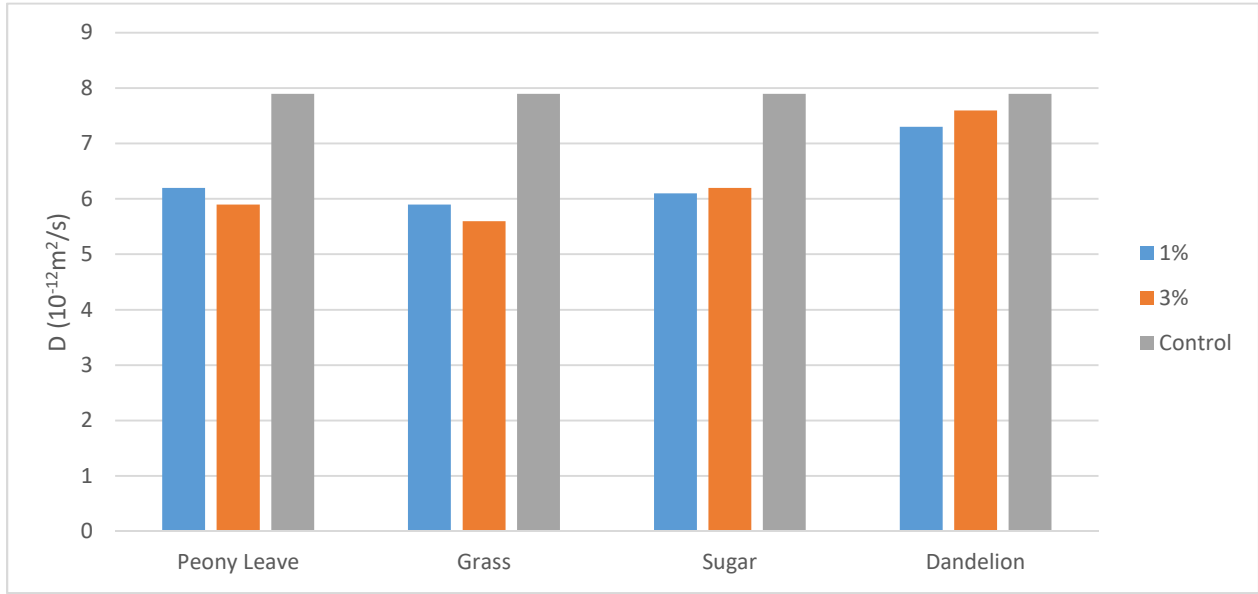


Fig. 11—Chloride diffusion coefficient measured from RCM test

The value of the chloride diffusion coefficient is not a measure that allows easy understanding of the advantage produced by the protection system. Service life was thus employed to facilitate the interpretation of the chloride diffusion coefficients results and the relationship was presented in Fig. 12. This type of representation allows comparison of different types of treatment systems through a relation between the depth of chloride penetration and the reinforced concrete's service life. Fick's second law [35] of diffusion (Equation 8 and 9) was used to produce Fig. 12, which indicates that the mortar mixed with PL-, KG- and SL-inhibitors can reduce the chloride ion penetration depth and thus increase the service life of reinforced concrete structures.

$$CP = 2(z)\sqrt{Dt} \quad (8)$$

$$\operatorname{erf}(z) = 1 - \frac{C_{Cl} - C_0}{C_s - C_0} \quad (9)$$

Where D is the chloride diffusion coefficient (cm^2/year), t is the service life (years), $\operatorname{erf}(z)$ is the Gauss error function, C_P (chloride penetration) is the depth at which the chloride concentration reached the threshold for reinforcement depassivation (cm), C_0 is the initial chloride concentration, C_s is the surface chloride concentration (%), C_{Cl} is the chloride concentration in depth and time (%).

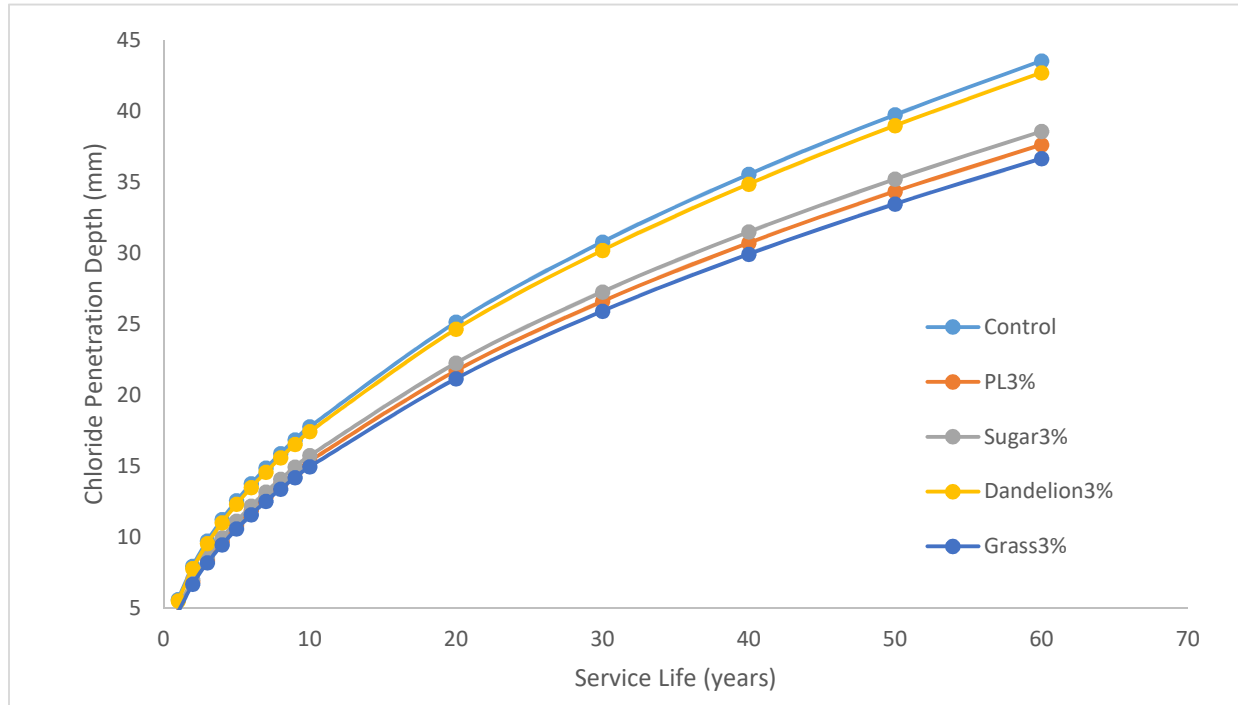


Fig. 12—Chloride penetration depth during service life of RC structures

CONCLUSIONS

This experimental study evaluated four types of green corrosion inhibitors as multi-function admixtures for mortar samples. From a comprehensive point of view, Peony leaves-based inhibitor and Kentucky blue grass-based inhibitor had the best performance among them.

Compressive strength of mortar specimens mixed with green corrosion admixtures were tested. Early age strength was slightly reduced due to PL-, KG- and SL-inhibitors. When more dosage of inhibitors was added, strength was compromised further. Water absorption test and gas permeability test were carried out to prove that the mixed green corrosion inhibitors had limited adverse effect on the transport properties of mortar.

Rheology tests including workability test and K-slump test were performed. The green corrosion inhibitors improved the rheology of mixed mortar, especially for the PL-inhibitor. Rheology test also indicated that the green corrosion inhibitors had the potential to be used as a water reducer to produce self-consolidation concrete. The green inhibitors also increased the initial setting time, thus working as a set retarder.

OCP, EIS and LPR were monitored during the accelerated immersion corrosion test. Results showed that all the green corrosion inhibitors had a good corrosion inhibiting efficiency. Based on the data from RCM test, PL-, KG- and SL-inhibitors could be used as effective corrosion inhibitors in mortar or concrete to resist chloride induced corrosion.

Future work may focus on understanding how green inhibitors affect the hydration process. Meanwhile, the influence of green corrosion inhibitors on microstructure and chloride binding capability of cement hydrates could be studied to further understand the inhibiting mechanism.

REFERENCES

- [1] S. M. Abd El Haleem, E. E. Abd El Aal, S. Abd El Wanees, and A. Diab, “Environmental factors affecting the corrosion behaviour of reinforcing steel: I. The early stage of passive film formation in Ca(OH)₂ solutions,” *Corros. Sci.*, vol. 52, no. 12, pp. 3875–3882, Dec. 2010.
- [2] S. M. Abd El Haleem, S. Abd El Wanees, E. E. Abd El Aal, and A. Diab, “Environmental factors affecting the corrosion behavior of reinforcing steel II. Role of some anions in the initiation and inhibition of pitting corrosion of steel in Ca(OH)₂ solutions,” *Corros. Sci.*, vol. 52, no. 2, pp. 292–302, Feb. 2010.
- [3] 222 ACI Committee, “Protection of Metals in Concrete Against Corrosion,” ACI, ACI 222R01, Sep. 2001.
- [4] A. E. Alvarez, A. E. Martin, and C. Estakhri, “A review of mix design and evaluation research for permeable friction course mixtures,” *Constr. Build. Mater.*, vol. 25, no. 3, pp. 1159–1166, Mar. 2011.
- [5] N. S. Berke and M. C. Hicks, “Predicting long-term durability of steel reinforced concrete with calcium nitrite corrosion inhibitor,” *Cem. Concr. Compos.*, vol. 26, no. 3, pp. 191–198, Apr. 2004.
- [6] T. A. Söylev and M. G. Richardson, “Corrosion inhibitors for steel in concrete: State-of-the-art report,” *Constr. Build. Mater.*, vol. 22, no. 4, pp. 609–622, Apr. 2008.
- [7] J. L. Kepler, D. Darwin, and C. E. Locke, “Evaluation of Corrosion Protection Methods for Reinforced Concrete Highway Structures,” University of Kansas Center for Research, Inc., Technical Report, May 2000.
- [8] C. L. Page, V. T. Ngala, and M. M. Page, “Corrosion inhibitors in concrete repair systems,” *Mag. Concr. Res.*, vol. 52, no. 1, pp. 25–37, Feb. 2000.
- [9] P. B. Raja, S. Ghoreishiamiri, and M. Ismail, “Natural corrosion inhibitors for steel reinforcement in concrete — a review,” *Surf. Rev. Lett.*, vol. 22, no. 03, p. 1550040, Feb. 2015.
- [10] S. A. Asipita, M. Ismail, M. Z. A. Majid, Z. A. Majid, C. Abdullah, and J. Mirza, “Green Bambusa Arundinacea leaves extract as a sustainable corrosion inhibitor in steel reinforced concrete,” *J. Clean. Prod.*, vol. 67, pp. 139–146, Mar. 2014.
- [11] P. B. Raja and M. G. Sethuraman, “Natural products as corrosion inhibitor for metals in corrosive media — A review,” *Mater. Lett.*, vol. 62, no. 1, pp. 113–116, Jan. 2008.
- [12] M. H. Nazari, M. S. Shihab, L. Cao, E. A. Havens, and X. Shi, “A peony-leaves-derived liquid corrosion inhibitor: protecting carbon steel from NaCl,” *Green Chem. Lett. Rev.*, vol. 10, no. 4, pp. 359–379, Oct. 2017.
- [13] S. Roux, N. Bur, G. Ferrari, B. Tribollet, and F. Feugeas, “Influence of a biopolymer admixture on corrosion behaviour of steel rebars in concrete,” *Mater. Corros.*, vol. 61, no. 12, pp. 1026–1033, 2010.
- [14] S. Roux, B. Tribollet, N. Serres, A. Lecomte, and F. Feugeas, “Use of Biopolymers to Improve the Reinforced Concrete Sustainability,” *Restor. Build. Monum.*, vol. 19, no. 2–3, pp. 163–170, Jan. 2013.
- [15] Ş. Erdoğdu, I. L. Kondratova, and T. W. Bremner, “Determination of chloride diffusion coefficient of concrete using open-circuit potential measurements,” *Cem. Concr. Res.*, vol. 34, no. 4, pp. 603–609, Apr. 2004.
- [16] Y.-S. Choi, J.-G. Kim, and K.-M. Lee, “Corrosion behavior of steel bar embedded in fly ash concrete,” *Corros. Sci.*, vol. 48, no. 7, pp. 1733–1745, Jul. 2006.
- [17] M. Kouřil, P. Novák, and M. Bojko, “Limitations of the linear polarization method to determine stainless steel corrosion rate in concrete environment,” *Cem. Concr. Compos.*, vol. 28, no. 3, pp. 220–225, Mar. 2006.
- [18] “C01 Committee - Specification for Portland Cement.pdf.” .
- [19] “C12 Committee - Specification for Aggregate for Masonry Mortar.pdf.” .

- [20] “A01 Committee - Specification for Deformed and Plain, Low-Carbon, .pdf.” .
- [21] “C01 Committee - Test Method for Compressive Strength of Hydraulic .pdf.” .
- [22] “C1362-WITHDRAWN.31080.pdf.” .
- [23] “C09 Committee - Test Method for Time of Setting of Concrete Mixtur.pdf.” .
- [24] “C09 Committee - Test Method for Measurement of Rate of Absorption .pdf.” .
- [25] “NT build 492_Concrete mortar and cement-based repair materials_Chloride migration coefficient from non-steady-state migration experiments_Nordtest Method.pdf.” .
- [26] M. A. Quraishi, V. Kumar, B. N. Singh, and S. K. Singh, “Calcium Palmitate: A Green Corrosion Inhibitor for Steel in Concrete Environment,” p. 9, 2012.
- [27] C. F. Ferraris, K. H. Obla, and R. Hill, “The influence of mineral admixtures on the rheology of cement paste and concrete,” *Cem. Concr. Res.*, vol. 31, no. 2, pp. 245–255, Feb. 2001.
- [28] C.-Z. Li, N.-Q. Feng, Y.-D. Li, and R.-J. Chen, “Effects of polyethylene oxide chains on the performance of polycarboxylate-type water-reducers,” *Cem. Concr. Res.*, vol. 35, no. 5, pp. 867–873, May 2005.
- [29] A. W. Saak, H. M. Jennings, and S. P. Shah, “A generalized approach for the determination of yield stress by slump and slump flow,” *Cem. Concr. Res.*, vol. 34, no. 3, pp. 363–371, Mar. 2004.
- [30] F. Mahmoodzadeh and S. E. Chidiac, “Rheological models for predicting plastic viscosity and yield stress of fresh concrete,” *Cem. Concr. Res.*, vol. 49, pp. 1–9, Jul. 2013.
- [31] R. Boncukcuoğlu, M. T. Yılmaz, M. M. Kocakerim, and V. Tosunoğlu, “Utilization of borogypsum as set retarder in Portland cement production,” *Cem. Concr. Res.*, vol. 32, no. 3, pp. 471–475, Mar. 2002.
- [32] J. H. Potgieter, S. S. Potgieter, R. I. McCrindle, and C. A. Strydom, “An investigation into the effect of various chemical and physical treatments of a South African phosphogypsum to render it suitable as a set retarder for cement,” *Cem. Concr. Res.*, vol. 33, no. 8, pp. 1223–1227, Aug. 2003.
- [33] S. Aggoun, M. Cheikh-Zouaoui, N. Chikh, and R. Duval, “Effect of some admixtures on the setting time and strength evolution of cement pastes at early ages,” *Constr. Build. Mater.*, vol. 22, no. 2, pp. 106–110, Feb. 2008.
- [34] T. Luping and L.-O. Nilsson, “Rapid Determination of the Chloride Diffusivity in Concrete by Applying an Electric Field,” *Mater. J.*, vol. 89, no. 1, pp. 49–53, Jan. 1993.
- [35] S. Chatterji, “On the applicability of Fick’s second law to chloride ion migration through portland cement concrete,” *Cem. Concr. Res.*, vol. 25, no. 2, pp. 299–303, Feb. 1995.

LIST OF CAPTIONS FOR TABLES AND FIGURES

Table 1—Mix Proportion of mortar mixed with four green corrosion inhibitor and control sample

Table 2—Strength reduction of mortar samples

Fig.1—Compressive strength of mortar cylinders

Fig. 2—Workability of mortar samples

Fig. 3—K-Slump of mortar samples

Fig. 4—Initial setting time of mortar samples

Fig. 5—Water absorption rate of mortar samples

Fig. 6—Gas permeability of mortar samples

Fig. 7—Open circuit potential of the reinforced mortar samples

Fig. 8— Equivalent circuit applied to analyze the EIS results

Fig. 9— EIS spectra of control group of reinforced mortar specimen during immersion test

Fig. 10—Time required to initiate corrosion for embedded steel rebar

Fig. 11—Chloride diffusion coefficient measured from RCM test

Fig. 12—Chloride penetration depth during service life of RC structures

Understanding Shrinkage in Alternative Binder Systems

Lisa E. Burris, Prasanth Alapati, Kimberly E. Kurtis, Amir Hajibabae, M. Tyler Ley

Synopsis: Cement production is one of the largest contributors to CO₂ emissions in the U.S. One method of reducing emissions associated with concrete is through usage of alternative cements (ACMs). Some of the more common ACMs include calcium sulfoaluminate cement, calcium aluminate cement, ternary calcium aluminate-calcium sulfate-portland cements, and chemically-activated binders, all of which have been shown to have lower carbon footprints than ordinary portland cement (OPC). However, the durability, and more specifically, the shrinkage behavior, of these cements has not been adequately examined, and must be better understood and able to be controlled before ACM concrete can be effectively used in the field. As a first step in increase understanding of shrinkage in ACMs, this paper examines chemical, autogenous, and drying shrinkage in the ACMs listed above. Results show that, despite greater quantities of chemical shrinkage, CSA, CAC, and chemically activated fly ash binder undergo less autogenous and drying shrinkage than OPC.

Keywords: Alternative cementitious materials; calcium sulfoaluminate cement; calcium aluminate cement; alkali activated binders; shrinkage; durability

ACI member **Lisa E. Burris** is an Assistant Professor in the Department of Civil, Environmental, and Geodetic Engineering at the Ohio State University. She received her B.S. and M.S. in Architectural and Civil Engineering, respectively, from Kansas State University; and her Ph.D. in Civil Engineering from the University of Texas at Austin. She is a member of ACI Committees 123 (Research), 236 (Materials Science of Concrete), and 242 (Alternative Cements).

Prasanth Alapati is a Ph.D. candidate at the Georgia Institute of Technology. He received his B.Tech. and M.Tech. in Civil Engineering from Indian Institute of Technology Madras. He has research interests in alternative cementing materials, hydration mechanisms, admixture interactions, and concrete durability, including understanding carbonation, alkali silica reactivity (ASR), sulfate testing, and corrosion in both portland and alternative cement systems.

ACI fellow **Kimberly E. Kurtis** is Associate Dean for Faculty Development and Scholarship and Professor of Civil Engineering at Georgia Institute of Technology. She received her B.S. in Civil Engineering from Tulane University; and her M.S. and Ph.D. in Civil Engineering from the University of California Berkeley. She is a member of ACI's Technical Activities Committee (TAC) and is a voting member of Committees 236 (Materials Science of Concrete), 225 (Hydraulic Cements) and 201 (Durability).

ACI member **Amir Hajibabae** is a Research Engineer at Ozinga Ready Mix Concrete, Inc. He received his B.S. in Civil Engineering from University of Tehran, and his M.S. and Ph.D. in Civil Engineering from Oklahoma State University. He is a member of ACI Committees 201 (Durability), 209 (Creep and Shrinkage), and 308 (Curing).

ACI member **M. Tyler Ley** is a Professor at Oklahoma State University. He received his B.S. in Civil Engineering from Oklahoma State University; and his M.S. and Ph.D. in Civil Engineering from the University of Texas at Austin. He is a member of ACI Committees 201 (Durability of Concrete), 211 (Proportioning of Concrete Mixtures), 236 (Material Science of Concrete), and ACI Subcommittee 130-A, Materials (Sustainability of Concrete).

INTRODUCTION

Concrete is the world's most prolifically used construction material, and as a result of the vast quantities produced each year it also represents a significant worldwide environmental impact, accounting for 4.8% of global anthropogenic carbon dioxide emissions (CO_{2e}).¹ Reduction of CO₂ emissions associated with concrete construction may be achieved through the use of binders and alternative cementitious materials (ACMs) that require lower production temperatures, and/or have lower calcium contents, than ordinary portland cement (OPC), and thus use less fuel and produce less CO₂ from calcination of calcium carbonate precursor materials. A substantial CO_{2e} savings, between 16 to 56%, has been shown to be possible to be possible to achieve through the use of ACMs.²

However, the durability, and more specifically, the shrinkage and cracking behavior, of these cements has not been adequately examined, and must be better understood, and able to be controlled, before alternative binder concretes can be effectively used in the field. As a first step

in increasing understanding of shrinkage cracking in alternative cements, this study examines current research on shrinkage of alternative binders, then builds on this understanding, evaluating the chemical, autogenous, and drying shrinkage potential, as well as the interplay between the three shrinkage mechanisms on overall shrinkage behavior of four commercially available alternative binder formulations, compared to a typical OPC.

RESEARCH SIGNIFICANCE

Little testing has been done to understand the propensity of alternative cements, including CSA, CAC, blended OPC-CAC-calcium sulfate systems, and commercial chemically activated systems towards shrinkage, despite the importance of understanding this property in order to ensure durability of alternative binder concrete infrastructure. Thus, this preliminary study investigated chemical, autogenous, and drying shrinkage in four commercially available alternative binder systems with the goal of making a quantitative comparison to help guide use of these materials.

BACKGROUND

Shrinkage Mechanisms

Chemical

The three shrinkage mechanisms investigated by this study include chemical, autogenous, and drying shrinkage. Chemical shrinkage occurs when water is consumed as binder phases chemically react, combine, and hydrate due to the fact that the water contained in cement hydrates is denser than the free mixture water.³ In OPC pastes, chemical shrinkage is linearly correlated with the degree of reaction of the cement^{3,4} and will not occur in pastes with w/cm greater than 0.6.⁵ Until around the time of initial set, chemical shrinkage and autogenous shrinkage are equivalent. After that time chemical shrinkage will continue to occur until anhydrous phases are exhausted or the density of microstructure considerably slows or stops water transport.

Autogenous

With the reduction in fluid transport throughout the hardened media the binder will begin to self-desiccate, with removal of water from the pores leading to increases in capillary pressures. Water will be removed from larger pores first, with the generated pressures inversely correlated with pore size. As the pressures increase the section will contract and autogenous shrinkage will occur. Autogenous shrinkage is based on many factors, including the rate and magnitude of chemical shrinkage after the paste reaches final set, the development of mechanical properties in the hardened binder, and the pore sizes and distribution of pores throughout the binder.⁶

Drying

Drying shrinkage is similar to autogenous shrinkage in that it is caused by the removal of water from pores in the hardened paste.⁶ The primary difference is that drying shrinkage occurs due to external drying as a result of the concrete's environment, rather than the progression of chemical reactions of the paste that remove water from the pores. Drying shrinkage is of particular concern for restrained sections of concrete. Additionally, drying from only one side of a concrete member, such as in slab-on-ground or pavement, results in differential shrinkage over the depth

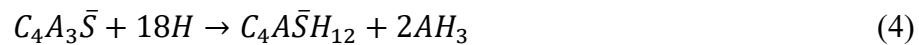
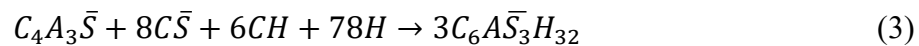
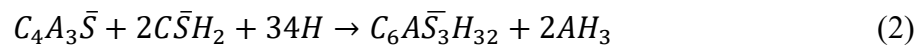
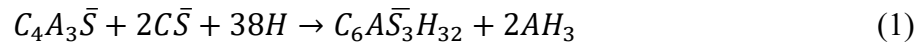
of the member.^{3,7-10} This differential strain can cause unwanted volume change which can lead to serviceability issues, or cracking from a loss of support from the foundation.¹¹⁻¹⁵

This work investigated the shrinkage in four types of commercially available binders: calcium sulfoaluminate (CSA2) cement; calcium aluminate cement (CAC3); a *CAC – OPC – C \bar{S}* (CAC2) blended cement; and a chemically activated binder (AA1), compared to OPC. A brief synopsis of the chemistry, hydration/reaction processes, and previous work investigating their proclivity towards shrinkage and cracking of each binder are outlined here to aid in understanding their demonstrated shrinkage behaviors.

Hydration and Shrinkage in Alternative Binders

Calcium sulfoaluminate cements (CSA)

CSA cements are primarily composed of ye’elinite ($C_4A_3\bar{S}$) and C_2S , with anhydrite or gypsum ($CaSO_2$ or $CaSO_4$) added in order to control the speed of the reaction resulting in initial set.¹⁶ Hydration and property development typically occurs more rapidly in CSA than in OPC. Hydration of CSA cements occurs rapidly as the ye’elinite reacts with calcium sulfate, and lime, if present, to form ettringite ($C_6A\bar{S}_3H_{32}$) (Eqs. 1 and 2), monosulfate ($C_4A\bar{S}H_{12}$) (Eq. 3) and/or aluminum hydroxide (AH_3) (Eqs. 1, 2, and 4).¹⁷⁻¹⁹



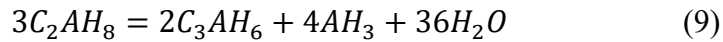
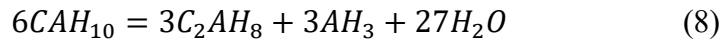
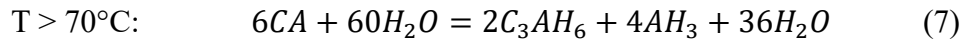
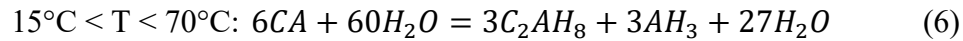
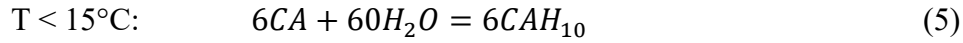
CSA cements are sometimes referred to as ‘shrinkage compensating’ or ‘self-stressing’ cements, however not all CSA mixtures are expansive. Chen and Juenger found that CSA expansion is based on cement composition and particle size, as well as the w/cm used in the mixture. Expansion of cements was found to be correlated with ye’elinite content, calcium sulfate content, and particle size.²⁰ The work of Bizzozero et al. confirmed this, observing that mortar bar expansions in mixtures with greater than 57 mol % gypsum became subject to macro-cracking and were destroyed within four days. Using less than 52 mol% gypsum minimized expansion to less than 0.25%.²¹ It has also been demonstrated that greater expansion occurs in lower w/cm CSA mixtures,²⁰ but even at high w/cm of 0.7 CSA cements were shown to have more than 4x the amount of chemical shrinkage of OPC mixtures at 0.3 or 0.5 w/cm.²² Significant amounts of chemical shrinkage are suggested to occur in CSAs due to greater density in the bound water within ettringite compared to the density of free water.¹⁶

With regard to autogenous shrinkage in CSA pastes, Bianchi et al.²³ found that after 180 days their CSA cement sample showed only -600 microstrain of drying shrinkage – 62.5% less than their reference OPC sample using the ring test (EN 196-1). Additionally, Beretka et al.²⁴ noted that their in-situ concrete samples showed “particularly good dimensional stability” with *expansions* of 0.19% after 1 year. Hargis et al.²⁵ investigated autogenous shrinkage in CSA pastes as a function of the ratio of calcium sulfate to ye’elinite, and found that mixtures with

very low calcium sulfate content (sulfate/ye'elimit = 0.1) showed expansions of 0.4% at 180 days, while higher sulfate content mixtures (sulfate/ye'elimit = 1 and 1.5) expanded only 0.05%.

Calcium aluminate cements (CAC)

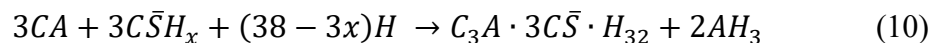
CAC is composed principally of monocalcium aluminate (CA) which usually amounts to 50 to 60% of the cement by weight. The hydration of CA produces CAH_{10} , C_2AH_8 , and/or C_3AH_6 along with alumina gel (AH_3), as shown in Eqs. 5-7, where T stands for the temperature of the casting environment.²⁶ The other major component of CAC, $C_{12}A_7$, is believed to hydrate to C_2AH_8 . The principal CAC hydration products, CAH_{10} and C_2AH_8 , are thermodynamically unstable and with time, and in the presence of moisture, both CAH_{10} and C_2AH_8 transform (or convert) to C_3AH_6 and alumina gel (Eqs. 8 and 9).²⁶ The original (pre-conversion) hydration products have a lower density than the products of conversion, resulting in an increase in the porosity of the concrete, significantly lower strength, and increased permeability.²⁶

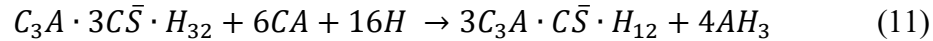


Of the limited testing that has been conducted to track shrinkage in CAC mixtures, most have found their chemical and drying shrinkage to be significantly greater than OPC mixtures.^{21,27,28} Chemical shrinkage of CAC systems has been shown to be 2 to 4 times greater than that of OPC pastes and is primarily due to the consumption of water during formation of the metastable CAC hydrates (CAH_{10}).^{16,27} Field testing also showed that significantly greater amounts of cracking developed over the first 7 days after placement, in CAC pavement sections compared to the OPC, CSA and AA mixtures used in that study.²⁸ However, no investigation was undertaken in the study to confirm that crack development was a result of shrinkage, and not other mechanisms, such as conversion.

Calcium aluminate-portland-calcium sulfate blended cements

In order to minimize the effects of conversion and offset the high costs of CAC, *CAC – OPC – $C\bar{S}$* blended cements, consisting of a large proportion of calcium aluminate cement with additions of portland cement and a small amount of gypsum or anhydrite, are becoming increasingly common.²⁹ When mixed with water both the C_3A and CA present in the *CAC – OPC – $C\bar{S}$* blend hydrate to form ettringite (Eq. 10) and monosulfate (Eq 11), after the depletion of the system's calcium sulfate.³⁰ Additionally, calcium silicate phases present in the OPC fraction of the blend will produce C-S-H and CH phases similar to normal OPC hydration processes.





The reaction of ternary CAC blends is dependent on the ratio of OPC, CAC, and calcium sulfate in the mixture, in addition to the form of calcium sulfate used (anhydrite, hemihydrate, or gypsum). In one study looking at mixture composed of 77.5/7.5/15.0 proportions of OPC/CAC/ $C\bar{S}$, at 28 days, mixtures utilizing anhydrite and hemihydrate showed expansive behavior, whereas mixtures utilizing gypsum showed shrinkage of ~0.1%.³¹

Chemically activated binders

Chemically activated binders form when an aluminosiliceous material, such as fly ash or metakaolin, is ‘activated’ using an alkaline solution, instigating dissolution of the aluminosiliceous media and leading to rearrangement and reformation of a new hardened calcium-alumina-silicate-hydrate (C-A-S-H), or calcium-silicate-hydrate (C-S-H) microstructure.³² Reactive silica content, amorphous phase content, gradation, calcium content, aluminum availability, and moisture content of the precursor materials can all affect reactivity, set time, and strength development of the binders,^{32,33} and may also affect shrinkage of the binder system.

Drying shrinkage in chemically activated binders has been found to be a function of many factors including water content, system chemistry, activator content, and curing temperature,^{34,35} with higher initial mixing water content, lower Si:Al ratios, and lower sodium contents leading to decreased drying shrinkage.^{34,36} High activator content was also found to result in greater shrinkage, however typical drying shrinkage in alkali activated materials was still very low compared to OPC mixtures, with alkali activated concrete showing drying shrinkage strain as low as 100 microstrain after one year^{37,38} compared to drying shrinkage as high as 500 to 1000 microstrain in some OPC concretes with w/cm of 0.5 and cured at 50% RH.^{39,40}

MATERIALS

This study evaluated shrinkage in four commercially available alternative binder systems: a ASTM C150 Type I/II ordinary portland cement (OPC), which served as a control; a calcium sulfoaluminate cement (CSA2); a calcium aluminate cement (CAC3); a CAC- $C\bar{S}$ -OPC blended product (CAC2); and a chemically-activated binder (AA1) consisting of a class C fly ash activated with a proprietary chemical solution. Oxide and phase contents for each cement, are shown in Table 1. The particle size distribution of each unhydrated binder, dispersed in isopropanol, was obtained using a Malvern Mastersizer 3000E, and is shown in Figure 1. Specific gravity, average particle size (d_{50}), and specific surface area (SSA) of the binders are shown in Table 3. Anhydrous ACS grade citric acid (Electron Microscopy, 99.5% purity) was used to retard setting in the CSA1, CSA2, and CAC2 systems. CAC3 used a plasticizing, retarding proprietary admixture, and AA1 also used a proprietary chemical activator. Crushed granite coarse aggregates from Vulcan Materials Company (Lithia Springs, Georgia) meeting the ASTM C33 #67 gradation was used in all concrete mixtures. River sand from the Lambert Sand and Gravel Plant (Shorter, Alabama), conforming to ASTM C33 specified gradations was used in all concrete and mortar mixtures.

TABLE 1 - OXIDE CONTENTS OF THE BINDERS, SHOWN AS PERCENTAGES OF THE TOTAL MATERIAL, DETERMINED USING X-RAY FLUORESCENCE.

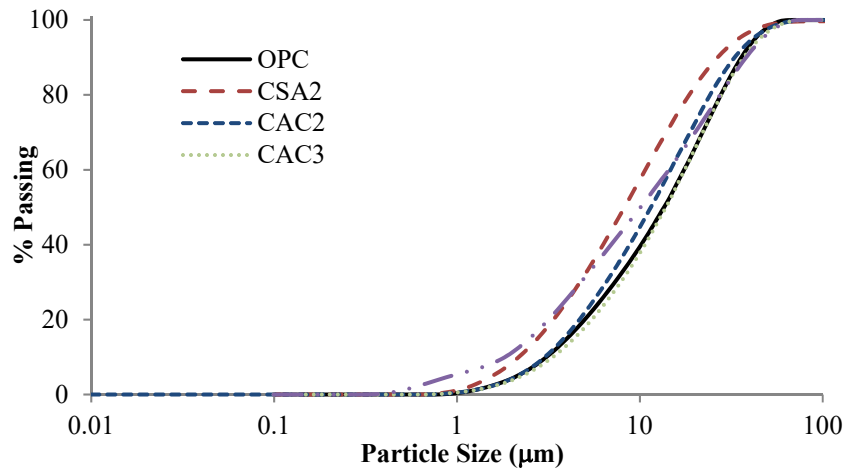
Oxide	OPC	CSA2	CAC3	CAC2	AA1-Class C Fly Ash Precursor
SiO ₂	17.3	14.2	5.5	15.0	35.6
Al ₂ O ₃	4.9	14.8	45.2	12.0	18.8
Fe ₂ O ₃	4.7	1.1	6.9	2.7	6.2
CaO	65.2	49.2	37.7	55.2	24.5
MgO	1.4	1.6	0.2	2.6	5.7
K ₂ O	2.5	13.6	0.3	7.7	2.3
Na ₂ O	0.5	0.7	0.0	0.8	1.8
P ₂ O ₅	0.5	0.2	0.1	0.3	0.9
TiO ₂	0.1	0.1	2.1	0.1	1.5

TABLE 2 - PHASE COMPOSITIONS OF THE BINDERS, SHOWN AS PERCENTAGES OF THE TOTAL MATERIAL, DETERMINED BY RIETVELD ANALYSIS OF X-RAY DIFFRACTION DATA.

Phase	OPC	CSA2	CAC3	CAC2	AA1-Class C Fly Ash Precursor
Alite	61.0	-	-	40.8	-
Belite	12.6	48.9	12.2	22.7	-
Aluminate	2.3	1.38	12.3	0.5	-
Ferrite	14.3	0.68	1.0	11.1	-
Calcite	6.7	3.36	-	0.7	-
Anhydrite	2.2	9.02	-	9.1	-
Gypsum	-	-	-	1.9	7.6
Ye'elimite – Cubic	-	6.62	-	-	-
Ye'elimite – Orthorhombic	-	20.41	-	-	-
Bassanite (Hemihydrate)	-	2.80	-	-	-
Quartz	-	0.26	-	0.1	28.1
Mayenite	-	-	1.4	0	-
Calcium Aluminum Oxide	-	-	-	0	-
Monocalcium Aluminate (CaAl ₂ O ₄)	-	-	56.9	15	-
Periclase	-	1.49	-	0	24.7
Gehlenite	-	0.90	16.2	-	-
Anatase	-	-	-	-	4.2
Hematite	-	-	-	-	21.0
Trydymite	-	-	-	-	10.8
Mullite	-	-	-	-	3.6
Portlandite	-	1.27	-	-	-
Ternesite	-	1.02	-	-	-

TABLE 3 - SPECIFIC GRAVITY AND AVERAGE PARTICLE SIZE OF THE BINDERS.

	OPC	CSA2	CAC2	CAC3	AA1
Specific Gravity	3.05	2.78	2.91	2.97	2.5
Mass-median Particle Size (d ₅₀) (μm)	12.8	8.8	14.3	15.3	9.3
Specific surface area (SSA) (m ² /kg)	333.3	453.2	302.7	306.4	550.7


FIGURE 1 - PARTICLE SIZE DISTRIBUTION FOR THE UNHYDRATED OPC AND ACM BINDERS.

METHODS

Paste, mortar, and concrete mixtures were used to test chemical, autogenous, and drying shrinkage of the alternative binder systems and are shown in Tables 4, 5, and 6, respectively. All paste mixtures used a w/cm of 0.4 by mass of binder, except the AA1 mixtures, which had a w/cm of 0.23, as recommended by the manufacturer. All the mortar mixes were mixed at w/cm of 0.4 (AA1 at 0.25 w/cm), and sand/cement of 2.0. The sand content was adjusted to account for the differences in the specific gravities of cements, and the water dosage was also adjusted to account for the sand absorption and water content of admixtures. The admixture dosages in the concrete mixtures were chosen so that the material had a slump of 200 mm +/- 25 mm.

TABLE 4 - PASTE MIXTURE PROPORTIONS.

Cement	w/cm	Admixture & Dosage (% of cement wt)
OPC	0.40	-
CSA2	0.40	Citric acid, 0.5%
CAC2	0.40	Citric acid, 1.5%
CAC3	0.40	Proprietary water reducer/set modifier.
AA1	0.23	Proprietary activator solutions: Admix 1 = 2.475%, Admix 2 = 2.207%

TABLE 5 - MORTAR MIXTURE PROPORTIONS FOR AUTOGENOUS SHRINKAGE TESTING.

Cement	w/cm	Set modifier, dosage (% of cement wt)	HRWR, dosage (ml/100kg cement)	Cement g (lbs)	Water g (lbs)	Sand g (lbs)
OPC	0.40		200ml	1000 (2.2)	408 (0.9)	2000 (4.4)
CSA2	0.40	Citric acid, 0.5%	400ml	1000 (2.2)	408 (0.9)	1926 (4.2)
CAC2	0.40	Citric acid, 1.5%		1000 (2.2)	408 (0.9)	1959 (4.3)
CAC3	0.40		200ml	1000 (2.2)	408 (0.9)	1977 (4.4)
AA1	0.25	Admix 1 = 2.47%, Admix 2 = 2.21%		1000 (2.2)	257 (0.6)	1843 (4.1)

TABLE 6 - CONCRETE MIXTURE PROPORTIONS.

Cement	w/cm	Cement (kg/m ³) lb/yd ³	Sand (kg/m ³) lb/yd ³	Coarse Aggregate (kg/m ³) lb/yd ³	Admixture & Dosage
OPC	0.41	765 (454)	1165 (691)	1789 (1061)	-
CSA2	0.41	765 (454)	1109 (658)	1789 (1061)	Citric acid, 0.5% of cement wt
CAC2	0.41	765 (454)	1134 (673)	1789 (1061)	Citric acid, 1.5% of cement wt
CAC3	0.41	765 (454)	1148 (681)	1789 (1061)	200 mL/100 kg cement
AA1	0.206	822 (488)	1359 (809)	1789 (1061)	Admix 1 = 2.475%, Admix 2 = 2.207% of cement wt

Chemical Shrinkage Testing

Chemical shrinkage of the ACM pastes was tracked using the ASTM C1608 dilatometry method. Pastes were first mixed using a 5-speed hand mixer at the lowest speed for 30 seconds, followed by high speed for 90 seconds. In all cases, the admixture dosage was weighed to ± 0.0005 g accuracy and dissolved into 18 M Ω -cm deionized water mixing water prior to mixing with the cement. After mixing, approximately 5g of paste was transferred to a glass vial, which was then filled with de-aerated, deionized water, capped with a rubber stopper fitted with a capillary pipette, and placed in a water bath maintained at 23°C. A droplet of colored hydraulic oil was added to the top of the capillary tubes in order to track the water consumed during hydration, or in the case of the AA1 system, reaction of the binders over the first seven days after mixing. Due to the rapid reaction of many of the alternative binders, initial readings were taken 30 minutes after the initial water contact time, in comparison with the 60-minute time recommended in ASTM C1608, in order to capture more of the early age changes. Measurements for five replicate samples were tracked for each binder system.

Autogenous Shrinkage Testing

The autogenous shrinkage of ACM mortar samples was measured according to ASTM C1698. All the mortar samples were mixed in a Hobart mixer according to ASTM C305. In all cases admixtures were added to 18 M Ω -cm deionized water mixing water prior to mixing with cement. After mixing, the corrugated tubes were filled and sealed completely according to the guidelines provided in the ASTM 1698, and were cured at 23°C during the entire testing period. The length measurements were made on 4 replicate samples at the time of final setting (shown in Table 7 and determined using Vicat needle of diameter 2mm) and ages of 1, 2, 3, 7, 14, 28 days of

hydration. The autogenous shrinkage strains were calculated with reference to the initial length measurements made at final setting time.

TABLE 7 - FINAL SETTING TIMES (IN MINUTES) OF ACM MORTARS.

OPC	CSA2	CAC2	CAC3	AA1
255	180	390	1080	1080

Drying Shrinkage Testing

Twelve concrete prisms were prepared for each cement type to measure the linear drying shrinkage according to the ASTM C157. All samples were cured for 7 days with wet burlap and AA1 samples were sealed for 7 days in plastic bags prior to shrinkage measurements. These samples were placed in a room at 50% RH and 73°F for the entire testing period.

One common criticism of ASTM C157 is that this technique cannot measure the early strains when the samples are still in the molds within the first 12 to 24 hours. However, the autogenous and chemical shrinkage measurements can provide insights into the performance of these materials at these early ages.

RESULTS AND DISCUSSION

The results of ASTM C1608 chemical shrinkage testing are shown in Figs. 2 and 3. All ACM mixtures, with the exception of CAC2, showed considerably greater quantities of chemical shrinkage than the OPC mixture. The bulk of the chemical shrinkage occurred, for the CAC3 and CSA2 mixtures, during the first 24 hours. After 24 hours the rate of chemical reaction slowed, but was similar to that of OPC. After 7 days of reaction, the CAC3 binders had greater than 3x the chemical shrinkage of the OPC mixture, while the CSA mixtures had nearly 2x that of OPC. The chemically activated binder had slower chemical shrinkage development during the first two days of reaction, but showed a much greater rate (Table 8), compared to the other binders, including OPC, from 2 to 7 days. Based on this result, more work to ascertain the link between water uptake, percent reaction of binder precursor materials, and development of physical and mechanical properties should be done in order to examine the importance of water curing for this material.

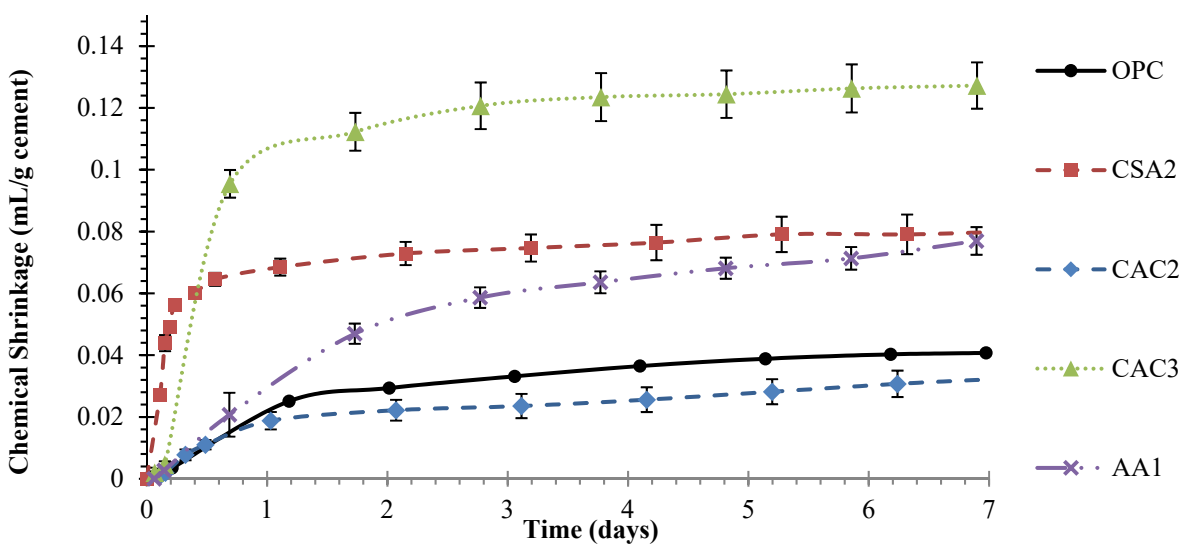


FIGURE 2 - AVERAGE CHEMICAL SHRINKAGE OF THE ACM PASTES.

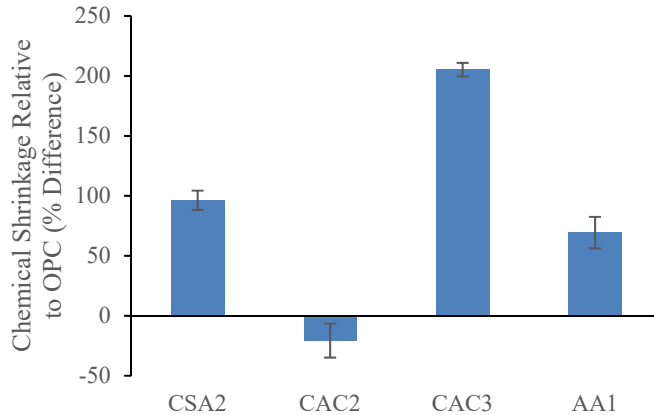


FIGURE 3 - CHEMICAL SHRINKAGE OF ALTERNATIVE CEMENT PASTES, RELATIVE TO THE CHEMICAL SHRINKAGE OF OPC PASTE, AFTER 7 DAYS OF HYDRATION.

While chemical shrinkage is not directly related to cracking, increased amounts of chemical shrinkage indicate higher water requirements for hydration of the cements. Use of mixing water in lower quantities than what is required for hydration will lead to self-desiccation and introduction of strains that can lead to autogenous shrinkage. However, development of autogenous shrinkage is based on many factors including the material's pore structure and the timing and extent of development of mechanical properties. Because of this, the chemical shrinkage of a material cannot directly predict the expected autogenous shrinkage.

The blended CAC-calcium sulfate-OPC material (CAC2) had very similar chemical shrinkage to OPC, up to 24 hours of hydration. After 24 hours its consumption of water slowed, resulting in it being the only binder tested which developed less chemical shrinkage than the OPC mixture. This reduction may be explained by the quantity of calcium sulfate present in the blended material. Calcium sulfate will dissolve into water, but not consume it, allowing the calcium sulfate present in the mixture to serve as an inert filler for consumption of water and therefore chemical shrinkage.

TABLE 8 - CHEMICAL SHRINKAGE RATES FOR OPC AND ACM MIXTURES.

Cement	Shrinkage Rate (mL/g/day)	
	0-2 days	2-7 days
OPC	0.0146	0.0023
CSA2	0.0339	0.0014
CAC2	0.0107	0.0020
CAC3	0.0648	0.0029
AA1	0.0271	0.0058

Fig. 4 shows the development of autogenous shrinkage in the OPC and ACM mixtures over 28 days of hydration, while Fig. 5 shows the change in shrinkage for each mixture relative to the OPC. The CSA2, CAC3, and AA1 mixtures generated significantly less total autogenous shrinkage at both 7 and 28 days, compared to the OPC mixture, while the CAC2 had equal or greater total autogenous shrinkage. Since all the autogenous shrinkage measurements were made from final setting time, it might be the reason for lower shrinkage values observed in case of

CSA2, CAC3 and AA1. Most of the shrinkage for these three cements occurred before final set, and thus is best captured during chemical shrinkage measurements (especially for CSA2 and CAC3) rather than autogenous shrinkage measurements. Additionally, of the shrinkage developed by CSA2, CAC3, and AA1, nearly all was developed during the first 48 hours of measurements, with only small increases continuing over the subsequent 26 days. Increases in shrinkage occurred over a much longer period for the CAC2 mixture, and were likely a result of continued hydration of the calcium silicates present in large proportion in that mixture as the continuing changes in the CAC2 mixture were similar to those occurring in the OPC mixture. Regression of shrinkage appeared to occur in the CAC3 sample near the very end of the testing period, and was believed to indicate the start of conversion in that sample.

The chemical shrinkage results for these binders did not necessarily correlate with the observed autogenous shrinkage. This may result from the different times and rates at which these phenomena occur. For example, early high chemical shrinkage can precede set and may not be fully captured by autogenous shrinkage measurements. The differences may also result from variations in the development of microstructure (e.g., fine porosity) and mechanical properties, among the ACMs. Further effort is required to better understand these variations in shrinkage.

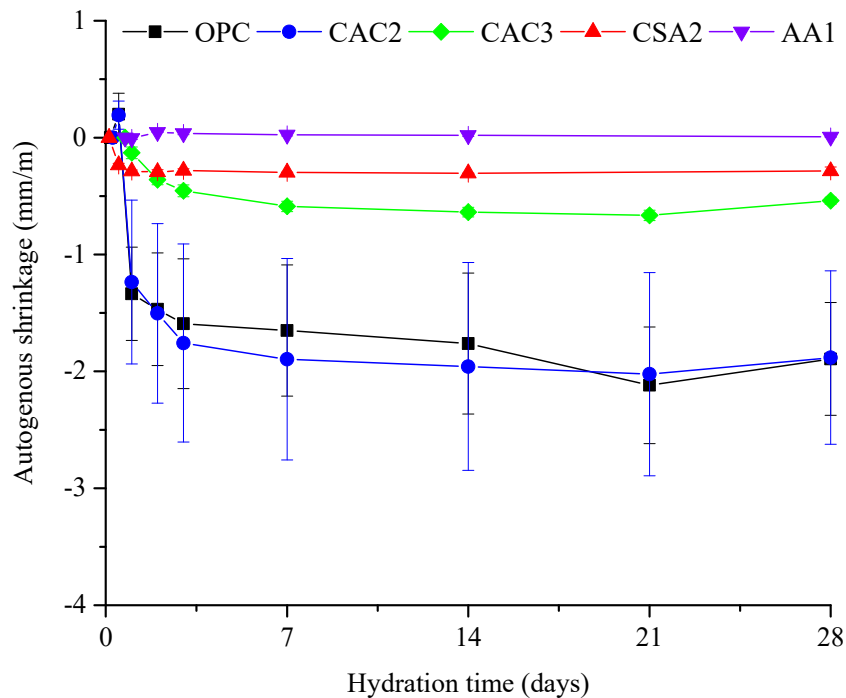


FIGURE 4 - AUTOGENOUS SHRINKAGE OF ACM MORTAR SAMPLES OVER 28 DAYS OF HYDRATION.

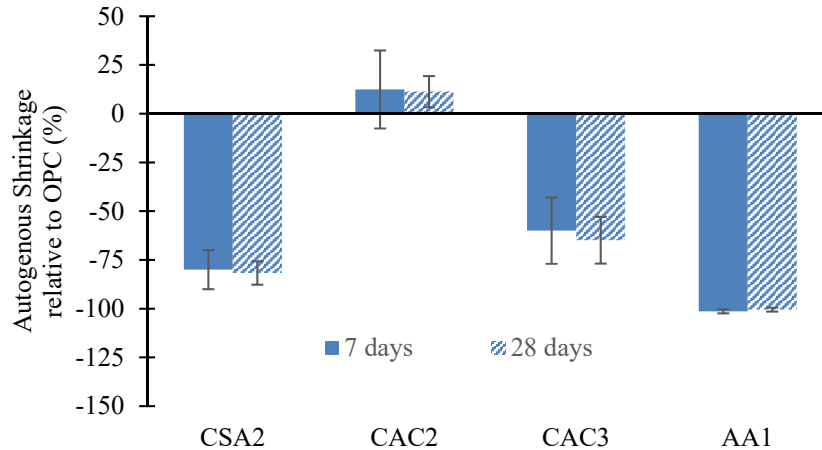


FIGURE 5 - RELATIVE AUTOGENOUS SHRINKAGE OF THE ACM MORTAR SAMPLES COMPARED TO THAT OF OPC AT 7 AND 28 DAYS OF HYDRATION.

Fig. 6 shows the average axial drying shrinkage of concrete beams according to ASTM C157 over 10 months for different ACMs compared to OPC. The measured data are shown by markers and their trends are shown by different line types. The trend lines were calculated using the best fit curves with R-squared larger than 0.96. Fig. 7 shows the difference in drying shrinkage of ACMs relative to OPC at 50, 150, and 300 days of drying. The trend lines shown in Fig. 5 were used to interpolate the shrinkage values at 50, 150, and 300 days and calculate the difference in ACM shrinkage relative to OPC.

For the samples tested, all of the ACM samples generated less shrinkage than OPC, except for CAC2, which had higher amounts of drying shrinkage than OPC. The CSA2, AA1, and CAC3 samples showed decreased drying shrinkage relative to OPC by greater than 52 to 54%, 58 to 65%, and 51 to 75% within 50 to 300 days from the exposure time, respectively. The AA1 samples showed the least shrinkage relative to OPC over the first 100 days. However, by 150 days CAC3 became the least expansive material. These results suggest that the conversion of CAC3 is likely an expansive process due to the release of water during conversion. However, more research is needed to better understand this mechanism. At 135 days the CAC3 sample began to increase in shrinkage, reaching nearly the same drying shrinkage as at 54 days.

Of the materials tested CSA2 had the rate of shrinkage change most similar to OPC, averaging 53% reduction in shrinkage compared to OPC over the full testing period. This property could be helpful in designing low-curling members where a small differential shrinkage from differential relative humidity over the depth of the member needs to be met.¹¹⁻¹⁵

On the other hand, CAC2 samples generated 32% more drying shrinkage than OPC after 50 days of drying, although this value did decrease over time, to 24% after 300 days. It is not clear why this occurred and this is an area of future research. Care should be taken in using this ACM when drying shrinkage is a major concern.

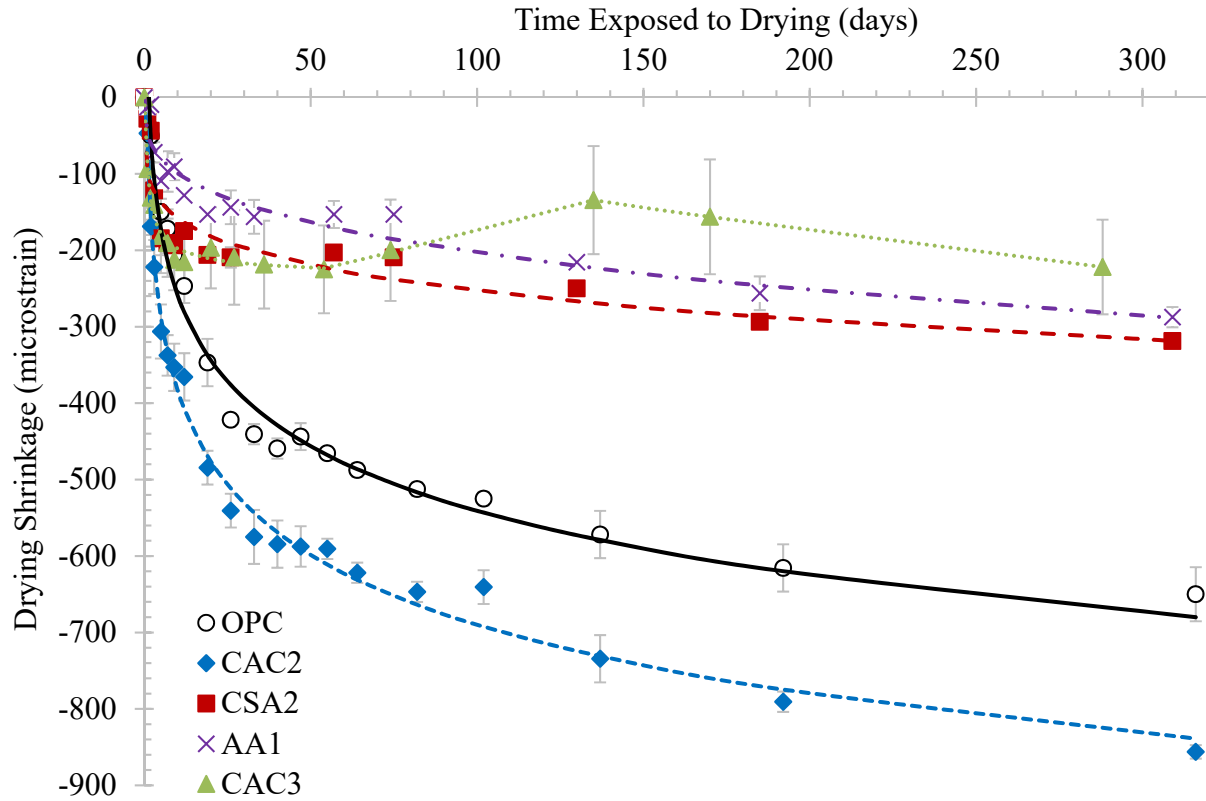


FIGURE 6 - AVERAGE AXIAL DRYING SHRINKAGE OF CONCRETE PRISMS.

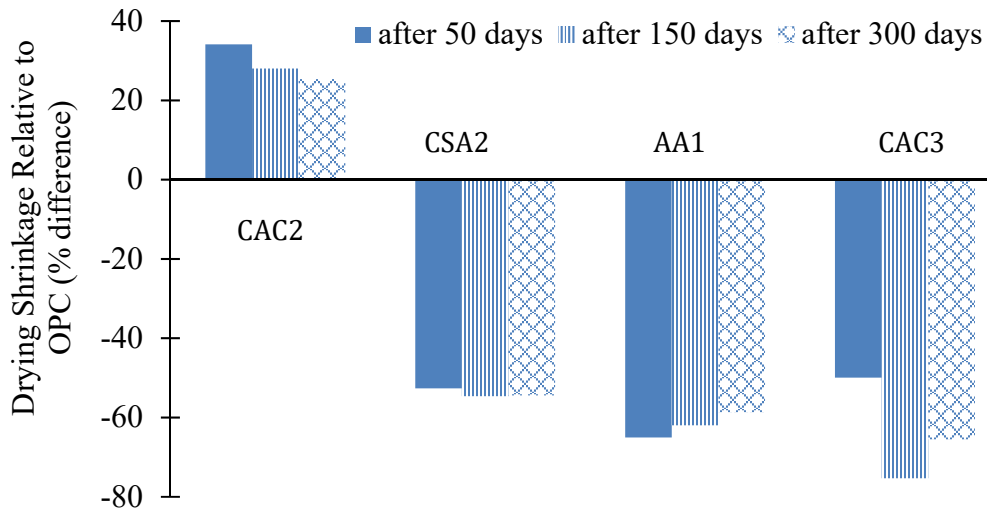


FIGURE 7 - DRYING SHRINKAGE RELATIVE TO OPC (% DIFFERENCE).

CONCLUSIONS

One approach to reducing the construction industry's carbon contributions will be through use of cements with lower associated emissions than those of portland cement. Reductions in cement emissions come from two places: materials-derived emissions, which can be obtained through substitution of cements requiring less calcium oxide than traditional portland cements, such as

calcium sulfoaluminate cement, calcium aluminate cement, and chemically activated fly ash binders; and fuel-derived emissions, which can be obtained using binders with reduced clinkering temperature requirements, such as calcium sulfoaluminate cement, or that do not require any clinkering, like chemically activated fly ash binders. In addition to the CO₂ savings associated with production of the material, further increases in sustainability can be achieved if: processing requirements (placing and curing) of alternative binders are understood and optimized; practices that contribute to increased durability of the alternative binders are prioritized during and after their construction; materials selections are made based on the application's requirements, keeping in mind the strengths and weaknesses of the particular binder choice, for example, choosing binders with low shrinkage, or expansive qualities, for applications where shrinkage cracking will reduce durability.

As cracking correlates with durability and reductions in concrete pavement service life, understanding and controlling shrinkage and cracking in pavements is essential for ensuring durability and reducing needs for repair and replacement of concrete pavements. Thus, in order to efficiently utilize alternative cements more must be understood about their shrinkage behavior and propensity towards cracking in order to determine if use of a material is suitable for a particular application. In order to increase understanding of shrinkage processes in alternative cementitious materials this study examined shrinkage from early ages through 10 months of hydration, tracking -- at various time periods appropriate for each test -- chemical shrinkage, autogenous shrinkage, and drying shrinkage of four commercially available ACMs.

Results showed that although the CSA2, CAC3, and AA1 binders consumed 2-3x higher quantities of water than the OPC mixture during hydration and initial reactions, translating to higher relative amounts of chemical shrinkage. Increased chemical shrinkage did not, however, lead to significant increases in autogenous shrinkage compared to OPC, and instead CSA2, CAC3, and AA1 all had lower total autogenous shrinkage than the portland cement did after 28 days of curing. Similarly, the CSA2, CAC3, and AA1 binders performed significantly better than the OPC mixture over 10 months of drying, generating between 45-55% less drying shrinkage than their OPC counterpart.

Conversely, the CAC2 binder generated slightly lower amounts of chemical shrinkage relative to OPC, but the same quantity of autogenous shrinkage, and approximately 25% greater levels of drying shrinkage than the OPC. Based on these results, CSA, CAC, and chemically activated binders may be good choices for projects in which shrinkage is a concern, while blended *CAC – OPC – CS* binders should be used with caution.

ACKNOWLEDGEMENTS

This work was supported by the Federal Highway Administration (FHWA) through an Exploratory Advanced Research Project (Project ID FHWA-PROJ-14-0134). Any opinions, findings, and conclusions expressed in this document are those of the authors and do not necessarily reflect those of the FHWA. The authors would also like to acknowledge Théotim Paul for his help conducting autogenous shrinkage testing, Natalia Stanley for her help with chemical shrinkage testing and Bijaya Rai and Katelyn Oquin for their help conducting the drying shrinkage testing.

REFERENCES

1. Olivier, J. G. J., Janssens-Maenhout, G., Muntean, M. & Peters, J. A. H. W. Trends in Global CO₂ Emissions 2014 report. *PBL Netherlands Environ. Assess. Agency* 60 (2014).
2. Burris, L. E., Ley, J. T., Berke, N., Moser, R. D. & Kurtis, K. E. Novel Alternative Cementitious Materials for Development of the Next Generation of Sustainable Transportation Infrastructure. *FHWA Techbr.* 38 (2015).
3. Scherer, G. W. Drying, Shrinkage, and Cracking of Cementitious Materials. *Transp. Porous Media* 110, 311–331 (2015).
4. Parrott, L. J., Geiker, M., Gutteridge, W. A. & Killoh, D. Monitoring Portland cement hydration: Comparison of methods. *Cem. Concr. Res.* 20, 919–926 (1990).
5. Lura, P., Jensen, O. M. & Van Breugel, K. Autogenous shrinkage in high-performance cement paste: An evaluation of basic mechanisms. *Cem. Concr. Res.* 33, 223–232 (2003).
6. Kovler, K. & Zhutovsky, S. Overview and Future Trends of Shrinkage Research. *Mater. Struct.* 39, 827–847 (2006).
7. Hajibabae, A. Reducing Curling from Drying Shrinkage of Concrete Pavements Through the Use of Different Curing Techniques. (Oklahoma State University, 2011).
8. Hajibabae, A. Impact of Different Curing Methods and Drying Conditions on Drying Shrinkage Induced Curling. (Oklahoma State University, 2016).
9. Hajibabae, A., Moradillo, M. K. & Ley, M. T. Comparison of curing compounds to reduce volume change from differential drying in concrete pavement. *Int. J. Pavement Eng.* 1–10 (2016).
10. Hajibabae, A. & Ley, M. T. The Impact of Wet Curing On Curling in Concrete Caused By Drying Shrinkage. *Mater. Struct.* 49, 1629–1639 (2016).
11. Hajibabae, A., Grasely, Z. C. & Ley, M. T. Mechanisms of dimensional instability caused by differential drying in wet cured cement paste. *Cem. Concr. Res.* 79, 151–158 (2016).
12. Hajibabae, A. & Ley, M. T. Impact of Wet and Sealed Curing on Curling in Cement Paste Beams from Drying Shrinkage. *ACI Mater. J.* 112, 79–84 (2015).
13. Ytterberg, R. Shrinkage and Curling of Slabs on Grade (Part a). *Concr. Int.* 9, 22–31 (1987).
14. Ytterberg, R. Shrinkage and Curling of Slabs on Grade (Part b). *Concr. Int.* 9, 54–61 (1987).
15. Ytterberg, R. Shrinkage and Curling of Slabs on Grade (Part c). *Concr. Int.* 9, 72–81 (1987).
16. Juenger, M. C. G., Winnefeld, F., Provis, J. L. & Ideker, J. H. Advances in alternative cementitious binders. *Cem. Concr. Res.* 41, 1232–1243 (2011).
17. Hargis, C. W., Kirchheim, A. P., Monteiro, P. J. M. & Gartner, E. M. Early age hydration of calcium sulfoaluminate (synthetic ye’elinite,) in the presence of gypsum and varying amounts of calcium hydroxide. *Cem. Concr. Res.* 48, 105–115 (2013).
18. Tang, S. W., Zhu, H. G., Li, Z. J., Chen, E. & Shao, H. Y. Hydration stage identification and phase transformation of calcium sulfoaluminate cement at early age. *Constr. Build. Mater.* 75, 11–18 (2015).
19. Bernardo, G., Telesca, A. & Valenti, G. L. A porosimetric study of calcium sulfoaluminate cement pastes cured at early ages. *Cem. Concr. Res.* 36, 1042–1047 (2006).

20. Chen, I. A., Hargis, C. W. & Juenger, M. C. G. Understanding expansion in calcium sulfoaluminate–belite cements. *Cem. Concr. Res.* **42**, 51–60 (2012).
21. Bizzozero, J., Gosselin, C. & Scrivener, K. L. Expansion mechanisms in calcium aluminate and sulfoaluminate systems with calcium sulfate. *Cem. Concr. Res.* **56**, 190–202 (2014).
22. Lura, P., Winnefeld, F. & Klemm, S. Simultaneous measurements of heat of hydration and chemical shrinkage on hardening cement pastes. *J. Therm. Anal. Calorim.* **101**, 925–932 (2010).
23. Bianchi, M. *et al.* Hydration Properties of Calcium Sulfoaluminate-Portland Cement Blends. *ACI Spec. Publ. - 261-13* 187–200 (2009).
24. Beretka, J., Marroccoli, M., Sherman, N. & Valenti, G. L. The influence of C4A3 \bar{S} content and ratio on the performance of calcium sulfoaluminate-based cements. *Cem. Concr. Res.* **26**, 1673–1681 (1996).
25. Hargis, C. W. *et al.* Further insights into calcium sulfoaluminate cement expansion. Further insights into calcium sulfoaluminate cement expansion. (2019).
26. Scrivener, K. L., Cabiron, J.-L. & Letourneux, R. High-performance concretes from calcium aluminate cements. *Cem. Concr. Res.* **29**, 1215–1223 (1999).
27. Ideker, J. H. Early-Age Behavior of Calcium Aluminate Cement Systems. (2008).
28. Dornak, M. L. Mechanical Properties, Early Age Volume Change, and Heat Generation of Rapid, Cement-based Repair Materials. (2014).
29. Torrens-Martin, D. & Fernandez-Carrasco, L. Long-term hydration and mechanical behaviour of portland cement, calcium aluminate cement and calcium sulfate blends. in *Proceedings of the International Conference on Calcium Aluminates* 242–249 (2014).
30. Lamberet, S. Durability of ternary binders based on portland cement, calcium aluminate cement and calcium sulfate. **3151**, (Ecole Polytechnique Federale de Lausanne, 2005).
31. Linglin, X., Peiming, W., Guangmin, W. & Guofang, Z. Effect of Calcium Sulfate on the Formation of Ettringite in Calcium Aluminate and Sulfoaluminate Blended Systems. *Key Eng. Mater.* **599**, 23–28 (2014).
32. Pacheco-Torgal, F., Castro-Gomes, J. & Jalali, S. Alkali-activated binders: A review. *Constr. Build. Mater.* **22**, 1305–1314 (2008).
33. Van Deventer, J. S. J., Provis, J. L. & Duxson, P. Technical and commercial progress in the adoption of geopolymer cement. *Miner. Eng.* **29**, 89–104 (2012).
34. Kuenzel, C., Vandeperre, L. J., Donatello, S., Boccaccini, A. R. & Cheeseman, C. Ambient Temperature Drying Shrinkage and Cracking in Metakaolin-Based Geopolymers. *J. Am. Ceram. Soc.* **95**, 3270–3277 (2012).
35. Puertas, F., Izquierdo, J. D., Granizo, M. L., Palomo, Fernández-Jiménez, Effect of superplasticisers on the behaviour and properties of alkaline cements. *Adv. Cem. Res.* **15**, 23–28 (2003).
36. Gunasekera, C., Setunge, S. & Law, D. W. Creep and Drying Shrinkage of Different Fly-Ash-Based Geopolymers. 39–50 (2019). doi:10.14359/51706941.
37. Janotka, I., Krajčí, L., Ray, A. & Mojumdar, S. . The hydration phase and pore structure formation in the blends of sulfoaluminate-belite cement with Portland cement. *Cem. Concr. Res.* **33**, 489–497 (2003).
38. Wallah, S. E. Drying shrinkage of heat-cured fly ash-based geopolymer concrete. *Mod. Appl. Sci.* **3**, 14 (2009).
39. Bissonnette, B., Pierre, P. & Pigeon, M. Influence of key parameters on drying shrinkage

- of cementitious materials. *Cem. Concr. Res.* **29**, 1655–1662 (1999).
40. Al-Saleh, S. A. & Al-Zaid, R. Z. Effects of drying conditions, admixtures and specimen size on shrinkage strains. *Cem. Concr. Res.* **36**, 1985–1991 (2006).

Durability of Recycled Aggregate Concrete

Nariman J. Khalil and Georges Aouad

Synopsis: The results of an experimental investigation into the mechanical properties and durability of recycled and natural coarse aggregates concrete are reported. A total of thirty-six specimens were tested. The percentages of replacement of coarse aggregates with recycled aggregates in the concrete mixes were 0%, 50%, and 100%. The source of recycled aggregates in this study was the concrete specimens tested in the laboratory. These specimens were crushed and then sieved into medium aggregates (4.75-9.5 mm) [0.19-0.37 in.] and coarse aggregates (9.5-19mm) [0.37-0.75 in.]. The replacement of fine aggregates was not considered in this study. The properties of concrete mixes containing natural aggregates as control mix and those containing Recycled Concrete Aggregates (RCAs) have been studied, including fresh properties, mechanical properties and durability. The influence of saturation state of RCA (dried or saturated) on the properties of concretes of identical compositions has first been studied. The theoretical amount of absorbed water is added at the beginning of mixing. Durability performance of hardened concrete made with recycled aggregates as partial or full replacement of natural coarse aggregates is reported. Resistance to pure water and sulfate attack is investigated. The results show that a replacement ratio of 50% does not have a significant effect on the performance of recycled aggregate concrete mixes. Moreover, the recycled aggregate concrete performs relatively satisfactorily under various conditions and has a comparable durability to natural aggregate concrete if properly designed.

Keywords: recycled aggregates, durability, mechanical properties, absorption, sulfate attack.

ACI member **Nariman J. Khalil** is an Associate Professor in the Department of Civil Engineering at the University of Balamand, Lebanon. She is the advisor to the University of Balamand Student Chapter-ACI. Her research interests encompass structural stability and design, concrete technology, high way materials, concrete sustainability and engineering education. She is a licensed consultant engineer in Lebanon.

George Aouad is an Associate Professor in the Department of Civil Engineering at the University of Balamand, Lebanon. His research activity concern the development of special concretes, the concrete durability, the reduction of the environmental impact of cement industries and 3D Printing.

INTRODUCTION

Concrete is the most used building material due to its adaptability and relatively low cost to produce. Nevertheless, it largely consumes the natural resources with serious environmental impacts. Sustainable development requires the reuse of Demolished Concrete Waste (DCW) in the production of new concrete which has been reported in literature for decades. Many researchers have studied different properties of concrete mixtures containing recycled concrete aggregates [1 till 19]; but there is still insufficient information on durability of Recycled Aggregates Concrete (RAC) and on the performance of structural elements made with such material.

This paper investigates the effect of different replacement levels of coarse RCA on the properties of fresh and hardened concrete. Some durability aspects of various RAC mixtures were investigated such as water absorption, porosity, and resistance to sulfate attack. Two levels of replacement were considered: 50% and 100%. Results were compared with a control concrete mix prepared using only natural aggregates. Seven and twenty-eight day compressive strengths, tensile strengths, moduli of rupture, and elasticity were measured for hardened concrete. This experimental study was performed in the civil engineering laboratory at the University of Balamand-Lebanon.

EXPERIMENTAL INVESTIGATION

In order to study the durability of RAC, three different concrete mixes were designed. The first mix was made entirely with natural aggregates and referred to as control mix (R0). The remaining two mixes were made by replacing the natural coarse aggregates (by volume) with recycled concrete aggregates. Two ratios were considered: 50% and the corresponding mix is referred to as (R50) and 100% replacement is referred to as (R100). Previous investigation by the first author [20] showed that the replacement level of 30% has no significant effect on concrete mechanical properties and therefore this percentage was eliminated from the current work. The work carried out was divided into four phases: characterisation of constituent materials, concrete mixture proportioning, study of the mechanical properties, and durability of concrete.

Characterisation of Constituent Materials

Ordinary Portland cement (Type I, 42.5), natural aggregates, water, and a high-range water-reducing admixture were used for the different concrete mixes prepared. The RCAs in this study were obtained by crushing concrete cylinders that were cast or brought to the civil engineering laboratory for testing of their compressive strength at 28 days age, as shown in Figure 1.

After crushing, the aggregates were sieved into two sizes: medium aggregates (4.75-9.5 mm) [0.19-0.37 in.] and coarse aggregates (9.5-19 mm) [0.37-0.75 in.], as per ASTM C33 [21], and proportioned as per each mix design, refer to Figure 2. The particle size distribution of both Natural Coarse Aggregates (NCAs) and RCAs were within the margins specified in ASTM C33. The test results on the physical properties of

natural and recycled aggregates are given in Table 1. The RCAs were dried in the oven at 110 ± 5 °C [230 ± 41 °F] and then stocked in closed containers until the mixing time.

Mix Proportions

Three concrete mixes using different recycled and natural aggregates were prepared. The main variable was the percentage of RCA, in order to study its effect on the mechanical properties and durability aspects. The effective water to cementitious material ratio (w/cm) used was fixed to 0.51 to account for the absorption properties of the RCAs that are considerably higher than the NCAs used. Recycled aggregates have not been soaked in water, instead the amount of absorbed water was calculated and added to the mixing water. The mix design is presented in Table 2.

Casting, Curing and Testing

All ingredients were fed into a 0.35 m^3 [12.36 ft^3] rotating drum mixer. About twenty percent of the mixing water was fed first to the mixer, then other ingredients in alternate manner were added to the turning mixer. A high-range water-reducing admixture was dissolved in one litre water and then added to the mix. Once all materials were in the mixer, the concrete was mixed for three minutes; followed by three minutes rest then two minutes mixing time, and immediately placed in the formwork. Immediate slump of each fresh concrete mixture was measured after mixing completion. Bulk density and air content of fresh concrete were also measured. Results are presented in Table 3.

Twelve specimens were cast for each mix, six cylinders 150 by 300 mm [6 by 12 in.] for the compressive strength at ages of 7 and 28 days and for the modulus of elasticity, three cylinders for the splitting tensile test at 28 days of age and three beams 150 by 600 mm [6 by 24 in.] for the flexural tensile test also at the age of 28 days.

The specimens were cast in a steel moulds and then covered with plastic sheets till the following day. After 24 hours the covers were removed and the specimens were left to air cure under laboratory conditions (temperature 24 ± 5 °C, relative humidity 60%) until the time of testing. Sampling and testing were done in accordance with the relevant ASTM standards.

Porosity

The total porosity of the paste part of each mix was measured by mercury intrusion porosimetry (MIP) (Micromeritics-Autopore IV system).

Resistance to Pure Water and Sulfate Attack

Cylindrical specimens (94 by 26 mm) [3.7-1.02 in.] were prepared from the R0, R50 and R100 mixes for durability tests. The specimens were immersed in a solution of 44g/l [2.75 lb/ft^3] Na_2SO_4 at 20 °C [68 °F]. The liquid/solid-volume ratio of the batches was 4 to 1. The sulfate concentration and the liquid/solid-volume ratio are the same as those of Schmidt et al. [26]. The sulfate solutions were changed after 7, 14, 28 and 56 days. For each mix, a reference test is realised in the same conditions by used distilled water instead of sulfate solution.

RESULTS AND DISCUSSIONS

Mechanical Properties

Table 4 summarises all test results on hardened concrete. Each result is the average of three specimens' tests. All tests are done in accordance with the relevant ASTM standards.

Compressive Strength

The effect of RCA replacement ratio on the compressive strength is shown in Figure 3. It can be seen that the early age strength has decreased by 9% as the RCA replacement ratio increased from zero to 100% while for the 28 day strength, the figure suggests an increase in strength up to 17% for R50 mix. This result is in agreement with the first author's previous work [20] and with literature. Surya et al [22] concluded that the replacement of NCA with RCA

does not have any adverse effect on the strength of the concrete. Yang et al [23], who studied the development of compressive strengths for RAC specimens for ages up to 91 days, concluded that the development of long-term strength is more favourable than that of natural aggregate concrete (NAC). Ulloa et al [15] agree with these findings, they stated that if the recycled aggregate is obtained from pure concrete, as is the case in the current study, a replacement ratio higher than 50% would only affect the workability but not the compressive strength.

Splitting Tensile Strength

Figure 4 represents the splitting tensile test results. Compared to R0 and R100 mixtures, a lower splitting tensile strength was recorded for R50 with 6% reduction when compared to R0. This value is comparable with the values obtained in previous work [20]. According to some researchers such as McNeil and Kang [24], the residual mortar improves the tensile capacity by creating a smoother transition between mortar and aggregates.

Flexural Tensile Strength

The flexural tensile strength, also known as the modulus of rupture, are reported in Table 4 and shown in Figure 5. There is an adverse effect of the replacement of NCA with RCA on the flexural tensile strength with a maximum reduction of 24% recorded for R50. This value is much higher than the reduction value of 6% obtained in the previous work [20]. This indicates the variable nature of RAC mixes.

Modulus of Elasticity

The modulus of elasticity values for RCA mixes recorded a maximum reduction value of 9% for R50 when compared with NAC mix R0. The results are given in Table 4 and illustrated in Figure 6. Larger reduction values were noted in reference [20] attaining 18%. Li [25] recorded a 45% reduction in E_c for 100% RCA replacement ratio. This could be explained by the variation in the properties of the aggregates used.

Porosity

Total porosity reveals a disparity of behaviours between mixes. In particular the porosity of R0 (23.6%) is higher than R50 (20.2%) and R100 (21.5%). This finding may explain the results of compressive strengths. The R0 mix which develops the lowest mechanical strength is the most porous.

Durability Properties

The expansion and mass changes were followed for R0, R50 and R100 concrete immersed at 20 °C [68 °F] in:

- 1) 44 g/l [2.75 lb/ft³] Na₂SO₄ solution (R0S, R50S and R100S)
- 2) Distilled water (R0W, R50W and R100W)

Figure 7 and Figure 8 present the mass change and expansion for the specimens of the mixture R0, R50 and R100 exposed to 44 g/l Na₂SO₄ solution. The results showed no significant difference in mass or in dimension between R0, R50 and R100 concrete after 56 days. No cracking was noted for all mixes in both media (water and sulfate). This finding is consistent with the results of Schmidt et al. [26] who concluded no expansion before 91 days. However, in the present study and for the sulfate condition, a white product was precipitated in the recycled aggregates specimens as shown in Figure 9. The amount of this white product varied in relation to the percentage of RCA; on one hand, a lack of it was noted in the RCA-free concrete (R0S) and on the other hand, an increasing amount of this product was seen on (R50S and R100S). The white product was characterised by X-Ray Diffraction (XRD) and the results show that it is a mix of ettringite and gypsum. This result is consistent with those in the literature for studies of sulfate attack on Ordinary Portland Cement concrete [26]. The durability tests were conducted up to 365 days (without measuring mass change or expansion) and no cracking was noted after this period.

CONCLUSIONS

- The mechanical properties of RAC mixes at the age of 28 days, such as splitting tensile and flexural strengths were comparable with those of NAC mixes. There was a favorable increase in the compressive strength for R100 compared to R0; whereas the modulus of elasticity of RAC was lower than that of NAC.
- The R50 mix exhibited the highest compressive strength and the lowest porosity.
- Durability tests up to 56 days revealed that recycled aggregate concrete performs satisfactorily under sulfate

exposure and has comparable durability behavior to natural aggregate concrete.

ACKNOWLEDGMENTS

The work presented in this paper was supported by the University of Balamand. The authors would like to thank the staff members of the civil engineering laboratory for their help during the experimental work.

REFERENCES

- [1] Hansen, T.C. recycling of demolished concrete and masonry. Taylor and Francis, Oxford shire, UK, (1992) 316.
- [2] ACI221R-96. Guide for use of normal weight and heavyweight aggregates in concrete. (Re approved 2001).
- [3] Katz, A. Properties of concrete made with recycled aggregate from partially hydrated old concrete. *Cement and Concrete Research*, (2003) 703-711.
- [4] Xiao, J., Li, J.B. and Zhang, C. On relationships between the mechanical properties of recycled aggregate concrete: An overview. *Materials and Structures* (2006) 39:655-664.
- [5] Etxeberria, M., Mari, A.R. and Vazquez, E. Recycled aggregate concrete as structural material. *Materials and Structures*, (2007) 40:529-541.
- [6] Gonzalez, B. and Martinez, F. Concrete with aggregates from demolition waste and silica fume. *Materials and mechanical properties, Building and Environment*, (2008) 429-437.
- [7] Florea, M. and Brouwers, H. The influence of crushing method on recycled concrete properties. *Advances in Cement and Concrete Technology in Africa*, (2009) 1041-1050.
- [8] M. Malesev, M., Radonjanin, V. and Marinkovic, S. Recycled concrete as aggregate for structural concrete production. *Sustainability* (2010), www.mdpi.com, 1204-1225.
- [9] Naguchi, T. Sustainable recycling of concrete structures. *Indian Concrete Institute Journal*, (2010) 41-53.
- [10] Husain, A. and Assas, M. Utilization of demolished concrete waste for new construction. *World Academy of Science, Engineering and Technology*, (2013) 69-74.
- [11] Belagraa, L. and Beddar, M. Study of the mechanical performance of a recycled aggregate concrete with admixture addition. *Open Journal of Civil Engineering*, <http://www.scirp.org/journal/ojce>, (2013).
- [12] Jeong, H. Processing and properties of recycled aggregate concrete. <http://hdl.handle.net/2142/26156>, 2011, (2014).
- [13] Cabral, A., Schalch, V., Dal Molin, D. and Ribeiro, J.L. Mechanical properties modelling of recycled aggregate concrete. *Construction and Building Materials* 24, ELSEVIER, (2010) 421-430.
- [14] McNeil K. and Kang T. H.-K. Recycled Concrete Aggregates: A Review. *International Journal of Concrete Structures and Materials*, Vol. 7, No. 1, (2013) 61-69.
- [15] Ulloa, V. A., Garcia-Taengua, E., Pelufo, M., Domingo, A., and Serna, P., 2013, "New views on effect of recycled aggregates on concrete compressive strength", *ACI Material Journal*, V. 110, No. 6, 687-696.
- [16] Limbachiya, M., Meddah, M. S., and Ouchagour, Y., 2012, "Performance of Portland/silica fume cement concrete produced with recycled concrete aggregate", *ACI Material Journal*, V. 109, No. 1, 91-100.
- [17] Seara-Paz, S., Corinaldesi, V., Gonzales-Fonteboa, B., and Martinez-Abella, F., 2016, "Influence of recycled coarse aggregates characteristics on mechanical properties of structural concrete", *European Journal of Environmental and Civil Engineering*, 20:sup1, s123-s139, DOI: 10.1080/19648189.2016.1246694.
- [18] Salem, R. M., Burdette, E. G., and Jackson, N. M., 2003, "Resistance to freezing and thawing of recycled aggregate concrete", *ACI Material Journal*, V. 100, No. 3, 216-220.
- [19] Faella, C., Lima, C., Martinelli, E., Pepe, M., and Realfonzo, R., 2015, "Strength and durability of sustainable concrete: an experimental study", *ACI*, V. 305, SP-305-10. 10.1-10.10.
- [20] Khalil, N.J., Touma, A., Touma, T., and Daher, R., 2016 "A Study into the Relationships between the Mechanical Properties of Recycled Aggregate Concrete", *Proceedings of the Second International Conference on Concrete Sustainability*", E-Book ISBN 978-84-945077-8-6, pp 1146-1158, Madrid- Spain.
- [21] ASTM-C33, Standard Specification for Concrete Aggregates.

- [22] Surya, M., Kanta Rao V. V. L. and Lakshmy, P., 2015, "Mechanical, durability and time-dependent properties of recycled aggregate concrete with fly ash", *ACI Materials Journal*, V. 112, No. 5, pp.653-660.
- [23] Yang, K., Chung, H. and Ashour, A., 2008, "Influence of type and replacement level of recycled aggregates on concrete properties", *ACI Material Journal*, V. 105, No. 3, 289-296.
- [24] McNeil K. and Kang T. H.-K., 2013, "Recycled Concrete Aggregates: A Review", *International Journal of Concrete Structures and Materials*, Vol. 7, No. 1, 61-69.
- [25] Li, X. 2008, "Recycling and reuse of waste concrete in china. Part I. Material behavior of recycled aggregate concrete, *Resources, Conservation and Recycling*", 53, ELSEVIER, 36-44
- [26] Schmidt, T., Lothenbach, B., Romer, M., Neuenschwander, J., Scrivener, K., 2009, "Physical and microstructural aspects of sulfate attack on ordinary and limestone blended Portland cements", *Cement and Concrete Research*, V. 39, 1111-1121.

TABLES AND FIGURES

Table 1- Properties of coarse aggregates. [1 in. = 25.4 mm]

Property	RCA		NCA	
	(4.75 – 9.5) mm [0.19-0.37 in.]	(9.5 – 19) mm [0.37-0.75 in.]	(4.75 – 9.5) mm [0.19-0.37 in.]	(9.5 – 19) mm [0.37-0.75 in.]
Specific gravity	2.415	2.390	2.654	2.676
Bulk density	1271	1311	1500	1505
Water absorption (%)	7.189	5.273	1.171	0.835
Los Angeles % of Mass Loss	29.05		22.1	

Table 2- Mix design [1 kg/m³=1.685 lb/yd³].

Mix	Cement (kg/m ³)	NCA*	NCA*	RCA†	RCA†	Natural Sand (kg/m ³)	Water (kg/m ³)	Super-plasticizer (kg/m ³)
		9.5-19 mm [0.37-0.75 in.]	4.75-9.5 mm [0.19-0.37 in.]	9.5-19 mm [0.37-0.75 in.]	4.75-9.5 mm [0.19-0.37 in.]			
R0	350	666	444	0	0	741	190.38	3.12
R50	350	333	222	285	202	741	214.21	3.46
R100	350	0	0	570	404	741	238.15	3.64

*NCA and RCA† refer to natural coarse aggregates and recycled coarse aggregates respectively.

Table 3- Results of fresh concrete tests [1 in.= 2.54 cm; 1 kg/m³=1.685 lb/yd³]

Mix	Slump	Bulk density	Air content
	cm	kg/m ³	%
R0	17.6	2291	5.40
R50	24	2261	2.35
R100	22	2243	2.40

Table 4- Results of hardened concrete tests [1000 psi= 6.895 MPa]

Concrete Type	Compressive strength f'_c		Density ρ	Splitting tensile strength f_{sp} , MPa	Flexural tensile strength f_t , MPa	Modulus of elasticity E_c MPa
	MPa		kg/m ³			
	7 days	28 days	28 days	28 days	28 days	28 days
R0	25.70	31.61	2299	3.90	5.30	32486
R50	23.73	37	2337	3.66	4.03	32521
R100	23.42	35.55	2217	3.87	4.05	29426



Figure 1- Laboratory waste



Figure 2- Characterized aggregates

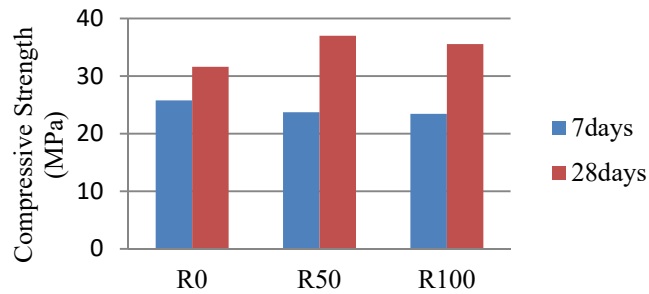


Figure 3- Effect of RCA percentage on concrete compressive strength
[1000 psi = 6.895 MPa]

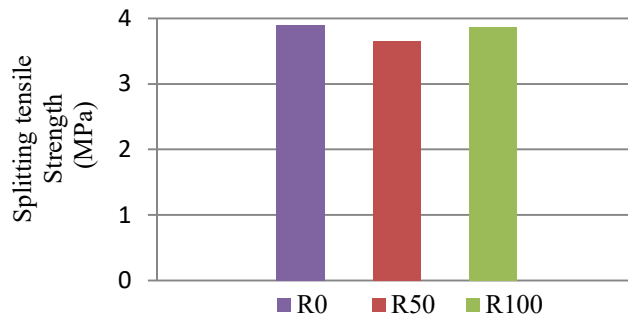


Figure 4- Effect of RCA percentage on the splitting tensile strength
[1000 psi = 6.895 MPa]

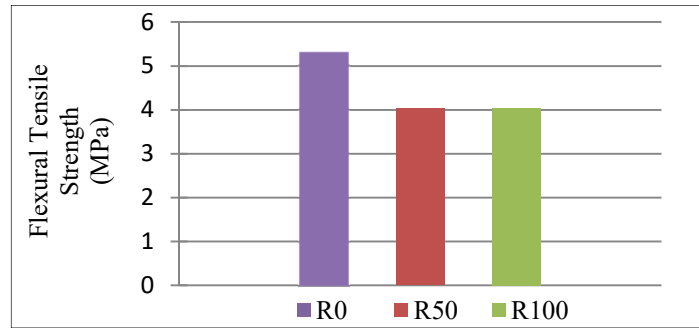


Figure 5- Effect of RCA percentage on the flexural tensile strength
[1000 psi = 6.895 MPa]

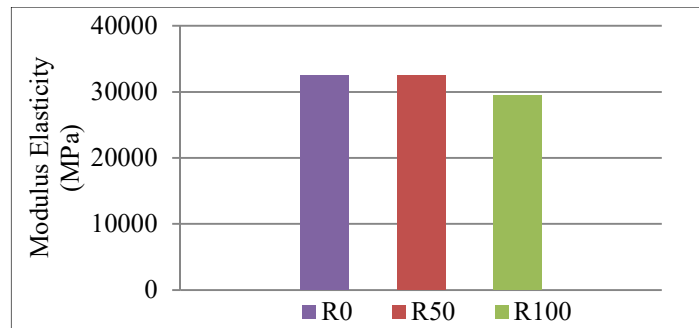


Figure 6- Effect of RCA percentage on the modulus of elasticity
[1000 psi = 6.895 MPa]

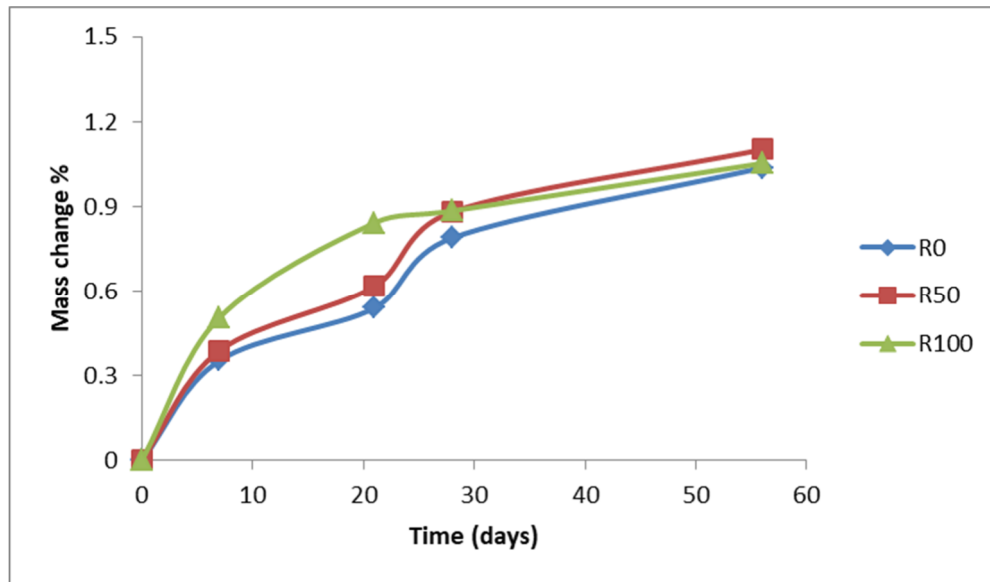


Figure 7- Mass change for the specimens of the mixture R0, R50 and R100 exposed to 44 g/l Na₂SO₄ solution.

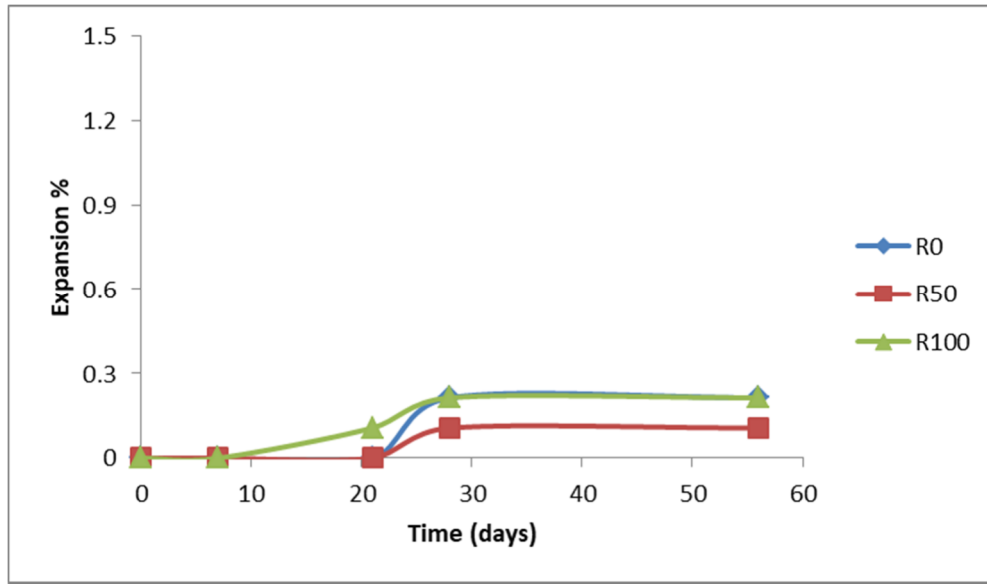


Figure 8- Expansion for the specimens of the mixture R0, R50 and R100 exposed to 44 g/l Na₂SO₄ solution.

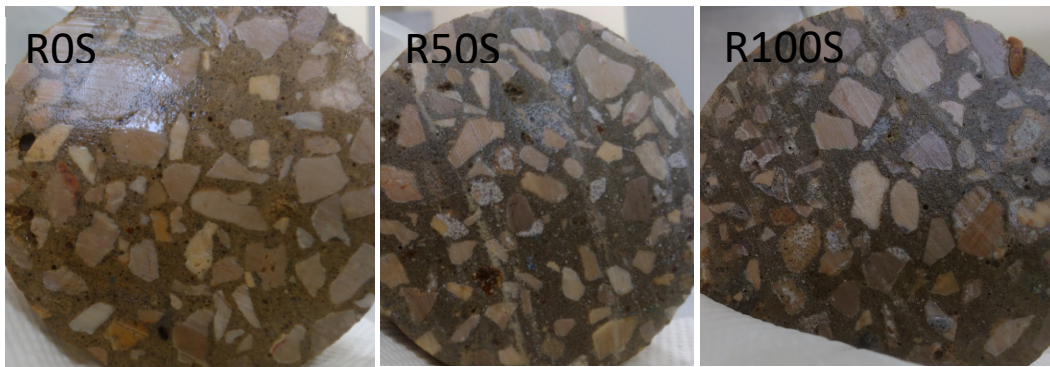


Figure 9- Concrete cylinders after 56 days of sulfate attack

Low-Cracking High-Performance Concrete (LC-HPC) for Durable Bridge Decks

David Darwin, Rouzbeh Khajehdehi, Muzai Feng,
James Lafikes, Eman Ibrahim, Matthew O'Reilly

Synopsis: The goal of this study was to implement cost-effective techniques for improving bridge deck service life through the reduction of cracking. Work was performed both in the laboratory and in the field, resulting in the creation of Low-Cracking High-Performance Concrete (LC-HPC) specifications that minimize cracking through the use of low slump, low paste content, moderate compressive strength, concrete temperature control, good consolidation, minimum finishing, and extended curing. This paper documents the performance of 17 decks constructed with LC-HPC specifications and 13 matching control bridge decks based on crack surveys. The LC-HPC bridge decks exhibit less cracking than the matching control decks in the vast majority of cases. Only two LC-HPC bridge decks have higher overall crack densities than their control decks, which are the two best performing control decks in the program, and the differences are small. The majority of the cracks are transverse and run parallel to the top layer of the deck reinforcement. The results of this study demonstrate the positive effects of reduced cement paste contents, concrete temperature control, limitations on or de-emphasis of maximum concrete compressive strength, limitations on maximum slump, the use of good consolidation, minimizing finishing operations, and application of curing shortly after finishing and for an extended time on minimizing cracking in bridge decks.

Keywords: bridge decks, consolidation, cracking, curing, finishing, high-performance concrete, temperature control

INTRODUCTION

Deterioration of bridges is a widespread and costly sustainability problem faced by society. In 2016, 9.1% of bridges in the U.S. were rated as structurally deficient (ASCE 2017). An average of 188 million trips were made over these deficient bridges daily. Cracking of concrete bridge decks is one major factor that causes bridges to become deficient. Cracks allow chlorides and moisture to reach the reinforcing steel in the bridge decks, resulting in corrosion. This in turn can lead to spalling of the concrete and a reduction in the service life of the bridge (Lindquist et al. 2005, Lindquist et al. 2006). Moreover, bridge deck cracking increases the vulnerability of concrete to freeze-thaw damage, further compromising the sustainability of bridge structures.

In response to these crack-related problems, a 13-year, two-phase pooled-fund program at the University of Kansas, titled *Construction of Crack-Free Bridge Decks*, was developed with the goal of implementing the most cost-effective techniques to reduce cracking construct more durable bridge decks. To accomplish this goal, the researchers completed the following tasks:

1. Developed a detailed plan to construct bridge decks with minimum cracking by incorporating “best practices” dealing with materials, construction procedures, and structural design. These practices were developed into Low-Cracking, High Performance Concrete (LC-HPC) specifications for high-quality sustainable concrete bridge decks.
2. Worked with state DOTs, designers, contractors, inspectors, and material suppliers to modify designs, specifications, contracting procedures, construction techniques, and materials to obtain decks exhibiting minimal cracking.
3. Selected and scheduled bridges to be constructed using LC-HPC specifications, and pre-qualify designers and contractors in application of the techniques.
4. Performed detailed crack surveys on bridge decks built following LC-HPC specifications as well as decks built following conventional practices.
5. Correlated the cracking measured in Task 4 with environmental and site conditions, construction techniques, design specifications, and material properties, and compared results with earlier data.
6. Documented the results of the study. Those results have been documented during the 13-year term of the study through a series of reports and papers describing the development of crack reduction technologies and the performance of the bridges constructed in the program. These are listed in a bibliography provided by Darwin et al. (2016).

The LC-HPC specifications involved concrete mixtures with low cement paste contents, low slump, and moderate rather than high strength. Improved construction procedures, including concrete temperature control, minimum finishing, and an early start coupled with extended curing, were also followed. The result was a reduction in plastic shrinkage, settlement, thermal, and drying shrinkage cracking, all of which contribute to cracking in bridge decks and compromise the sustainability of bridge structures.

The study involved cooperation between state departments of transportation, cement companies and other material suppliers, contractors, and designers. Work was performed both in the laboratory and in the field, resulting in the construction of 17 bridge decks (in 22 placements) in Kansas that were let under LC-HPC specifications. The study was performed in two phases, concluding in 2016. In addition, two bridge decks were constructed in Minnesota under LC-HPC specifications, along with control decks, the performance of which was reported by Pendergrass et al. (2013).

In 2005, the Kansas Department of Transportation (KDOT) with participation of the University of Kansas as part of this study started constructing bridge decks following LC-HPC specifications covering aggregate, concrete, and construction practices. Thirteen of these decks were paired by KDOT with control decks that had similar structural design, traffic volume, age, and environmental exposure conditions.

Seventeen LC-HPC bridges were planned for construction. The specifications were not followed for one of the bridge decks; all 17, however, remained in the study. Bridges that were constructed in accordance with the LC-HPC specifications are labeled as LC-HPC-1 through 13, 15, 16, and 17. The single bridge that was not constructed in accordance with LC-HPC specifications is labeled as OP-14 (Overland Park 14) and is the only one of the 17 bridges not constructed under the supervision of the Kansas Department of Transportation. Control bridges are labeled Control-1/2, 3 through 7, 8/10, 9, 11, 12, and 13. LC-HPC-1 and LC-HPC-2 were paired to the same control deck, designated as Control-1/2; and LC-HPC-8 and LC-HPC-10 were paired to one control deck, designated as Control-8/10. The bridge numbers reflect the order in which the bridges were let, not the order in which they were constructed. Most of the bridge decks in this study are supported by steel girders. LC-HPC-8, LC-HPC-10, and Control-8/10, however, are supported by precast-prestressed concrete girders.

Every year, crack surveys were performed to compare the cracking performance of the LC-HPC decks with that of the control decks. In this paper, crack survey data for years 2014 through 2017 are summarized. Four prior reports have been published with the specific goal of summarizing the crack survey results for 2006 through 2015. Gruman, Darwin, and Browning (2009) summarized the crack survey results for 2006, 2007, and 2008. Pendergrass, Darwin, and Browning (2011) summarized the crack survey results for 2009 and 2010. Kaul, Darwin and Browning (2012) and Bohaty, Riedel, and Darwin (2013) summarized the crack survey results for 2011, 2012 and 2013, and Alhmoode, Darwin, and O’Reilly (2015) summarized the crack survey results for 2014 and 2015. This paper extends the work of Alhmoode et al. (2015) to include the last surveys performed in 2016 and 2017. Full details are presented by Darwin et al (2016). In addition to the summaries of the crack survey results, four in-depth reports by Lindquist, Darwin, and Browning (2008), McLeod, Darwin, and Browning (2009), Yuan, Darwin, and Browning (2011), and Pendergrass and Darwin (2014) have been issued that address the evaluation of crack reduction technologies for both effectiveness and their impact on the durability of the resulting concrete (some of the findings are being implemented in follow-on studies and by programs outside of this pooled-fund study), the key parameters that control cracking in bridge decks, and the experiences involved in the construction of the LC-HPC decks, the performance of the bridge decks constructed under this program, and the lessons learned from the construction and evaluation of those decks.

RESEARCH SIGNIFICANCE

The studies described in this paper have had a major impact on the construction of bridge decks in the U.S. Many of the recommendations have been adopted by departments of transportation in multiple states within their regular bridge deck specifications, including reduced cementitious material and cement paste contents, improved early-age and long-term curing, limitations on or de-emphasis of maximum concrete compressive strength, limitations on maximum slump, and minimizing finishing operations. The result has been a significant reduction in cracking and improvement in durability of concrete bridge decks.

SPECIFICATIONS

Three special provisions of the Kansas Department of Transportation (KDOT) standard specifications have been developed for LC-HPC bridge decks. These special provisions cover the requirements for aggregate, concrete, and construction practices with the goal of reducing cracking of concrete bridge decks (Kansas Department of Transportation 2007a, b, c). The latest versions of the special provisions are presented by Darwin et al. (2016). The special provisions are written to minimize the potential for plastic shrinkage and settlement cracking in plastic concrete and drying shrinkage and thermal cracking in hardened concrete. The background for the approach taken to achieve these goals is presented by Schmitt and Darwin (1995, 1999), Darwin et al. (2004, 2010, 2012), Lindquist et al. (2005), Browning et al. (2007, 2009), and Darwin (2014). The requirements of the LC-HPC specifications are summarized below.

Aggregate

The coarse aggregate must be gravel, chat, or crushed stone. The minimum soundness and the maximum absorption should be 0.9 and 0.7, respectively. Table 1 lists the maximum allowable percentages of deleterious substances.

The fine aggregate must be natural sand (Type FA-A) or chat (Type FA-B). Moreover, these aggregate types must meet both the KDOT and the AASHTO requirements for mortar strength and organic impurities, respectively. Table 2 and Table 3 show the provisions on deleterious substances for natural sand and chat, respectively.

The combined aggregate gradation must be obtained by implementing a proven optimization method such as the KU Mix (Lindquist et al. 2008, 2015) or Shilstone (1990) Methods.

Table 1—Deleterious substance requirements for coarse aggregate

Substance	Maximum % Allowable by Weight
Material passing No. 200 sieve	2.5%
Shale or shale-like material	0.5%
Clay lumps and friable particles	1.0%
Sticks (including absorbed water)	0.1%
Coal	0.5%

Table 2—Deleterious substance requirements for type FA-A (Natural Sand)

Substance	Maximum % Allowable by Weight
Material passing No. 200 sieve	2.0%
Shale or shale-like material	0.5%
Clay lumps and friable particles	1.0%
Sticks (including absorbed water)	0.1%

Table 3—Deleterious substance requirements for type FA-B (Chat)

Substance	Maximum % Allowable by Weight
Material passing No. 200 sieve	2.0%
Clay lumps and friable particles	0.25%

Concrete

The cement content must be between 500 and 540 lb/yd³ (297 and 320 kg/m³). The water-cement ratio (by weight) must be between 0.44 and 0.45. The combined requirements for cement content and water-cement ratio ensure that the cement paste content will be below 26 percent by volume. The engineer in charge may approve a reduction in the water-cement ratio to 0.43 at the bridge construction site. All of the LC-HPC bridge decks discussed in this report, with the exception of LC-HPC 15 and 16, were constructed using 535 or 540 lb/yd³ of concrete (317 and 320 kg/m³). Bridge decks for LC-HPC 15 and 16 contained concrete with cement contents of 500 lb/yd³ (297 kg/m³) and 520 - 540 lb/yd³ (308 to 320 kg/m³), respectively. Table 4 and Table 5 list the concrete mix proportions for LC-HPC and control bridges, respectively.

Concrete must be sampled at the discharge of the pump, conveyor, or bucket. The allowable air content (by volume) ranges from 6.5 to 9.5%. To limit settlement cracking over the reinforcing bars, current specifications state that the concrete slump should range from 1½ to 3 in. (38 to 76 mm); the maximum allowable slump at the truck is 3½ in. (90 mm). When LC-HPC 1 through 13 were constructed, the specifications had a maximum limit on slump of 4 in. (100 mm). The concrete temperature at the time of placement should not exceed 70°F (21°C) and should not be lower than 55°F (13°C). The construction engineer in charge may permit the temperature to be 5°F (3°C) outside of this range. After the construction of LC-HPC 1 through 13, the LC-HPC specifications were modified to set a lower and upper limit for the compressive strength of concrete, with a 28-day compressive strength between 3500 and 5500 psi (24.1 and 37.0 MPa).

The use of vinsol resin or tall oil-based air-entraining admixtures is permitted per the LC-HPC specifications. The use of mineral, set-accelerating, or set-retarding admixtures is prohibited. The current specification allows for a Type A water-reducer or dual-rated Type A-F water-reducer. A Type F high-range water-reducer can be used if concrete complies with the plastic and hardened concrete properties specifications. If slump on site needs to be adjusted, it can be done only by adding water-reducing or high-range water-reducing admixtures. Withholding any portion of water during batching is not allowed.

Construction

Ambient temperature, wind speed, relative humidity 12 in. (30 cm) above the deck, and the plastic temperature of concrete must be measured at least once per hour by KDOT personnel. At all times during the construction process, the evaporation rate must remain under 0.2 lb/ft²/hr (1 kg/m²/hr). If the evaporation rate upper limit is exceeded, concrete cooling, wind break installation, or other procedures must be implemented to reduce the evaporation rate; fogging the concrete, however, is prohibited.

LC-HPC specifications allow contractors to use buckets, conveyors, or pumps to place concrete. A concrete pump may only be used if the contractor has demonstrated the ability to pump the LC-HPC concrete during the construction of the qualification slab. To avoid loss of entrained air in concrete, it is not acceptable to drop concrete from a height greater than 5 ft (1.5 m), and concrete pumps must have an air cuff or bladder valve to limit the free fall of concrete that may cause a loss in air. The concrete must be consolidated using vertically-mounted internal gang vibrators placed on 1-ft (305 mm) centers across the bridge deck. Saturated burlap must be placed on the finished concrete within 10 minutes of finishing, and the decks must be wet-cured for 14 days using soaker hoses under plastic. Curing is followed by application of curing compound for seven days to slow the rate of evaporation, which allows the concrete more time for creep to relieve tensile stresses due to early-age drying shrinkage.

The concrete supplier and contractor must demonstrate the ability to meet all the specifications by preparing both a qualification batch and a qualification concrete slab using LC-HPC concrete before the bridge deck is

constructed (Kansas Department of Transportation 2007c). Before the qualification batch is verified, the actual jobsite haul time must be simulated. All admixtures must be included in the qualification batch. The same personnel and equipment must be used to place both the qualification slab and the LC-HPC bridge deck. If the concrete meets the LC-HPC specifications during the construction of the qualification slab, those mixture proportions may be used for the bridge deck.

Table 4—Mix design properties for LC-HPC bridges

Bridge	Cement (lb/yd ³)	Water (lb/yd ³)	w/c	Fine Aggregate		Coarse Aggregate Max Size Agg.			Paste Content (% by volume)
				#1	#2	3/4 in. (CA-5)	1-1/2 in. (CA-6)	3/8 in. (CA-7)	
				(lb/yd ³)		(lb/yd ³)			
LC-HPC-1 p1	540	243	0.45	1246*	-	565	890	266	24.6
LC-HPC-1 p2									
LC-HPC-2									
LC-HPC-3	535	241	0.45	1071*	387 [†]	862	654	-	24.4
LC-HPC-4 p1	535	225	0.42	526*	1001 [†]	774	723	-	23.4
LC-HPC-4 p2	535	225	0.42	1089*	393 [†]	877	665	-	23.4
LC-HPC-5	535	225	0.42	1089*	393 [†]	877	665	-	23.4
LC-HPC-6	535	241	0.45	1071*	387 [†]	862	654	-	24.4
LC-HPC-7	540	243	0.45	1407**	-	599	988	-	24.6
LC-HPC-8	535	223	0.42	465*	1122 [§]	745	707	-	23.4
LC-HPC-9 [‡]	535	235	0.44	1419 [§]	-	1189	373	-	24.1
LC-HPC-10	535	223	0.42	465*	1122 [§]	745	707	-	23.4
LC-HPC-11	535	225	0.42	1467 ^{##}	-	312 ^{††}	312	1030	23.4
LC-HPC-12 p1	540	238	0.44	1438**	-	360	1199	-	24.3
LC-HPC-12 p2	535	239	0.45	1415**	-	855	805	-	24.2
LC-HPC-13	535	235	0.44	415*	1059 [§]	-	1510	-	24.1
OP p1	535	241	0.45	974**	392 [†]	875	745	-	24.4
OP p2									
OP p3									
LC-HPC-15	500	225	0.45	1472 ^{##}	-	1166	429 ^{##}	-	22.8
LC-HPC-16 [#]	500	225	0.45	1472 ^{##}	-	1166	429 ^{##}	-	22.8
LC-HPC-17	540	243	0.45	1470 ^{##}	220 ^{§§}	789	497 ^{##}	-	24.6

[‡] Cement content increased to 540 lb/yd³ for deck placement; [#] Cement content was increased to 520 and 540 lb/yd³ for deck placement; *Designated as FA-A; ** Designated as MA-2 in KDOT Specs; ^{##} Designated as MA-3 in KDOT Specs; [†] Manufactured sand; ^{††} Designated as CA-1 in KDOT Specs; ^{##} Designated as MA-4 in KDOT Specs; [§] Designated at BD-2 in KDOT Specs; ^{§§} Pea Gravel.

Note: 1 lb/yd³ = 0.5933 kg/m³, 1 in. = 25 mm

Table 5—Mix design properties for Control bridges

Bridge	Deck Section	Cement (lb/yd ³)	Class F Fly Ash (lb/yd ³)	Silica Fume (lb/yd ³)	Water (lb/yd ³)	w/c	Fine Aggregate (FA-A)	Coarse Aggregate		Paste Content (% by volume)
							(lb/yd ³)	CA-5	CA-7	
							(lb/yd ³)	(lb/yd ³)		
Control 1/2 p1	Subdeck	602	-	-	241	0.40	1493	1493	-	25.6
	Overlay	583	-	44	233	0.37	1488	-	1488	26.0
Control 1/2 p2	Subdeck	605	-	-	241	0.40	1493	1493	-	25.7
	Overlay	583	-	44	233	0.37	1488	-	1488	26.0
Control 3	Subdeck	536	133	-	268	0.40	Not Available			29.0
	Overlay	583	-	44	233	0.37	Not Available			26.0
Control 4	Subdeck	536	133	-	268	0.40	Not Available			29.0
	Overlay	583	-	44	233	0.37	Not Available			26.0
Control 5	Subdeck	536	133	-	268	0.40	Not Available			29.0
	Overlay	583	-	44	233	0.37	Not Available			26.0
Control 6	Subdeck	536	133	-	268	0.40	Not Available			29.0
	Overlay	583	-	44	233	0.37	Not Available			26.0
Control 7 p1	Subdeck	536	133	-	268	0.40	1419	1419	-	29.0
	Overlay	583	-	44	233	0.37	1488	-	1488	26.0
Control 7 p2	Subdeck	536	133	-	268	0.40	1419	1419	-	29.0
	Overlay	583	-	44	233	0.37	1488	-	1488	26.0
Control 8/10	Monolithic	612	-	-	244	0.40	Not Available			26.0
Control 9	Subdeck	612	-	-	244	0.40	1478	1478	-	26.0
	West Overlay	590	-	44	234	0.37	1485	-	1485	26.2
	East Overlay									
Control 11	North Subdeck	602	-	-	241	0.40	1508	1478	-	25.6
	South Subdeck	602	-	-	241	0.40	1508	1478	-	25.6
	Overlay	583	-	44	233	0.37	1490	-	1490	26.0
Control 12 p1	Subdeck	602	-	-	265	0.44	1455	1455	-	27.1
	Overlay	581	-	44	231	0.37	1475	-	1475	25.8
Control 12 p2	Subdeck	602	-	-	265	0.44	1455	1455	-	27.1
	Overlay	581	-	44	231	0.37	1475	-	1475	25.8
Control 13	Subdeck	612	-	-	244	0.40	1478	1478	-	26.0
	Overlay	590	-	44	234	0.37	1485	-	1485	26.2

Note: 1 lb/yd³ = 0.5933 kg/m³, 1 in. = 25 mm

CRACK SURVEY PROCEDURE

Crack surveys for both LC-HPC and control bridge decks are performed annually. The surveys are performed in accordance with the specifications presented by Darwin et al. (2016) and are summarized next.

Procedure

To provide accurate and comparable results, a standard procedure is followed for crack surveys. Crack surveys must be performed only on a day that is at least mostly sunny. The air temperature should not be less than 60°F (16°C) at the time of surveying. Moreover, the bridge deck should be completely dry. The crack survey is invalid if it rains during the time of the survey or if the sky becomes overcast.

A scaled plan (map) for the bridge deck is developed and printed before the survey. These plans serve as the template to indicate the location and length of the cracks on the bridge deck, and they should include a compass

indicating north. Plans should be developed at a scale of 1 in. = 10 ft (25.4 mm = 3.048 m). Furthermore, a 5 ft × 5 ft (1.524 m × 1.524 m) grid should be printed on a separate paper and placed underneath the deck plan; this grid should match the bridge grid that is placed on the deck. The grid helps the surveyors keep track of crack location and length. Some human error is involved when drawing the cracks.

Traffic control is provided to ensure the safety of the surveyors during the bridge survey. After closing at least one lane of the bridge to traffic, two surveyors draw a 5 ft × 5 ft (1.524 m × 1.524 m) grid on the bridge deck using chalk or lumber crayons. This grid is called the bridge grid and should match the grid drawn on the plans. Surveyors mark any cracks they can see while bending at waist height. Surveyors should not mark any crack that cannot be seen from waist height. When surveyors see a crack, they may bend closer and trace the crack to its end, including portions of the same crack that cannot be seen from waist height. If the surveyors see another crack while tracing a crack (not attached to the crack being traced), they do not mark it unless it can also be seen when bending from waist height. After marking a crack, the surveyors return to the location where they started marking the crack and continue surveying. At least two surveyors inspect each section of the bridge. This method results in consistent crack survey results between surveys (Lindquist et al. 2005, 2008). After cracks are marked on the bridge, another surveyor draws the marked cracks on the scaled bridge plan.

In addition to marking cracks, a standard crack comparator is used for measuring the width of the cracks. In case of a low cracking deck, all crack widths are measured. When the crack density is high, a representative number of cracks over the deck is selected for crack width measurements.

To determine crack density, the bridge plans with the marked cracks are scanned into a computer and converted to AutoCAD files. In AutoCAD, any lines on the bridge plan not representing cracks (such as bridge abutments or boundaries) are erased. The total length of the cracks can then be measured using AutoCAD. Crack density is calculated by dividing the total length of the cracks by the area of the bridge deck. Crack densities are reported in m/m^2 for the whole bridge, each placement, and each span.

RESULTS

The type of results obtained in the bridge deck cracking surveys can be illustrated by LC-HPC 4 and Control-4. LC-HPC-4 is the first unit of the southbound US-69 ramp to I-35 over 103rd Street in Overland Park, Kansas (Kansas City metro area), and Control-4 is the Antioch Road to westbound I-435 ramp that spans over the 103rd Street to US-69 south ramp, also in Overland Park. The deck on LC-HPC-4 was constructed in two placements. Placement 1 was cast on September 29, 2007 and Placement 2 was cast on October 2, 2007. The bridge deck for Control-4 was constructed on August 5, 2007. Both decks have been surveyed 8 times, with the most recent surveys in 2015.

Figures 1 and 2 show, respectively, the crack maps for LC-HPC-4 and Spans 1 and 2 of Control-4. As can be seen in the figures, the majority of cracks present are transverse, although longitudinal cracks do form, especially adjacent to abutments. As observed on most bridges decks in the study, both decks exhibit cracking within the positive and as well as the negative moment regions. The average crack density for LC-HPC-4 shown in Fig. 1 is $0.217 m/m^2$. The density for Spans 1 and 2 of Control-4 shown in Fig. 2 are 0.458 and $0.774 m/m^2$, respectively. For all of Control-4, the average crack density is 0.755 . Figure 3 compares crack densities of LC-HPC 4 and Control-4 over time. As shown in the figure, both LC-HPC-4 placements have exhibited much less cracking than Control-4.

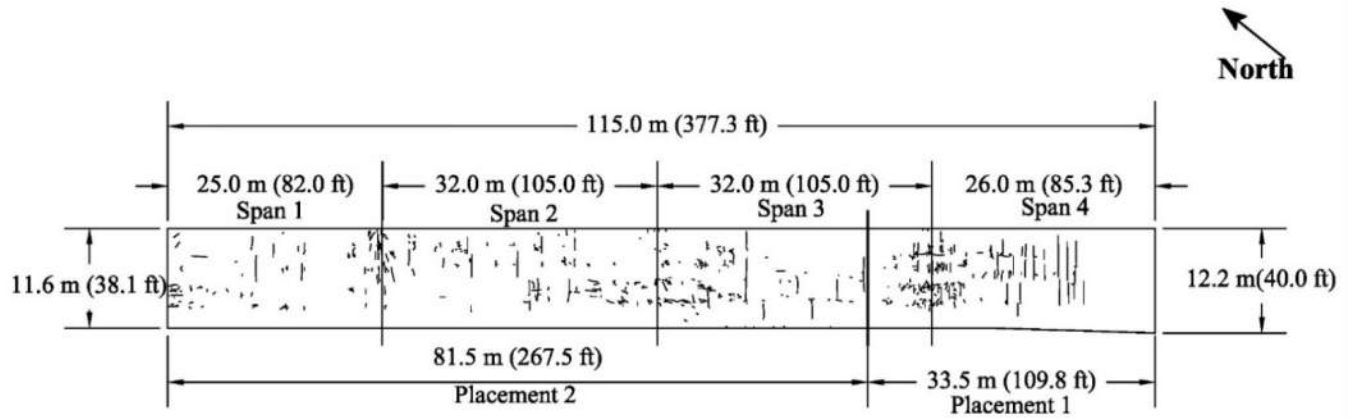


Fig. 1—2015 crack map of LC-HPC-4

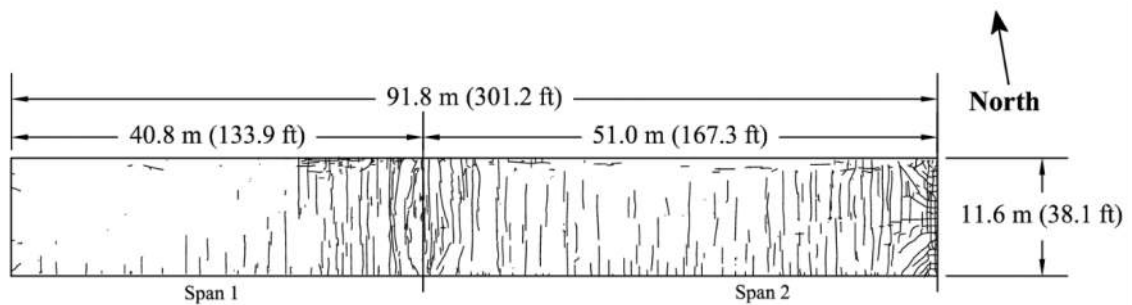


Fig. 2—2015 crack map of Spans 1 and 2 of Control-4

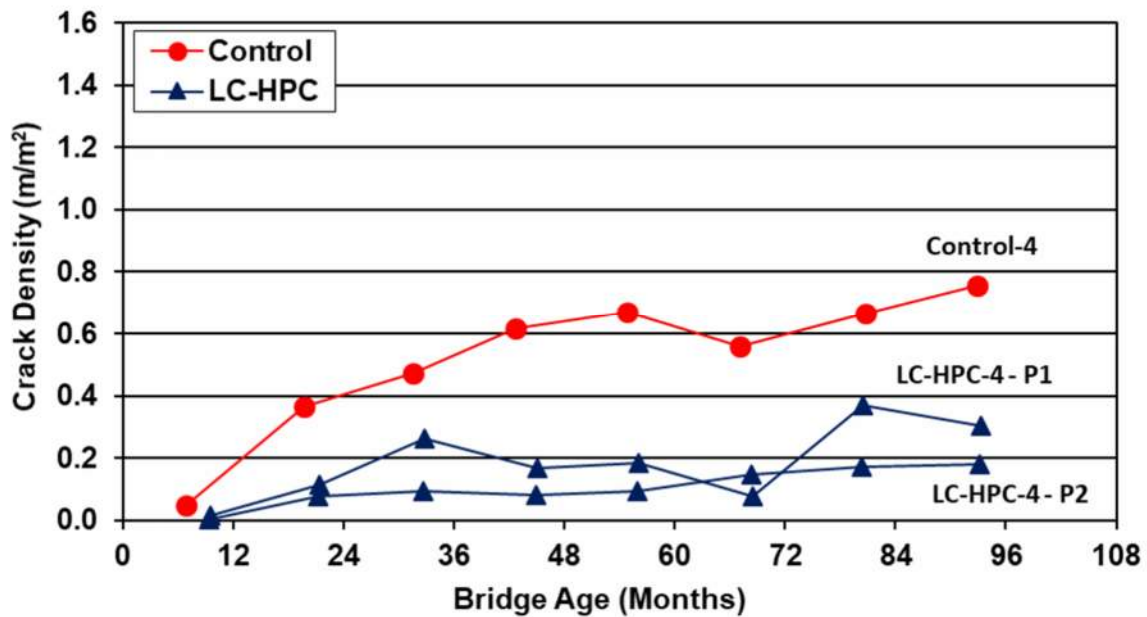


Fig. 3—Crack Densities versus Deck Age for LC-HPC-4 and Control-4

Tables A.1 and A.2 in Appendix A summarize the crack densities for the bridge decks surveyed in 2014 and 2015, respectively. Table A.3 summarizes the crack densities for the bridge decks surveyed in 2016 and 2017. Due to

high amounts of cracking, surveys on Control-5 ended in 2011 and surveys on Control-7, LC-HPC-12, and Control-12 ended in 2014. The crack densities obtained in the final surveys are included in the tables. Four decks were surveyed in 2016 (LC-HPC-3, Control-3, LC-HPC-11, and Control-11) and three decks in 2017 (LC-HPC-15, LC-HPC-16, and LC-HPC-17) to obtain final data for those projects (Table A.3). The crack maps for the 2014, 2015, and 2016 surveys are reported by Darwin et al. (2016). The results of the surveys performed in 2006, 2007, and 2008 were reported by Gruman, Darwin, and Browning (2009), those performed in 2009 and 2010 were reported by Pendergrass, Darwin, and Browning (2011), and those performed in 2011, 2012, and 2013 were reported by Kaul, Darwin and Browning (2012) and Bohaty, Riedel, and Darwin (2013).

The highest recorded crack density on an LC-HPC deck was 0.66 m/m^2 (LC-HPC-3 at 79.3 months) and the highest crack density on a control deck was 1.165 m/m^2 (Placement 1 of Control-7 at 98.5 months). Bridge deck OP-14 was not constructed in accordance with LC-HPC specifications; high slump concrete was used, the concrete was not properly consolidated, and the deck was over-finished, delaying curing. As a result, OP-14 has exhibited excessive cracking throughout its life. Two of the three placements of OP-14 exhibit the highest crack densities among all decks included in this study (1.331 m/m^2 for Placement 2 and 1.387 m/m^2 for Placement 3).

Figure 4 shows crack density versus time for the bridge decks included in this study, including OP-14. The south lane of LC-HPC-11 and decks LC-HPC-12 and Control-12 have been excluded. The south lane of LC-HPC-11 experiences a high amount of heavy truck traffic and, as a result, exhibits structural cracking. LC-HPC-12 and Control-12 were subjected to unusual torsional loading during construction that has affected the cracking performance of both decks. Although, the south lane of LC-HPC-11 and LC-HPC-12 have been excluded, both LC-HPC 11 (before excluding the south lane) and LC-HPC-12 have lower cracking than their control pairs. As shown in Fig. 4, the LC-HPC decks have exhibited lower overall cracking than the control decks. There is, however, some overlap, with some of the LC-HPC decks exhibiting higher crack densities than some of the control decks because they were constructed by different contractors (Yuan et al. 2011, Pendergrass and Darwin 2014) and have experienced different conditions.

Figure 5 shows that when the crack density of each LC-HPC deck (if a bridge had more than one placement, the average crack density of the placements are used) is compared with its corresponding control deck, LC-HPC decks have performed better than their control pairs in 10 of 12 cases. The two control decks (Control 1/2 and Control 3) that are performing better than their paired LC-HPC decks are the two best performing control decks in the program, and the differences in crack density between the LC-HPC and control deck is each case is small. As shown in Fig. 5, both LC-HPC decks supported by precast-prestressed girders (LC-HPC-8 and LC-HPC-10) performed better than the control deck (Control-8/10).

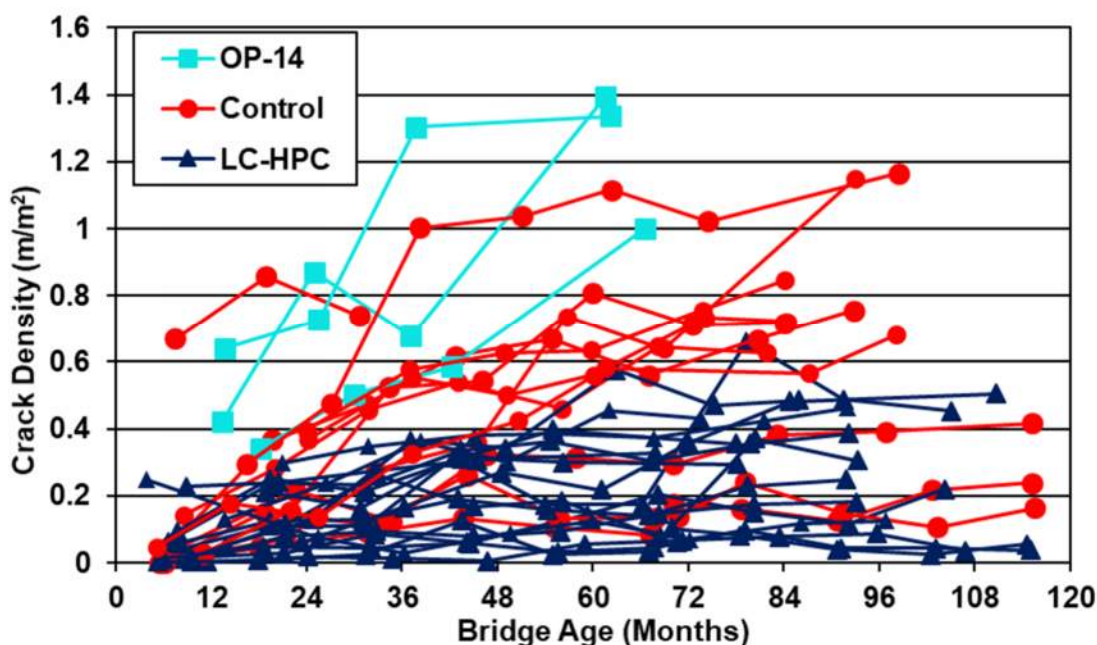


Fig. 4— LC-HPC and Control decks crack densities versus deck age*
 *LC-HPC-12, Control-12, and south lane of LC-HPC-11 are not shown

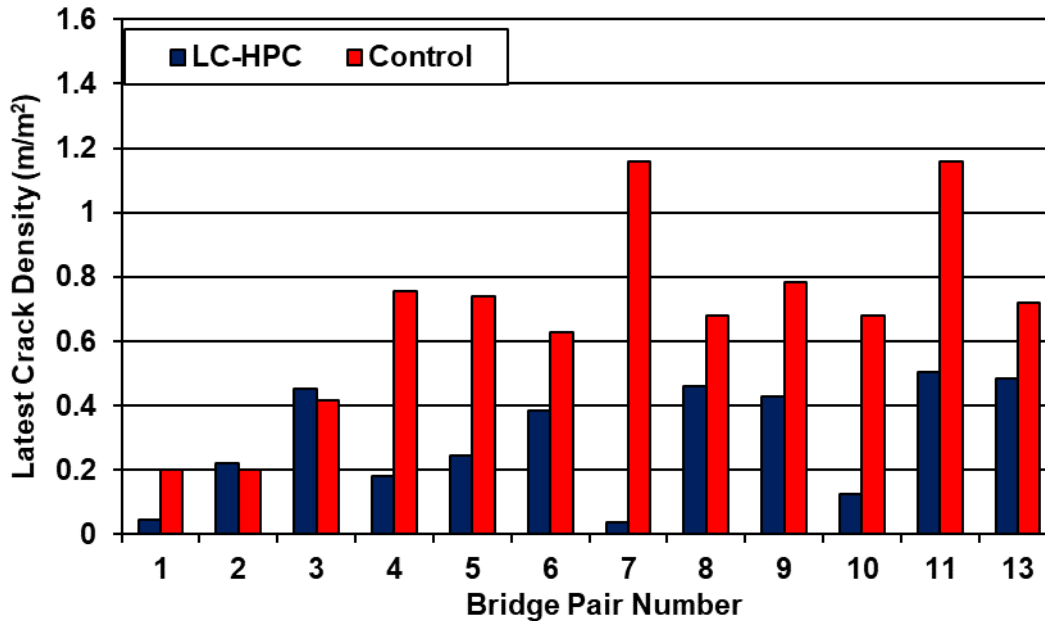


Fig. 5—Comparison of Crack Density between each LC-HPC and its Control pair*
 * LC-HPC-12 and Control-12 are not shown

Starting in the summer of 2015, crack widths were measured for most of the bridges that were surveyed. Crack widths were measured using a wallet-sized crack comparator. The accuracy of the comparator was verified with multiple devices. Results of more than 500 cracks width measurements indicate that most of the crack widths for cracks that can be seen from waist height have widths between 0.006 and 0.025 in. (0.150 mm to 0.635 mm).

SUMMARY AND CONCLUSIONS

Low-Cracking High-Performance Concrete (LC-HPC) specifications have been developed by KDOT and the University of Kansas for the purpose of increasing the expected service life of concrete bridge decks by the reduction of cracking. Surveys of LC-HPC and control bridge decks were performed and crack densities compared to examine the benefits of implementing LC-HPC specifications. Comparisons between 13 LC-HPC and matching control bridge decks are made based on the crack density and changes in crack density over time.

Based on the results of this study, the following conclusions can be drawn:

1. The LC-HPC bridge decks exhibit less cracking than the matching control decks in the vast majority of cases.
2. Most of the cracks observed on the bridge decks in this study were transverse cracks. Cracks of this type appear to run directly over and parallel to the top layer of reinforcement in the decks.
3. Near the abutments, cracks usually propagate perpendicular to the abutments.
4. The widths of the cracks generally range from 0.006 to 0.025 in. (0.15 to 0.64 mm).
5. Reduced cementitious material and cement paste contents, improved early-age and long-term curing, limitations on or de-emphasis of maximum concrete compressive strength, limitations on maximum slump, concrete temperature control, and minimizing finishing operations help minimize cracking in bridge decks.
6. High-slump concrete, poor consolidation, delayed curing, and over-finishing result in increased cracking in bridge decks.

ACKNOWLEDGEMENTS

Funding for this research was provided by the Kansas Department of Transportation (KDOT) serving as the lead agency for the “Construction of Crack-Free Bridge Decks, Phase II” Transportation Pooled Fund Study, Project No. TPF-5(174). The Colorado DOT, Idaho Transportation Department, Indiana DOT, Michigan DOT, Minnesota DOT, Mississippi DOT, New Hampshire DOT, New York DOT, North Dakota DOT, Ohio DOT, Oklahoma DOT, Texas DOT, Wisconsin DOT, the University of Kansas Transportation Research Institute, BASF Construction

Chemicals, and the Silica Fume Association provided funding to the pooled fund. Representatives from each sponsor served on a Technical Advisory Committee that provided advice and oversight to the project. Thanks are also due to the KDOT personnel who provided support, guidance, and construction supervision, the contractors, material suppliers, and subcontractors who worked on the bridges, and the sponsors of the first phase of “Construction of Crack-Free Bridge Decks” Transportation Pooled Fund Study, Project No. TPF-5(051), including Kansas Department of Transportation serving as the lead agency, the Federal Highway Administration (FHWA) of the U.S. Department of Transportation (DOT), Delaware DOT, Idaho Transportation Department, Indiana DOT, Michigan DOT, Minnesota DOT, Mississippi DOT, Missouri DOT, Montana DOT, New Hampshire DOT, North Dakota DOT, Oklahoma DOT, South Dakota DOT, Texas DOT, Wyoming DOT, Overland Park, KS, and the University of Kansas Transportation Research Institute. LRM Industries, BASF Construction Chemicals, Holcim US, Fordyce Concrete, Grace Construction Products, Ash Grove Cement, and Lafarge North America provided concrete materials for laboratory studies. Last, but certainly not least, it is important to acknowledge the contributions of Dr. JoAnn Browning, Dean of Engineering at the University of Texas at San Antonio (UTSA), who served at the Co-Principal Investigator of this project prior to joining UTSA, and the earlier graduate students who contributed to the project: Drs. Will Lindquist, Heather McLeod, Jiqui Yuan, Ben Pendergrass, and Miriam Toledo, and Diane Reynolds, Dan Gruman, Maria West, Nathan Tritsch, Swapnil Deshpande, Amber Harley, Vinur Kaul, Jeff Peckover, Pankaj Shrestha, Brent Bohaty, Elizabeth Riedel, Grant Polley, Osama Al-Qassag, and Ryan Brettmann.

REFERENCES

- Alhmoode, A.; Darwin, D.; and O'Reilly, M., 2015, “Crack Surveys of Low-Cracking High-Performance Concrete Bridge Decks in Kansas 2014-2015,” *SL Report* 15-3, University of Kansas Center for Research, Lawrence, KS, Sep., 118 pp.
- ASCE, 2017, “2017 Infrastructure Report Card,” American Society of Civil Engineers. <<https://www.infrastructurereportcard.org/cat-item/bridges/>>
- Bohaty, B.; Riedel, E.; and Darwin, D., 2013, “Crack Surveys of Low-Cracking High-Performance Concrete Bridge Decks in Kansas 2011-2013,” *SL Report* 13-6, University of Kansas Center for Research, Lawrence, KS, Dec., 153 pp.
- Browning, J.; Darwin, D.; and Hurst, K., 2007, “Specifications to Reduce Bridge Deck Cracking,” *HPC Bridge Views*, Issue No. 46, Sep./Oct., pp. 1-2.
- Browning, J.; Darwin, D.; and Hurst, K., 2009, “Specifications to Reduce Bridge Deck Cracking,” *HPC Bridge Views*, Issue No. 55, May/June, pp. 1-3.
- Darwin, D.; Browning, J.; and Lindquist, W. D., 2004, “Control of Cracking in Bridge Decks: Observations from the Field,” *Cement, Concrete and Aggregates*, ASTM International, V. 26, No. 2, Dec. pp. 148-154.
- Darwin, D.; Browning, J.; Lindquist, W.; McLeod, H. A. K.; Yuan, J.; Toledo, M.; and Reynolds, D., 2010, “Low-Cracking, High-Performance Concrete Bridge Decks – Case Studies Over the First 6 Years,” *Transportation Research Record: Journal of the Transportation Research Board*, No. 2202, pp. 61-69.
- Darwin, D.; Khajehdehi, R.; Alhmoode, A.; Feng, M.; Lafikes, J.; Ibrahim, K.; and O'Reilly, M., 2016, “Construction of Crack-Free Bridge Decks: Final Report,” *SM Report* No. 121, University of Kansas Center for Research, Lawrence, KS, Dec., 160 pp.
- Darwin, D.; Browning, J.; McLeod, H. A. K.; Lindquist, W.; and Yuan, J., 2012, “Implementing Lessons Learned From Twenty Years of Bridge-Deck Crack Surveys,” *Andy Scanlon Symposium on Serviceability and Safety of Concrete Structures: From Research to Practice*, SP-284, American Concrete Institute, Farmington Hills, MI, pp. 8-1-8-17.
- Darwin, D., 2014, “Low-Cracking High-Performance Bridge Decks,” *Concrete Bridge Views*, Issue No. 78, September/October. <http://www.concretebridgeviews.com/i78/Article2.php>
- Gruman, D.; Darwin, D.; and Browning, J., 2009, “Crack Surveys of Low-Cracking High-Performance Concrete Bridge Decks in Kansas 2006-2008,” *SL Report* 09-1, University of Kansas Center for Research, Lawrence, KS, Jan., 50 pp.

- Kansas Department of Transportation, 2007a, "Low-Cracking High-Performance Concrete - Aggregates," Standard Specifications for State Road and Bridge Construction, Topeka, KS.
- Kansas Department of Transportation, 2007b, "Low-Cracking High-Performance Concrete," Standard Specifications for State Road and Bridge Construction, Topeka, KS.
- Kansas Department of Transportation, 2007c, "Low-Cracking High-Performance Concrete - Construction," Standard Specifications for State Road and Bridge Construction, Topeka, KS.
- Kaul, V., Darwin, D., and Browning, J., 2012, "Crack Surveys of Low-Cracking High-Performance Concrete Bridge Decks in Kansas 2010-2011," *SL Report 12-4*, University of Kansas Center for Research, Lawrence, KS, Dec., 77 pp.
- Lindquist, W.; Darwin, D.; and Browning, J., 2005, "Cracking and Chloride Contents in Reinforced Concrete Bridge Decks," *SM Report No. 78*, University of Kansas Center for Research, Lawrence, KS, Feb., 453 pp.
- Lindquist, W.; Darwin, D.; Browning, J.; and Miller, G. G., 2006, "Effect of Cracking on Chloride Content in Concrete Bridge Decks," *ACI Materials Journal*, V. 103, No. 6, Nov.-Dec., pp. 467-473.
- Lindquist, W. D.; Darwin, D.; and Browning, J. P., 2008, "Development and Construction of Low-Cracking High-Performance Concrete (LC-HPC) Bridge Decks: Free Shrinkage, Mixture Optimization, and Concrete Production" *SM Report No. 92*, University of Kansas Center for Research, Lawrence, KS, Nov., 540 pp.
- Lindquist, W.; Darwin, D.; Browning, J.; McLeod, H. A. K.; Yuan, J.; and Reynolds, D., 2015, "Implementation of Concrete Aggregate Optimization," *Construction & Building Materials*, V. 74, Jan., pp. 49-56.
- McLeod, H. A. K.; Darwin, D.; and Browning, J., 2009, "Development and Construction of Low-Cracking High-Performance Concrete (LC-HPC) Bridge Decks: Construction Methods, Specifications, and Resistance to Chloride Ion Penetration," *SM Report No. 94*, University of Kansas Center for Research, Lawrence, KS, Sep., 815 pp.
- Pendergrass, B.; Darwin, D.; and Browning, J., 2011, "Crack Surveys of Low-Cracking High-Performance Concrete Bridge Decks in Kansas 2009-2010," *SL Report 11-3*, University of Kansas Center for Research, Lawrence, KS, Oct., 103 pp.
- Pendergrass, B.; Shrestha, P.; Riedel, E.; Polley, G.; and Darwin, D., 2013, "Evaluation of Cracking Performance of Bridge Decks in Minnesota," *SL Report 13-4*, University of Kansas Center for Research, Lawrence, KS, Oct., 24 pp.
- Pendergrass, B., and Darwin, D., 2014, "Low-Cracking High-Performance Concrete (LC-HPC) Bridge Decks: Shrinkage-Reducing Admixtures, Internal Curing, and Cracking Performance," *SM Report No. 107*, The University of Kansas Center for Research, Lawrence, KS, Jan., 664 pp.
- Schmitt, T. R., and Darwin, D., 1995, "Cracking in Concrete Bridge Decks," *SM Report No. 39*, University of Kansas Center for Research, Lawrence, KS, Apr., 151 pp.
- Schmitt, T. R. and Darwin, D., 1999, "Effect of Material Properties on Cracking in Bridge Decks," *Journal of Bridge Engineering*, ASCE, V. 4, No. 1, Feb., pp. 8-13.
- Shilstone, J. M., Sr., 1990, "Concrete Mixture Optimization," *Concrete International*, V. 12, No. 6, June, pp. 33-39.
- Yuan, J.; Darwin, D.; and Browning, J., 2011, "Development and Construction of Low-Cracking High-Performance Concrete Bridge Decks: Free Shrinkage Tests, Restrained Shrinkage Tests, Construction Experience, and Crack Survey Results," *SM Report No. 103*, University of Kansas Center for Research, Lawrence, KS, Sep., 505 pp.

AUTHOR BIOS

ACI Honorary Member **David Darwin** is the Deane E. Ackers Distinguished Professor and Chair of the Department of Civil, Environmental, and Architectural Engineering at the University of Kansas and a Past President of ACI.

ACI member **Rouzbeh Khajehdehi**, is a Graduate Research Assistant at the University of Kansas. He received his MS in civil engineering from the Southern Illinois University, Edwardsville, IL.

ACI member **Muzai Feng**, is a Graduate Research Assistant at the University of Kansas. He received his MS in civil engineering from the University of Kansas, Lawrence, KS.

ACI member **James Lafikes** is a Graduate Research Assistant at the University of Kansas. He received his MS in civil engineering from the University of Kansas, Lawrence, KS.

ACI member **Eman Ibrahim**, is a Graduate Research Assistant at the University of Kansas. She received her MS in civil engineering from the Mosul University, Mosul, Iraq.

ACI member **Matthew O'Reilly**, is an Assistant Professor at the University of Kansas. He received his Ph.D. in civil engineering from the University of Kansas, Lawrence, KS.

APPENDIX A—CRACK DENSITY COMPARISONS

Table A.1—2014 Crack Density Comparisons of LC-HPC vs. Control decks

Bridge Name	Bridge Location	Deck Age (months)	2014 Crack Density (m/m ²)	Bridge Girder Type
LC-HPC-1	EB Parallel Pkwy over I-635	102.5/103.1 ^Y	0.043/0.024 ^Y	Steel
Control-1/2	WB Parallel Pkwy over I-635	103.3/102.7	0.106/0.217	
LC-HPC-2	34th St. over I-635	92.2	0.116	Steel
Control-1/2	WB Parallel Pkwy over I-635	103.3/102.7	0.106/0.217	
LC-HPC-3	WB 103rd over US-69	79.4	0.759	Steel
Control-3	EB 103rd St. over US-69	83.2	0.376	
LC-HPC-4	SB US-69 to I-435 Rp over 103rd St	80.4/80.3	0.371/0.173	Steel
Control-4	Antioch to WB I-435 & NB US-69/Rp/WB I-435 to NB US-69 Rp	80.7	0.667	
LC-HPC-5	SB US-69 to WB I-435 Rp over Quivera Rp	79.4	0.229	Steel
Control-5*	SB US-69 to EB I-435 Rp over US-69 Hwy and I-435	30.6	0.738	
LC-HPC-6	SB US-69 to WB I-435 Rp over WB I-435 to Quivera Rp	79.7	0.356	Steel
Control-6	SB US-69 to EB I-435 Rp over US-69 Hwy and I-435	68.2	0.646	
LC-HPC-7	Co Rd 150 over US-75	95.7	0.087	Steel
Control-7	NB Antioch over I-435	74.5/68.9	1.022/0.638	
LC-HPC-8	E 1350 Rd over US-69	81.6	0.425	Precast Prestressed Concrete
Control-8/10	K-52 over US-69	87.2	0.566	
LC-HPC-9	NB US-69 over Marais Des Cygnes River	62	0.454	Steel
Control-9	SB US-69 over Marais Des Cygnes River	73.8/74.1	0.733	
LC-HPC-10	E 1800 Rd over US-69	86.2	0.117	Prestressed Concrete
Control-8/10	K-52 over US-69	87.2	0.566	
LC-HPC-11	EB US-50 over K&O RR	84.8	0.842	Steel
Control-11	US-50 over BNSF RR	98	0.922	
LC-HPC-12	Unit 2 K-130 over Neosho River	64.9/76.3	0.657	Steel
Control-12	Unit 1 K-130 over Neosho River	64.0/76.4	1.152	
LC-HPC-13	NB US-69 over BNSF RR	75.2	0.471	Steel
Control-13	SB US-69 over BNSF RR	72.5	0.711	
LC-HPC-15	NB K-7 over Johnson Dr./55th St	43	0.317	Steel
LC-HPC-16	SB K-7 over Johnson Dr./55th St	43.5	0.311	Steel
LC-HPC-17	Clear Creek Parkway over K-7	32.5	0.274	Steel

^Y Slash separates age and density for different placements; * 2011

Table A.2—2015 Crack Density Comparisons of LC-HPC vs. Control decks

Bridge Name	Bridge Location	Deck Age (months)	2015 Crack Density (m/m ²)	Bridge Girder Type
LC-HPC-1	EB Parallel Pkwy over I-635	15.1/114.5	0.045	Steel
Control-1/2	WB Parallel Pkwy over I-635	115.6/115.3	0.189	
LC-HPC-2	34th St. over I-635	104.2	0.222	Steel
Control-1/2	WB Parallel Pkwy over I-635	115.6/115.3	0.189	
LC-HPC-3	WB 103rd over US-69	91.5	0.487	Steel
Control-3	EB 103rd St. over US-69	96.9	0.391	
LC-HPC-4	SB US-69 to I-435 Rp over 103rd St	93.3/93.2	0.217	Steel
Control-4	Antioch to WB I-435 & NB US-69/Rp/WB I-435 to NB US-69 Rp	92.9	0.775	
LC-HPC-5	SB US-69 to WB I-435 Rp over Quivera Rp	91.8	0.247	Steel
Control-5*	SB US-69 to EB I-435 Rp over US-69 Hwy and I-435	30.6	0.738	
LC-HPC-6	SB US-69 to WB I-435 Rp over WB I-435 to Quivera Rp	92.2	0.386	Steel
Control-6	SB US-69 to EB I-435 Rp over US-69 Hwy and I-435	81.9	0.628	
LC-HPC-7	Co Rd 150 over US-75	106.9	0.036	Steel
Control-7 [#]	NB Antioch over I-435	74.5/68.9	1.022/0.638	
LC-HPC-8	E 1350 Rd over US-69	92.0	0.462	Precast Prestressed Concrete
Control-8/10	K-52 over US-69	98.1	0.680	
LC-HPC-9	NB US-69 over Marais Des Cygnes River	73.6	0.430	Steel
Control-9	SB US-69 over Marais Des Cygnes River	84.4/84.1	0.779	
LC-HPC-10	E 1800 Rd over US-69	96.8	0.125	Prestressed Concrete
Control-8/10	K-52 over US-69	98.1	0.680	
LC-HPC-11 [#]	EB US-50 over K&O RR	84.8	0.842	Steel
Control-11 [#]	US-50 over BNSF RR	98	0.922	
LC-HPC-12 [#]	Unit 2 K-130 over Neosho River	64.9/76.3	0.657	Steel
Control-12 [#]	Unit 1 K-130 over Neosho River	64.0/76.4	1.15*	
LC-HPC-13	NB US-69 over BNSF RR	85.9	0.486	Steel
Control-13	SB US-69 over BNSF RR	84.1	0.718	
LC-HPC-15	NB K-7 over Johnson Dr./55th St	56.2	0.299	Steel
LC-HPC-16	SB K-7 over Johnson Dr./55th St	55.0	0.397	Steel
LC-HPC-17	Clear Creek Parkway over K-7	45.5	0.308	Steel

^Y Slash separates age and density for different placements; * 2011; [#] 2014

Table A.3—2016 and 2017 Crack Density Comparisons of LC-HPC vs. Control decks

Bridge Name	Bridge Location	Deck Age (months)	2016 Crack Density (m/m²)	Bridge Girder Type
LC-HPC-3	WB 103rd over US-69	105	0.453	Steel
Control-3	EB 103rd St. over US-69	115.3	0.416	
LC-HPC-11	EB US-50 over K&O RR	110.7	0.883	Steel
Control-11	US-50 over BNSF RR	124.9	1.16	
			2017 Crack Density (m/m²)	
LC-HPC-15	NB K-7 over Johnson Dr./55th St	78.2	0.293	Steel
LC-HPC-16	SB K-7 over Johnson Dr./55th St	78	0.356	Steel
LC-HPC-17	Clear Creek Parkway over K-7	67.9	0.327	Steel